Advanced dose calculations and imaging in prostate brachytherapy treatment planning.

Joshua William Mason

Submitted in accordance with the requirements for the degree of
Doctor of Philosophy

The University of Leeds
Faculty of Medicine and Health
School of Medicine
Division of Medical Physics

December 2014

The candidate confirms that the work submitted is his/her own, except where work which has formed part of jointly authored publications has been included. The contribution of the candidate and the other authors to this work has been explicitly indicated below. The candidate confirms that appropriate credit has been given within the thesis where reference has been made to the work of others.

List of jointly authored publications

1) Mason J, Al-Qaisieh B, Bownes P, Henry A, Thwaites D. Monte Carlo investigation of I-125 interseed attenuation for standard and thinner seeds in prostate brachytherapy with phantom validation using a MOSFET. *Medical Physics* 2013;40:031717-031728.

   This work is included in sections 2 and 3. The work in this publication is attributable to J Mason; the co-authors contributed to the research ideas, provided supervision support and proof-read the manuscripts.

2) Mason J, Al-Qaisieh B, Bownes P, Wilson D, Buckley DL, Thwaites D, Carey B, Henry A. Multi-parametric MRI-guided focal tumor boost using HDR prostate brachytherapy: A feasibility study. *Brachytherapy* 2014;13:137-45.

   This work is included in section 5. The work in this publication is attributable to J Mason; the co-authors contributed to the research ideas, provided supervision support and proof-read the manuscripts.

3) Mason J, Al-Qaisieh B, Bownes P, Henry A, Thwaites D. Investigation of interseed attenuation and tissue composition effects in 125I seed implant prostate brachytherapy. *Brachytherapy* 2014;13:603-610.

   This work is included in section 4. The work in this publication is attributable to J Mason; the co-authors contributed to the research ideas, provided supervision support and proof-read the manuscripts.

4) Mason J, Al-Qaisieh B, Bownes P, Thwaites D, Henry A. Dosimetry modeling for focal high-dose-rate prostate brachytherapy. *Brachytherapy* 2014; 13:611-617.

   This work is included in section 6. The work in this publication is attributable to J Mason; the co-authors contributed to the research ideas, provided supervision support and proof-read the manuscripts.

Acknowledgements

I would like to thank GE Healthcare for their financial support to this research and for supplying the radioactive seeds used in the experimental measurements described in section 3.

I would like to thank my supervisors, Peter Bownes, Dr Ann Henry, Professor David Buckley and Professor David Thwaites for their input, direction and support, and for very helpful reviews of publications and the material in this thesis.

I would like to thank other members of the brachytherapy physics team at St James's Institute of Oncology for their assistance and support with various aspects of this research, including Shaun St Clair, Elizabeth St Clair, Owen O'Connell, Gavin Wright, Carolyn Richardson and, particularly, Dr Bashar Al-Qaisieh. I would like to thank other members of the clinical staff at St James's Institute of Oncology including the MRI radiographers, theatre staff, Dr Brendan Carey, Dr Jonathan Smith, Dr Kevin Franks and Dr David Bottomley. I would like to thank Dr Dan Wilson and Professor David Buckley for assistance with the MRI aspects of this project, and Brian Metcalfe and Tim Clarkson in radiation engineering services for making the phantom used in experimental measurements. I would like to thank the patients who participated in the prostate MRI study.

Finally I would like to thank my wife Shelley and children Isabel and Alex for their support and encouragement while I have been undertaking this PhD research.

Abstract

Brachytherapy using low dose rate (LDR) permanent seed implant or high dose rate (HDR) temporary implant is a well established treatment for prostate cancer. This study investigates the use of advanced dose calculation and imaging techniques to improve clinical prostate brachytherapy treatments. Monte Carlo (MC) simulations are used to assess the impact of source interactions and tissue composition effects that are ignored by the TG-43U1 dose calculation algorithm used in clinical practice. MC simulation results are validated using experimental phantom measurements. The development of prostate cancer may be driven by a dominant intra-prostatic lesion (DIL) but standard brachytherapy treatments prescribe the same dose level to the whole prostate. This study assesses the feasibility of multi-parametric (mp-MRI) guided focal boost treatments that escalate dose to the DIL to improve tumour control and of focal treatments that target the DIL to reduce treatment related side effects.

Source interactions and tissue effects are shown to reduce the dose that is delivered to patients in LDR treatments, particularly for patients with calcifications, however the dosimetric impact is small compared to other uncertainties in LDR seed implant brachytherapy. For HDR treatments attenuation by steel catheters has only a small impact on dose distributions. Feasibility of mp-MRI guided focal boost HDR prostate brachytherapy is demonstrated in terms of tumour delineation and the ability to dose escalate the DIL without increased dose to normal tissues. The dosimetric feasibility of LDR and HDR focal therapy treatments is demonstrated. Focal therapy treatments are shown to be more sensitive to source position errors than whole gland treatments. MC simulations of focal therapy treatments show that there are no additional concerns in terms of dosimetric accuracy compared to standard whole gland treatments. Advanced dose calculation and imaging techniques can improve clinical prostate brachytherapy treatments.

Table of Contents

List of Tables

List of Figures

List of abbreviations

^{103}Pd	Palladium-103
^{125}I	Iodine-125
^{192}Ir	Iridium-192
6711	Oncura 6711 ^{125}I seed
9011	Oncura 9011 ^{125}I seed
Λ	Dose rate constant (TG-43U1)
ADC	Apparent diffusion coefficient
AIF	Arterial input function
AKR	Air kerma rate
AISI	American Iron and Steel Institute
ANSI	American National Standards Institute
CT	X-ray computed tomography
CTR1/2	Contour 1/2 in Figure 16
D0.1cm^3	Minimum dose in the 0.1 cm^3 of the volume that receives the highest dose
D2cm^3	Minimum dose in the 2 cm^3 of the volume that receives the highest dose
D10	Minimum dose in the 10% of the volume that receives the highest dose
D30	Minimum dose in the 30% of the volume that receives the highest dose
D90	Minimum dose in the 90% of the volume that receives the highest dose
D98	Minimum dose in the 98% of the volume that receives the highest dose
DCE-MRI	Dynamic contrast enhanced MRI
DICOM	Digital Imaging and Communications in Medicine standard
DIL	Dominant intra-prostatic lesion
DVH	Dose-volume histogram
DWI	Diffusion weighted imaging

EES	Extravascular extracellular space
Elekta AB	Elekta AB, Stockholm, Sweden
EPI	Echo planar imaging
$F(r,\theta)$	Anisotropy function (TG-43U1)
$g_L(r)$	Radial dose function (TG-43U1)
$G_L(r,\theta)$	Geometry function (TG-43U1)
GEC-ESTRO	Groupe Européen de Curiethérapie-European Society for Radiotherapy & Oncology
F-GTV	Focal-gross tumor volume
F-PTV	Focal-planning target volume
FOV	Field of view
H-PTV	Hemi-planning target volume
HDR	High dose rate
HEMI	Hemi-gland focal therapy treatment plan
HIFU	High-intensity focused ultrasound
HU	Hounsfield unit
IMRT	Intensity-modulated radiation therapy
ISA	Inter-seed attenuation and scatter
k_{ep}	Rate constant between the EES and blood plasma
K^{trans}	Volume transfer constant
LDR	Low dose rate
MBDCA	Model-based dose calculation algorithm
MC	Monte Carlo
MC-CT-TISSUE	MC simulated CT based dose distribution including tissue and ISA effects
MC-ISA	MC simulated dose distribution including ISA effects
MC-STR-TISSUE	MC simulated structure based dose distribution including tissue and ISA effects
MC-SUP	MC simulated superposition dose distribution
MC-SUP 100% VOL	The volume enclosed by the 100% isodose in MC-SUP
mHDR-v2r	MicroSelectron HDR v2r source
MOSFET	Metal-oxide-semiconductor field-effect transistor

mp-MRI	Multiple parametric-MRI
MRI	Magnetic resonance imaging
MRSI	Magnetic resonance spectroscopic imaging
NNDC	National Nuclear Data Centre
OAR	Organ at risk
PMMA	Polymethyl methacrylate
PSA	Prostate-specific antigen
PTV	Planning target volume
ROI	Region of interest
SE	Spin-echo
S_k	Air kerma strength
SNR	Signal-noise ratio
T1	MRI T1 relaxation time
T2W	T2-weighted MRI
TE	Echo time
TG-137	AAPM Task Group No. 137 Report
TG-186	AAPM Task Group No. 186 Report
TG-43U1	AAPM Task Group No. 43 Report - Update 1
TLD	Thermoluminescent dosimeter
TR	Repetition time
TPS	Treatment planning system
TRAK	Total reference air kerma
TRUS	Trans-rectal ultrasound
UF	Ultra-focal focal therapy treatment plan
V100	Percentage of the volume that receives 100% dose
V150	Percentage of the volume that receives 150% dose
V200	Percentage of the volume that receives 200% dose
v_e	Fractional volume of the EES
VMAT	Volumetric modulated arc therapy
WG	Whole-gland focal therapy treatment plan

1 Introduction

1.1 Research project overview

Brachytherapy is an established treatment option for prostate cancer (1), either as a stand alone or in combination with external beam radiotherapy and/or hormone therapy. Brachytherapy uses radioactive sources that are implanted into the prostate using needles inserted through the perineum. The sources are permanently implanted for low dose rate (LDR) treatments using iodine-125 (^{125}I) or palladium-103 (^{103}Pd) seeds. Temporary high dose rate (HDR) prostate brachytherapy treatments are delivered using an afterloader device driving a single iridium-192 (^{192}Ir) source through catheters inserted into the prostate. Brachytherapy treatments have been shown to have comparable results to other radical treatments such as prostatectomy and external beam radiotherapy in terms of tumour control and survival (2).

This research investigates whether advanced dose calculation methods and imaging techniques can improve routine clinical treatment planning of prostate brachytherapy, as follows.

- Advanced dose calculations using Monte Carlo (MC) simulation are applied to clinical prostate brachytherapy treatment plans to investigate whether more accurate knowledge of clinical dose distributions can be applied to improve the effectiveness of patient treatments.
- MC simulations are used to assess the impact of simplifying assumptions made by the TG-43U1 (3) dose calculation algorithm used in routine clinical dose calculations. Effects are compared for several brachytherapy sources. Simulation results are verified using experimental phantom measurements.
- Multi-parametric MRI (mp-MRI) imaging techniques are investigated as a means to define tumour volumes for targeted treatments.

- Dosimetry of targeted treatments that escalate dose to tumour within the prostate, or that treat a sub-volume of the prostate incorporating the tumour, are compared to standard treatments that prescribe the same dose level to the whole prostate gland.

The remainder of this chapter explores the background to prostate cancer treatments and describes the brachytherapy techniques that are investigated in this study. The technical background to the study is explained, including TG-43U1 (3), advanced dose calculations and mp-MRI techniques. Finally a detailed overview of the objectives and work included in the study is presented.

1.2 Prostate cancer overview

Prostate cancer is the most common cancer in men in the UK (1) with 41,736 new cases and 10,793 deaths in the UK in 2011 (4). Incidence increases with age: cases in men younger than 45 are rare and post-mortem studies have shown malignancies are present in the majority of men over 80 years old. The overall incidence of prostate cancer in the UK is rising due to an ageing population and increased use of screening. The latest UK survival data (from 2005-2009) shows relative survival (survival of prostate cancer patients relative to the general population) across all age groups of 93.5% 1 year after diagnosis and 81.4% 5 years after diagnosis (5). Prostate cancer can be a slow progressing disease so patients surviving 5 years are not considered cured and survival rates continue to fall beyond 5 years. Survival is strongly linked to the stage of disease at diagnosis: five year relative survival recorded in 1999-2002 was 90% for patients with disease confined to the prostate and only 30% for patients with metastatic disease (5). Survival rates are improving which may be due to increased use of screening, leading to earlier diagnosis, as well as improvements to treatments.

Men with prostate cancer may present with urinary symptoms but many are asymptomatic with investigations carried out only after an abnormal result

in a prostate-specific antigen (PSA) test and/or digital rectal examination (1). PSA blood tests measure levels of prostate-related protein in circulation. PSA levels are often raised in prostate cancer but may also be high due to benign prostate conditions. The UK advises against routine PSA screening because of the sub-optimal sensitivity and specificity of this test. Despite this, unofficial 'screening' with the PSA test has contributed to an increase in the number of prostate cancer cases that are diagnosed at an early stage (1). If the possibility of prostate cancer is raised, patients are investigated using ultrasound guided prostate biopsies to obtain histology and grade the aggressiveness of any cancer present. Almost all prostate cancers found in adults are adenocarcinomas, and are generally multi-focal and heterogeneous (6). The Gleason score is used to grade prostate adenocarcinomas with the score ranging from 1 (well differentiated, resembling normal prostate tissue) to 5 (poorly differentiated, hardly recognizable as glandular tissue). The scores for the two most common appearances are combined to give an overall score, for example 6 (3+3), Gleason scores of 6, 7 and 8-10 are defined as low, intermediate and high grade respectively. Higher Gleason score has been shown to correlate with poorer survival outcomes (6). Following a positive biopsy, MRI or CT scans and nuclear medicine bone scans are used to determine the extent of the primary tumour, and look for evidence of nodal or distant spread.

A small proportion of men (12% in UK population (1)) will present with disease that has spread outside the pelvis and in this situation hormone manipulation to suppress testosterone and control the prostate cancer is the mainstay of treatment. A higher proportion (25%) will present with locally advanced disease where the cancer has breached the prostate capsule (T3a), grown into the seminal vesicles (T3b) or spread to local lymph glands (N1). Treatment again is aimed at controlling cancer and involves long-term hormones combined with radiotherapy treatments. The majority of patients present with localised prostate cancer and are classified as low, intermediate and high risk according to their PSA level, Gleason score and tumour stage. In these men treatments are aimed at curing the cancer and in some with low

risk disease a policy of observation (active surveillance) is preferred as these cancers often take many years to progress and the individual patient may be more likely to die with rather than from their disease. Table 1 summarises the definitions of prostate cancer tumour stages and classifications.

Radical treatments aiming at curing prostate cancer may have permanent side effects impacting sexual, bowel and urinary function. For this reason the 2014 UK guidelines recommend active surveillance should be offered to men with low risk prostate cancer and to men with intermediate risk prostate cancer who do not want immediate radical treatment (1). However patients suitable for active surveillance may still prefer radical treatment to avoid anxiousness caused by the knowledge of carrying untreated cancer (7).

Following treatment, outcomes are assessed by serial PSA blood test measurements. PSA is expected to drop to a low level, referred to as biochemical control. Small rises in PSA, so called ‘PSA bounce’, can be seen particularly in the first 3 years after treatment. Consistent rises in PSA may represent cancer recurrence and require investigation with repeat imaging. As survival rates for localised prostate cancer are high, prostate cancer treatments are often compared in terms of biochemical control which is assumed to be a surrogate for an actual survival benefit. It is also an early indicator of recurrence as biochemical relapse can precede clinical progression by three to five years. The toxicities of treatments are assessed using standardized tests of urinary and sexual function.

The majority of radical treatments are prostatectomy or radiotherapy, with high-intensity focused ultrasound and cryotherapy also offered as radical treatments in clinical trials. There is insufficient evidence from randomised controlled trials to establish whether any particular treatment is superior in terms of patient outcomes (8). Therefore choice of treatment is often determined by patient preferences, particularly in terms of the relative likelihood of treatment induced side-effects. All prostate brachytherapy treatments result in urethritis although in the majority of patients this will resolve after 6 weeks (for HDR) or 9 months (for LDR). LDR seed implant

brachytherapy has been shown to have the lowest rate of erectile dysfunction of all prostate cancer treatment modalities (6).

Table 1 Prostate cancer tumour stage and risk classification (1)

Tumour stage	**Description**
T1	Tumour too small to be seen on scans or felt during examination
T2	Tumour is completely inside the prostate capsule (T2a-c depending on how much of prostate contains tumour)
T3a	Tumour has broken through the prostate capsule
T3b	Tumour has invaded the seminal vesicles
T4	Tumour has spread to other organs close to the prostate
Classification	**Criteria**
Low risk	PSA < 10ng ml^{-1} Gleason score <= 6 T1-T2a
Intermediate risk	At least one of: PSA 10-20ng ml^{-1} Gleason score = 7 T2b
High risk	At least one of: PSA > 20ng ml^{-1} Gleason score = 8-10 T2c, T3 or T4

A systematic review of radical prostate cancer treatments comparing prostatectomy, external beam radiotherapy and brachytherapy by Grimm *et al*. (9) concluded that in terms of biochemical control, brachytherapy achieves superior outcomes for low risk patients and equivalent outcomes to combined external beam and brachytherapy for intermediate risk patients. For high risk patients external beam and brachytherapy combination treatments were found to be superior any of the three treatments alone.

There are many published studies of prostate brachytherapy clinical follow-up data showing that the majority of patients remain biochemical relapse free even 10 or more years after treatment. However biochemical relapse occurs more often in higher risk patients. Typical results from our own centre analysing 1298 patients treated with LDR seed implants and median follow up of 10 years showed that the percentage of patients free of biochemical failure was 72%, 74% and 58% in low risk, intermediate risk and high risk patients respectively (10). Results for HDR brachytherapy combined with external beam show very good results with many centres reporting biochemical relapse free survival greater than 80% even in high risk patients (6). However comparison with LDR seed implant results is difficult as follow up duration is much lower for HDR brachytherapy, due to it being a relatively recently developed technique.

1.3 Radiotherapy for prostate cancer

Radiotherapy for prostate cancer may be external beam radiotherapy, brachytherapy or a combination of the two. Tumour control in prostate radiotherapy has been shown to improve when increased dose is delivered to the prostate (11). Brachytherapy treatments are well suited for dose escalation as the radiation is delivered by sources placed inside the prostate. Radiation dose falls off rapidly with distance from a brachytherapy source – this means that a highly conformal radiation dose can be delivered to the prostate whilst minimizing toxicity to surrounding normal tissues such as the bladder or rectum. However this high conformality also limits the volume that can be treated, so that brachytherapy on its own is not suitable for patients whose cancer has spread extensively beyond the prostate capsule.

External beam radiotherapy without brachytherapy is widely used for all patients suitable for radical treatment. Reasons for using external beam rather than brachytherapy include patient preference, patients being unfit for surgery, large prostate glands, tumour extending significantly beyond the prostate capsule or patients having existing urinary symptoms. Standard UK

external beam treatment delivers at least 74Gy to the prostate using a schedule of the order of 2 Gy per fraction delivering treatment over 7 to 8 weeks treating Mondays to Fridays.

LDR brachytherapy treatment using permanent ^{125}I seed implants is offered as monotherapy for patients with low and selected intermediate risk localised prostate cancer (12-14) and whose prostate volume is <60 cm^3. Larger prostates may still be treated with seed implants after three months of hormone therapy to reduce the size of the gland.

HDR brachytherapy in combination with external beam therapy is suitable for patients with intermediate and high risk localised disease or those with locally advanced disease (15). Earlier guidelines suggested a limit on prostate volume of <60 cm^3 for HDR treatments but a recent update has removed this restriction (15). Nonetheless difficulties in access to the prostate due to pubic arch interference can make implantation technically difficult for larger prostates. Neo-adjuvant hormone therapy is recommended for intermediate and high risk patients in addition to radiotherapy (1) as it has been shown to improve cancer control rates, and this will generally reduce the prostate volume. There is growing evidence to support HDR brachytherapy as monotherapy, even using single fraction treatments (16).

There may be a radiobiological advantage in delivering a small number of very high dose treatments for prostate cancer (17) as it appears that prostate cancer has a low radiation fractionation sensitivity and more cancer cell killing occurs with a small number of high dose per fraction treatments rather than a large number of lower dose treatments as traditionally used in external beam radiotherapy.

Pathological studies looking at the distribution of cancer in surgical specimens demonstrate that prostate cancer is a multi-focal disease. Conventional therapies address this by treating the whole gland. There is

evidence that a dominant intra-prostatic lesion (DIL) within the prostate may drive the aggressiveness of the disease and be the focus of post-treatment recurrence (18). Pathological studies suggest that the DIL drives prostate cancer progression whereas it may be safe to leave satellite lesions with lower Gleason grade untreated (19). Studies of patients in whom prostate cancer has recurred after treatment have shown that the DIL is the most common site of recurrence (20, 21). This has lead to interest in targeting the DIL using either focal boost or focal treatments.

Focal boost treatments

In higher risk patients there is interest in escalating the dose delivered to the DIL while treating the whole gland. Treatments that escalate dose to the DIL in an attempt to increase tumour control have been investigated using intensity modulated radiotherapy (IMRT), stereotactic radiotherapy and both LDR and HDR brachytherapy but there is no consensus on the best approach to achieve these treatments (18). For focal boost dose escalation with whole gland treatment, very large numbers of patients would be required to achieve a statistically significant improvement in actual or biochemical relapse free survival compared to standard whole gland treatment. Therefore published studies have focused on demonstrating that focal boost dose escalation can be achieved without increasing treatment related toxicities. A recent systematic review of these studies covering external beam and brachytherapy treatments concluded that toxicity rates were low but the boost doses achieved were modest, and there was too much difference between the methodologies used in individual studies to allow more robust conclusions to be drawn (18). Because of this relative lack of evidence, the focal boost treatments described in this work were introduced as a pilot study. Meanwhile a prospective randomized trial is also underway (22).

Focal therapy treatments

In lower risk patients, there is increasing interest in focal treatments, where only the region containing the DIL is treated, as a potential way of reducing

overall treatment related toxicity (23-26). These treatments aim to achieve equivalent levels of tumour control to conventional whole gland treatments but with reduced side effects of urinary, bowel and sexual function. Focal therapy using LDR and HDR brachytherapy techniques is at an early stage but there have been some pilot studies and initial investigations (24, 27). Focal therapy is seen as a treatment option for patients who may be suitable for active surveillance yet prefer to receive radical treatment (25). Potential disadvantages of focal treatments are that PSA can't be used to monitor response to treatment (26) because some of the prostate gland remains untreated, and the complexities of planning subsequent treatments if the initial treatment fails. There is only one study reporting long term results for focal therapy, and it concluded that after 5.1 years median follow up, for low risk patients it was too early to say whether cancer control rates were equivalent to whole gland treatments, but that for intermediate risk patients the focal treatment was not suitable. In that study the treatment targeted the entire peripheral zone of the prostate (28). Current ongoing studies mentioned above are investigating a different focal treatment technique treating either a hemi-gland or the DIL alone – techniques for which there is currently no long term evidence. In this study focal therapy is investigated in a retrospective planning study to evaluate dosimetry and uncertainties of potential focal therapy treatment approaches.

1.4 Prostate brachytherapy techniques

1.4.1 Permanent ^{125}I seed implants

^{125}I is an ideal radionuclide for permanent implantation as the low energy of its emissions (mean energy 28 keV) minimizes the radiation hazard to others. Prostate cancer treatments using implanted ^{125}I seeds have been under development since the 1960s (29). Initially small numbers of high activity seeds were implanted using an open retropubic approach. Two major developments that improved the quality of seed implants were the introduction of trans-rectal ultrasound (TRUS) guided transperineal implantation in the later 1960s, which made the procedure much less invasive and provided image guidance, and the use of larger numbers of low

activity seeds by a group in Seattle in the 1980s, which substantially improved the dosimetry of the technique (29). The Seattle technique is essentially the approach now used around the world and in Leeds, the first and remaining one of the largest practices in the UK, nearly 3000 patients have been implanted since 1995 (10).

Treatments are planned on intra-operative 2-D TRUS acquired with the patient under anaesthetic in the lithotomy position. A 0.5 cm spaced grid is overlaid on the TRUS images – the grid points correspond to the positions of holes in the template through which needles are inserted. The prostate gland is delineated on the TRUS images and the treatment is planned by determining the seed positions required to deliver the prescribed dose of 145 Gy to the prostate. The seeds are inserted using needles placed through the template and perineum, using TRUS guidance to verify the needle grid position and depth. This procedure is often delivered in a single procedure. However the TRUS volume study for treatment planning and the seed implantation may be in separate sessions – for example if there are doubts over whether an implant will be technically feasible. Figure 1 illustrates the treatment set up. The procedure is described in more detail in 0.

In prostate seed implant brachytherapy, the actual dose delivered can be different from the planned treatment, because seeds may not be positioned exactly as planned, or because of seed migration or the effects of prostate oedema. Therefore, as a quality control check, post-implant dosimetry is carried out using CT and/or MRI to assess the actual dose received for each patient (30).

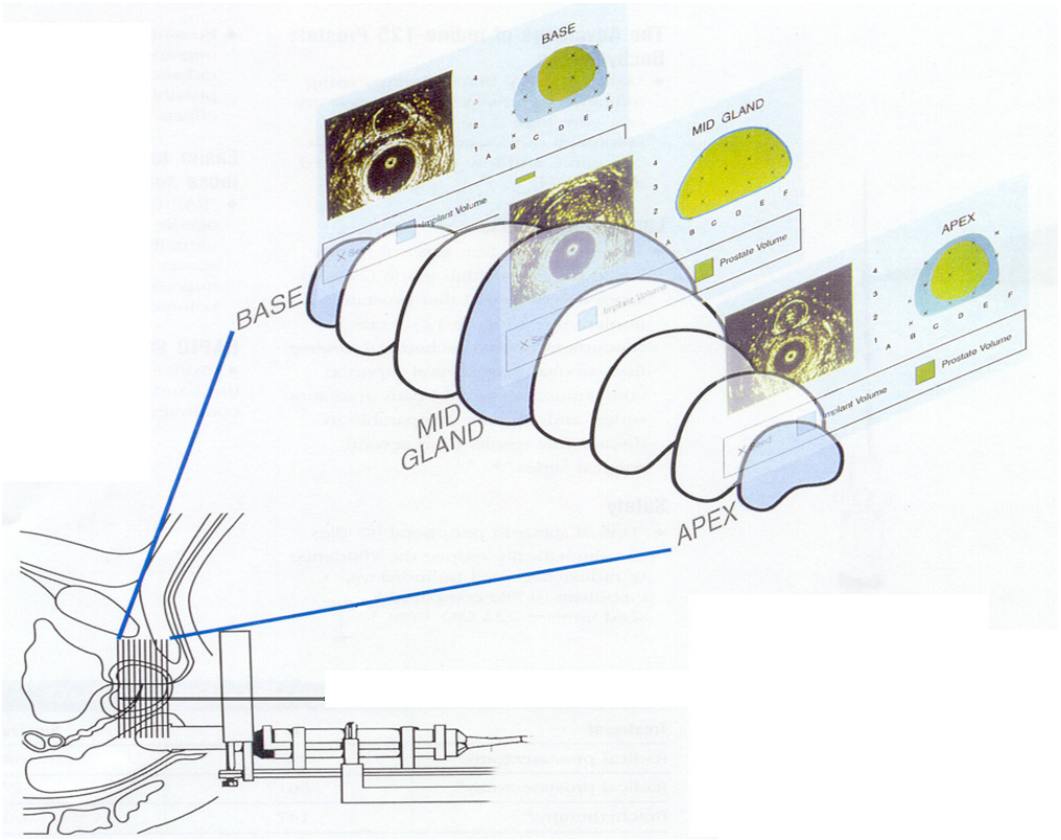

Figure 1 Trans-rectal ultrasound guided prostate brachytherapy (reproduced with permission of Jane Garrud, Medical Illustrations Services, LTH NHS Trust)

Studies have shown a correlation between the dose assessed in post-implant scans and the probability of achieving biochemical control (31, 32). LDR prostate brachytherapy has been demonstrated to have excellent patient outcomes, with many centres having patient data stretching back 10-20 years. A recent systematic review by Rodrigues et al (33) found that permanent seed implant brachytherapy is at least as effective as external beam radiotherapy or radical prostatectomy. Seed implant brachytherapy was associated with less urinary incontinence and sexual impotency but more urinary irritation and rectal morbidity than radical prostatectomy, in the 6 months to 3 years after treatment. Seed implant brachytherapy was also associated with less risk of impotency and rectal morbidity than external beam radiotherapy in the 3 years after treatment.

1.4.2 Temporary high dose rate ^{192}Ir treatments

Temporary transperineal implants for prostate cancer have been applied since the mid 1980's (34). The technique has some similarities to that presented for LDR permanent implants above – TRUS is used to guide implantation of steel or plastic catheters through a template grid and the perineum with the patient under anaesthetic in the lithotomy position. The treatment may be planned using TRUS, MRI or CT (14, 15). Treatment is delivered by a single ^{192}Ir source driven by a remote afterloader to different positions (dwell positions) within the catheters. The time that the source spends in each dwell position (dwell time) is optimised to achieve dose objectives. Unlike LDR seed implant brachytherapy, there is not yet a single well established prescription dose, or fractionation schedule. Multiple fraction treatments may use a single implant to deliver all fractions or a separate implant for each fraction. Given the evidence of radiobiological advantage of high doses per fraction in prostate cancer, discussed in 1.3, there has been a move to single fraction treatments and in Leeds patients receive 15Gy in a single fraction followed by external beam therapy delivering a further 37.5 Gy in 15 fractions over three weeks to the prostate and seminal vesicles(35). Since July 2007 over 300 patients have received this treatment in our centre (the first 50 patients used a different HDR fractionation schedule of 2 x 8.5 Gy fractions). Many patients receiving the combined HDR prostate brachytherapy and external beam treatment are also prescribed neo-adjuvant and adjuvant hormone therapy as they fall into higher risk groups.

A recent systematic review of HDR brachytherapy in combination with external beam therapy demonstrated excellent patient outcomes but did not find sufficient multi-centre or trial data to compare the technique to other prostate cancer treatments (36). A UK randomized controlled trial comparing HDR brachytherapy combined with external beam to external beam alone found a statistically significant improvement in biochemical control in patients receiving the combined treatment (37). HDR brachytherapy has potential advantages in that there is less risk of

geographical miss compared to external beam radiotherapy and less risk of source position errors and no risk of source migration compared to LDR permanent implants (2). A recent review of brachytherapy uncertainties estimated the total uncertainty (k=1) in key dosimetric parameters of 5% for TRUS planned HDR prostate brachytherapy compared to 11% for LDR permanent seed implants (38). Use of a remote afterloader means that there is no need for staff to handle sources and no radioactive sources remain in the patient after the procedure.

1.5 Brachytherapy dosimetry

1.5.1 TG-43U1

The TG-43U1 (3) algorithm is routinely used for dose calculations in LDR and HDR prostate brachytherapy treatments. In TG-43U1 the dose due to a single source is calculated using the 2D formalism shown in Equation 1. For prostate brachytherapy implants with multiple sources, dose at a point is calculated using a superposition of the doses due to all sources in the implant. Brachytherapy sources are designed with cylindrical symmetry so this method allows a 3D dose distribution to be derived. The values of the terms and functions in the TG-43U1 dose formalism for a given source type are derived from single source dose distributions, either from phantom measurements or from MC simulation. As independent measurements of source dose distributions may vary due to experimental or source construction uncertainties, TG-43U1 also defines consensus datasets for commonly used sources.

$$D(r,\theta) = S_k \Lambda \times \left[\frac{G_L(r,\theta)}{G_L(r_0,\theta_0)} \right] \times g_L(r) \times F(r,\theta)$$

Equation 1 TG-43U1 dose formalism

Figure 2 shows the dose calculation co-ordinate system and defines r, θ, r_0 and θ_0.

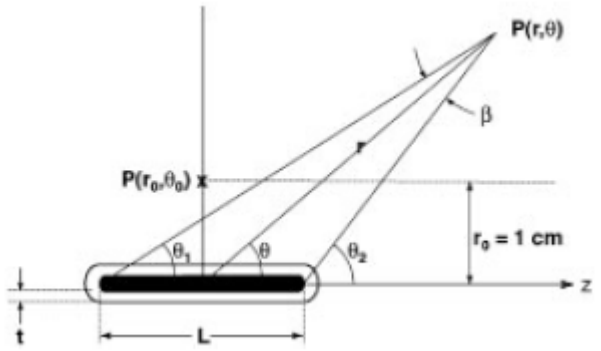

Figure 2 TG-43U1 dose calculation co-ordinate system (from TG-43U1 (3))

The terms in Equation 1 are as follows:

S_k - air kerma strength, is the air kerma rate (AKR) at a calibration distance d measured along the transverse bisector of the source, multiplied by the square of d. It has units U ($Gyh^{-1}m^2$). S_k is usually specified at reference distance of 1m, where the value will be the same as AKR.

Λ- dose rate constant, the dose rate to a water phantom at $r_{0,}$ θ_0 for unit S_k.

$G_L(r,\theta)$ - geometry function, defines the fall off of dose with distance from the source based on the spatial distribution of the source radioactivity approximated to a line source.

$g_L(r)$ - radial dose function, which defines the fall off of dose due to attenuation and scatter along the source transverse axis.

$F(r,\theta)$ - anisotropy function, describes the variation in dose with polar angle due to attenuation and scatter in the source and the source encapsulation.

1.5.2 Advanced dose calculations in brachytherapy

TG-43U1 (3) dose calculations make some simplifying assumptions, as follows (39):

- TG-43U1 calculates dose due to multiple sources using a superposition of single source dose distributions and therefore ignores any attenuation and scatter between sources.
- Dose is calculated in water. This ignores any difference in density and composition between tissue and water, tissue heterogeneities, and attenuation and scatter due to applicators used for treatment delivery.

- Dose distributions are measured or calculated in a phantom assumed large enough to provide full scatter. However depending on the proximity of the treatment site to the patient surface this assumption may be incorrect.

Approaches to addressing these potential causes of dosimetric errors are summarised in report TG-186(40), which also makes recommendations for implementing advanced dose calculations, referred to as model-based dose calculation algorithms (MBDCAs). Three MBDCA methods are proposed: collapsed-cone superposition/convolution, deterministic solutions to the linear Boltzmann transport equation and MC simulation. The first two methods are commercially available for high energy sources in brachytherapy treatment planning systems (TPSs): a collapsed cone algorithm is implemented in Oncentra® Brachy (Elekta AB, Stockholm, Sweden) (40) and a deterministic grid-based Boltzmann equation solver is implemented in the Acuros® system from Varian Medical Systems (Palo Alto, CA) (40). However there are no commercially available systems that implement these MBDCA methods for low energy sources. MC simulation was therefore selected for this study for the following reasons:

- MC simulation is the method most widely used in the literature for brachytherapy dosimetry and is considered the current state of the art computational dosimetry method in brachytherapy (40).
- There are freely available MC simulation packages that are benchmarked for brachytherapy dose calculations, similar packages are not available for the collapsed cone or linear Boltzmann solutions.
- A common MC simulation framework can be implemented for low and high energy brachytherapy dosimetry.

MC simulation uses random number sampling and probability distribution functions to model the processes associated with radiation emission and transport (41). This includes modeling source emissions, transport of particles and interactions in source components, encapsulation and

patient/phantom material, and estimating the energy deposited in defined "tally cells" to give a measure of dose. Simulation results are statistical in nature and random uncertainties reduce as the number of MC simulation histories is increased. For this reason MC simulation is not suitable for real-time brachytherapy treatment planning. The accuracy of MC simulation results also depends on the accuracy of the simulation input model and the implementation of the MC simulation code.

1.5.3 Experimental brachytherapy dosimetry

Experimental brachytherapy dosimeters need to be small due to high dose gradients and very sensitive due to low dose rates (for a clinical LDR implant the maximum initial urethral dose rates is around $10cGyh^{-1}$) (41). Energy dependent detector response can also be a problem (41).

Possible dosimeters include thermo-luminescent diodes (TLDs), film, metal-oxide-semiconductor field-effect transistors (MOSFETs), scintillation detectors and polymer gels.

TLDs

TLDs use crystals (typically LiF doped with Mg and Ti (known as TLD-100 (41)) with lattice defects such that electrons are raised into a metastable energy state between valence and conductivity bands by ionising radiation. When the crystal is heated the trapped electrons escape, releasing photons, and the light output is measured to produce a glow curve of light intensity versus temperature, with the area under the glow curve being related to dose (41). The small size and sensitivity of TLDs (doses down to cGy can be measured) means they are considered the standard method for brachytherapy dosimetry (41). However TLDs do not give instant readout and require a substantial amount of processing including reproducible annealing and readout cycles (41).

Before use TLDs require individual calibration of each chip, repeat measurement stability checks, and also a response linearity check if the dose is not in the region known to be linear (1-100cGy for TLD-100 (42)).

Additional corrections to experimental measurements are required to correct for the difference in response at measurement energy compared to calibration energy (this can be simulated using Monte Carlo methods and is ~1.4 for ^{125}I relative to Co-60 (43)).

Film

Gafchromic EBT® film (International Specialty Products, Wayne, NJ, US) is a self-developing radiochromic film commonly used in radiation dosimetry. Radiation causes polymerisation of the active layer, leading to changes in the absorption spectrum that can be assessed visually and quantified using a scanner. GafChromic films measure 2D dose distributions and have superior resolution compared to TLDs (44). GafChromic EBT® has a linear dose response over a wide range and low energy dependence but require larger doses compared to TLDs (41). GafChromic EBT2® can be used to measure dose in the cGy range (45). There are relatively few studies on the use of GafChromic EBT for low dose rate brachytherapy dosimetry.

MOSFETs

MOSFET dosimeters measure dose from a permanent shift in threshold voltage across the MOSFET due to radiation induced increase in trapped holes in a silicon oxide layer in a specially designed field effect transistor. MOSFET dosimeters have a smaller sensitive volume than the 1mm^3 TLD chips that are typically used in brachytherapy dosimetry and have similar sensitivity to TLDs (41). MOSFET dosimeters can be made waterproof and used for in-vivo dosimetry of brachytherapy treatments (46-49). Real time dosimetry is possible.

MOSFET response is energy dependent so calibration must be at the measurement energy. Individual calibration of each MOSFET detector is required (47), MOSFET response is linear with dose (49), is anisotropic (47, 49) and can vary as the threshold voltage increases (with accumulated dose) (50), requiring frequent re-calibration. MOSFET measurement uncertainty varies with dose rate and total dose (50). The total accumulated dose that a

MOSFET can measure over its lifetime is fixed, so there are ongoing costs associated with a MOSFET dosimetry system.

Scintillation detectors

Scintillation detectors use a miniature glass cylinder coupled to a photomultiplier using fiber optic cable. They have good dose linearity and reproducibility and no energy dependence above 100keV. They do suffer from stem effects (light created in the optical fiber) but it is possible to correct for this (51). Typical size of the glass detector is 1x3mm. There are no commercial systems for brachytherapy scintillation detection at the time of this study and there are no published studies of low energy brachytherapy dosimetry using these systems.

Polymer gels

Polymer gels consist of an aqueous solution of vinyl monomers with a gelling agent. Ionising radiation triggers radical polymerisation increasing the opacity of the gel. The same process changes the tranverse relaxation (T2) properties of the gel, with a linear relationship between the transverse relaxation rate (R2=1/T2) and dose, so that an MRI acquired T2 map of the gel post radiation exposure gives 3D information on the spatial distribution of dose (41). Polymer gels effectively form phantom and detector in one and as a phantom material are 85% water so corrections to obtain dose to water are small compared to other phantom materials (~3% for I125 energies and negligible for Ir192 energies (52). Dose resolution of $0.7mm^3$ is achievable, with volume averaging errors <2% (41).

The main disadvantage of gels for ^{125}I dosimetry is that doses ~Gy are required which can lead to exposure times of weeks for single source measurements (53). Other disadvantages are toxicity of many gels and the need for access to an MRI scanner to analyse results (41). Gel response is energy dependent so calibration requires a source with the same energy distribution as the experimental source, and calibration and experimental gel must be handled simultaneously and identically in terms of production,

irradiation, storage and MR scanning (54). Gels must be tightly enclosed to avoid oxygen diffusion into the gel during long irradiation exposures (52) which creates a problem with placing the radioactive sources into the gel.

Choice of dosimeter for this study

From the dosimeters discussed above, scintillation detectors were disregarded due to lack of availability. Polymer gels and film were considered not suitable due to the low dose rates in LDR seed implant measurements and relative lack of existing published data using these dosimeters for low energy brachytherapy sources. MOSFETs and TLDs each have pros and cons for use in this study and could be considered equally suitable. MOSFETs have the advantage over TLDs of providing instant readout so would be more suitable for in-vivo dosimetry. As there is interest in pursuing in-vivo dosimetry in the future in our centre, it was desired to gain experience of MOSFET use and so MOSFETs were chosen as the dosimeter for this study.

1.6 Prostate multi-parametric MRI

Treatments that target dominant intra-prostatic lesion (DIL) sub-volumes within the prostate require advanced imaging techniques for DIL delineation. Conventional T2- weighted (T2W) MRI is a sensitive tool for locating areas of tumour tissue within the prostate but not very specific in terms of distinguishing tumour from benign growths (55). Using mp-MRI techniques such as magnetic resonance spectroscopic imaging (MRSI), dynamic contrast enhanced MRI (DCE-MRI) and diffusion weighted imaging (DWI) in combination with T2W MRI**,** improves sensitivity and specificity of prostate cancer detection (56) (57) (58) (59).

1.6.1 Diffusion weighted imaging

In DWI large symmetric magnetic field gradients are applied either side of the 180° refocusing pulse in a T2W spin-echo (SE) echo planar imaging (EPI) sequence. The additional gradients reduce signal from moving molecules. Loss of signal depends on the amount of diffusion (or other incoherent motion) and the strength of the diffusion weighting gradients

(referred to as the b-value). For prostate studies b-values are generally in the range 0-1000 s/mm^2. Signal decay is roughly exponential with increasing b-value and decay constant referred to as the apparent diffusion coefficient (ADC). Tumour tissue generally has more restricted diffusion and so a lower ADC value compared to normal tissue, due to tumour having higher cellular density (56) (60). DWI can differentiate between tumour and normal tissue in both the central gland and peripheral zone (61-65) and more aggressive, higher risk or higher Gleason score cancer is associated with lower ADC values (64, 66-68).

DWI techniques suffer from distortions generated by the EPI sequence, particularly if there are susceptibility issues for example caused by air in the rectum (61). In DWI signal intensity decreases and noise increases with increasing b-value. This causes underestimation of ADC values; underestimation increases with increasing ADC, increasing b value and lower signal-noise ratio (SNR) (69). Incoherent motion also contributes to the loss of signal particularly at low b-values and will cause ADC values to be overestimated (70) unless a bi-exponential model of signal loss is used or low b-values are excluded (71).

1.6.2 Dynamic Contrast Enhanced MRI

In DCE-MRI a T1 weighted sequence is used to repeatedly image a volume and track changes in signal intensity caused by an intravenous contrast agent over time. The contrast agent acts to reduce T1 leading to signal enhancement. Prostate cancers induce angiogenesis so will take up contrast agent more avidly than normal prostate tissue (72). The concentration of contrast agent - and hence also the change in signal intensity - depend on blood perfusion, the permeability of vessel walls, and diffusion within extravascular space (73).

The variation in signal over time in the dynamic series is used to characterise tissue. This can be done simply by visually reviewing the change in image intensity over the time course of the acquisition however this is subjective and labour intensive. Semi-quantitative and quantitative

methods of analysis have been developed to get around this and can be applied to regions of interest (ROIs) or on a voxel-by-voxel basis. For each ROI or voxel, a curve of the signal intensity over time is generated. Semi-quantitative analysis measures the time of onset of enhancement (increase in signal intensity), gradient of enhancement slope (wash-in rate), maximum enhancement, wash-out rate and the area under the enhancement curve (74). Semi-quantitative analysis has the advantage of being relatively straightforward but the disadvantage that results for different tissue types can't be directly compared, results may be influenced by scanner settings, and do not directly relate to tissue physiology (74).

In quantitative analysis of DCE-MRI data the signal intensity/time curve is fitted to a model to provide estimates of physiological parameters. Model fitting requires an arterial input function (AIF) which can be based on population data but modelling results are more accurate if the AIF is measured for each patient by including in the field of view an artery of reasonable size as close as possible to the tissue of interest (75).

The extended Tofts model (76) represents tissue as two compartments: the intravascular space and the extravascular extracellular space (EES) and fits the dynamic data to the formula shown in Equation 2. Here C(t) is the tissue contrast agent concentration and $C_a(t)$ is the arterial contrast agent concentration. Contrast agent concentrations are determined from signal intensity using either assumed or measured tissue T1 values. The extended Tofts model assumes highly perfused tissue with a small blood volume.

$$C(t) = v_p C_a(t) + K^{trans} e^{-tkep} * C_a(t)$$

Equation 2 Extended Tofts model (76)

The extended Tofts model produces values for K^{trans}, the volume transfer constant that describes the rate of transfer from the intravascular compartment to the EES, v_e, the fractional volume of the EES, v_p the

fractional volume of plasma, and k_{ep}, the rate constant between the EES and blood plasma ($k_{ep} = K^{trans}/ v_e$) (76).

Quantitative DCE-MRI parameters, particularly K^{trans}, can be used to distinguish tumour and central gland tissue in the peripheral zone of the prostate (74) (77) (78, 79). Higher grade tumours have higher enhancement gradients and wash-out rates whereas smaller low grade tumours may not show abnormal enhancement (80). Abnormal enhancement is also seen in benign prostatic hyperplasia making it hard to distinguish from tumour in central gland tissue (80). Accurate characterization of tissue requires a low temporal resolution in DCE-MRI acquisitions but there is a trade-off between temporal resolution and the spatial resolution and field of view that can be achieved (73).

K^{trans} incorporates two different physiological parameters, the blood plasma flow per unit volume and the permeability of blood vessel walls/surface area of perfusing vessels (permeability surface area product) (81). Flow tends to dominate in malignant tissue with chaotic, heterogeneous vascular structure consisting of highly permeable vessels, whereas permeability dominates in fibrotic/atrophied regions (73). More accurate characterisation of tissue may be achieved if these two parameters are estimated separately (82), however this requires more complex models that may be more difficult to apply on a voxel basis. For radiotherapy treatment planning voxel-by-voxel fitting is preferable to facilitate tumour delineation. As detailed above, studies have shown the Tofts model to be suitable for distinguishing tumour and normal tissue in the prostate, and so this model was chosen for DCE-MRI analysis in this study.

1.6.3 Magnetic resonance spectroscopic imaging

In proton MRSI of the prostate the ratio of metabolic concentrations of choline plus creatine to citrate is measured through analysis of the MR frequency spectrum on a voxel-by-voxel basis. Choline is associated with increased proliferation and growth and is considered a marker of aggressiveness. Creatine is included because it can’t be separated from the

choline resonance peak. Citrate levels are reduced in cancer cells. Voxels are considered suspicious for cancer when the metabolic ratio is at least 2 standard deviations above the average for normal peripheral zone tissue, and are considered very suspicious when the ratio is more than 3 standard deviations above average (55). MRSI adds specificity to prostate cancer diagnosis and can significantly improve tumour localisation within the peripheral zone (72). MRSI parameters have been shown to correlate with tumour aggressiveness assessed using histopathology (83). Problems with MRSI are low SNR and metabolic peak separation (which can be improved using a 3T magnet) (80), magnetic field inhomogeneities, large voxel sizes and the fact that MRSI data is time consuming to acquire.

1.6.4 Other MRI issues

Choice of coils

Prostate MRI may be acquired using an endorectal coil or with phased-array pelvic coils. Histological studies have shown MRIs acquired using endorectal coils have better image quality, SNR and staging accuracy (84) (85). However images acquired with an endorectal coil suffer more from distortion and susceptibility artefacts which may make them less suitable as a basis for radiotherapy treatment planning which relies on high geometric accuracy. Phased-array pelvic coils are therefore acceptable for tumour localization in radiotherapy and brachytherapy applications (86).

Effects of hormone therapy

Hormone therapy has a number of physical and functional effects on the prostate gland. Hormone therapy reduces prostate volume, T2W signal intensity of normal tissue, and also reduces tumour volume and permeability(74). The volume of the peripheral zone is reduced more than the transition zone (87). Hormone therapy also reduces the contrast between normal and cancerous peripheral zone tissue in T2W, DWI, MRSI and DCE-MRI (88) (89) (90, 91). However it is possible to successfully identify prostate tumour using mp-MRI after hormone therapy (92).

Biopsy haemorrhage

Biopsy haemorrhage can be confused with tumour in mp-MRI. However it can be distinguished using T1 weighted images where it is high intensity (55). Ideally mp-MRI imaging should be carried out at least 6-8 weeks post biopsy(72)

1.6.5 Use of mp-MRI for tumour delineation

Studies assessing the validity of mp-MRI for prostate cancer detection generally focus on the sensitivity and specificity of the technique for tumour detection in cancer staging and benchmark the techniques by comparison to histo-pathological data. Correlation to histo-pathology is not possible for benchmarking mp-MRI for radiotherapy treatment planning as the prostate remains intact. Targeted biopsies could be performed to validate mp-MRI results but would be much less precise than histo-pathological data and have associated co-morbidities. Therefore studies of mp-MRI in radiotherapy treatment planning, including the work described here, assume that results from histo-pathology based studies can be carried across to the radiotherapy treatment planning case even though the underlying patient groups for radiotherapy and radical prostatectomy may not necessarily have the same clinical characteristics.

Several studies have successfully used MRSI to delineate tumour regions in studies of small numbers of prostate brachytherapy patients (permanent seed implant (93, 94) and HDR (95, 96)). All studies reported that DILs could be successfully identified, and in many cases patients had multiple DILs. The volumes of DILs identified in these studies ranged from 0.5-15cc and were located across all areas of the peripheral zone. Also DCE-MRI in combination with MRSI has been used to define DILs in prostate IMRT patients (97).

A study of automatic prostate segmentation techniques by Ozer et al. (59), analysed three parameters from functional MRI studies: T2 values (from multi echo T2 mapping scans), ADC (from DWI) and k_{ep} (from DCE-MRI) on single slices known to contain tumour from 20 patient's MRI studies.

The results were compared to radical prostatectomy sections. The study found that tumour detection was significantly more accurate when all 3 parameters were used compared to T2 and ADC alone, and that detection using T2 and ADC together was significantly better than either T2 or ADC alone. Franiel et al did a similar study using MRSI in addition, compared to biopsy results and concluded that T2W, DWI and either DCE or MRS was the best combination in terms of sensitiviy and specificity (78, 79).

Use of all three of DWI, DCE-MRI and MRSI would result in an uncomfortably long scan time for the patient. DWI is the simplest to acquire and is the best established technique; DCE-MRI is preferred to MRSI due to faster acquisition and better resolution (particularly important for accurate tumour delineation for treatment planning). For these reasons DWI and DCE-MRI, along with anatomical T2W MRI, were the techniques used in this study.

A single tumour ROI is required for treatment planning and there are often differences in the tumour region that would be delineated from each of the mp-MRI datasets. Groenendaal et al. (58) analysed DWI and DCE-MRI studies from 21 patients with biopsy proven prostate cancer. The area under the ROC curve (AUC) was used to measure consistency between DWI and DCE results. It was found that AUC values could be as high as 0.9 in individual patients but the average was 0.6. The AUC values increased with tumour stage and PSA value. There is very limited published data in this area so it was decided for this study that the safest approach was to include any area that was suspicious for cancer on any one of the mp-MRI datasets in the delineated tumour volume.

1.7 Study overview

The objective of this research is to improve clinical prostate brachytherapy treatments through better understanding of dose distributions from advanced dose calculation algorithms and more accurate targeting of dose to the prostate tumour using advanced imaging techniques.

There is a strong dose-response relationship in prostate radiotherapy (11) and accurate dosimetry is important for understanding this relationship and also for evaluating the impact of treatments on patient's urinary, rectal and sexual function. There also may be a radiobiological advantage of delivering increased doses to the prostate and accurate dosimetry is very important if higher doses are to be delivered safely. The TG-43U1 (3) dose calculation algorithm allows fast calculations for inter-operative treatment planning but ignores effects of source interactions and tissue heterogeneities on patient dose. Advanced dose calculation algorithms can take account of these effects. In this study the impact of source interactions and tissue heterogeneities on TG-43U1 dose distributions is evaluated using MC simulations of clinical brachytherapy implants. Experimental validation of MC simulation results is performed using a purpose built phantom and a MOSFET dosimeter.

The dose-response relationship in prostate radiotherapy can also be exploited by increasing the dose that is delivered but it is not possible to escalate dose to the entire prostate because this would overdose organs at risk (OARs). As discussed in 1.3, DILs can be targeted for dose escalation as these may drive the development of the cancer overall, are a common site of recurrence and tumour control may be increased if increased dose is delivered to areas of known tumour tissue within the prostate (11). In this study two techniques for targeting DILs using mp-MRI are investigated: focal boost treatments where dose to the DIL is escalated with the objective of increasing tumour control probability (98-100) and focal therapy which treats only the sub-volume of the prostate where the DIL is located, with the objective of reducing normal tissue complication probability (25). The

feasibility of these techniques is investigated in terms of DIL delineation using mp-MRI, dosimetry of treatments for LDR and HDR and comparison between MC simulations and TG-43U1 (3) dose calculations.

The objectives of this research are as follows:

- Develop a framework for advanced brachytherapy dose calculations based on MC simulation, for permanent ^{125}I seed implants and ^{192}Ir HDR implants. Validate the framework against published source data and using experimental phantom measurements.
- Investigate inter-seed attenuation and scatter (ISA) and tissue heterogeneity effects for ^{125}I seed implants in terms of the differences from TG-43U1 dose calculations. Using retrospective data, assess the clinical significance of the effects and determine whether it is necessary or possible to allow for these effects in real-time treatment planning.
- Determine whether the ISA effect can be reduced by using a thinner ^{125}I seed model.
- Investigate the feasibility of incorporating mp-MRI into HDR brachytherapy treatment planning for focal dose escalation, using data from a pilot study, initially as a retrospective planning study and then prospectively to deliver focal boost treatments to patients.
- Compare the dosimetric feasibility of treatment planning for focal therapy using ^{125}I seed implants or HDR brachytherapy, based on mp-MRI and template biopsy data from a clinical trial of patients treated with high intensity focused ultrasound (HIFU) focal therapy at University College London. Feasibility is assessed in terms of achievable dosimetry, plan robustness to source position uncertainties and MC simulation results.

The following outlines in more detail the work undertaken and describes what is included in each section of this thesis.

Section 2 – Preliminary validation work

In the first stage of the study the MC simulation and dose analysis framework is validated. The brachytherapy sources used are the 6711 and 9011 (ThinSeed™) (Oncura, a Unit of GE Healthcare, Chalfont St Giles, UK) for ^{125}I seed implant brachytherapy, and the MicroSelectron HDR v2r (mHDR-v2r) (Elekta AB) for ^{192}Ir HDR brachytherapy. Each source is simulated as a single source in a water phantom with the results compared to consensus data to validate the MC source input models. Multiple source MC simulations are implemented using code to automatically generate MC input files from DICOM files exported from TPSs. Code to calculate clinical dose distributions by superposing dose from multiple sources, and to calculate plan dose-volume histogram (DVH) parameters, are benchmarked by comparison to TPS calculations. Finally advanced MC simulation techniques are investigated including phase space source files, implementation of lattice tissue models and an investigation into the effects of varying the number of simulation histories on statistical uncertainties.

Section 3 – Phantom ISA and MOSFET measurements

In this section the effects of ISA in ^{125}I seed implant brachytherapy are investigated for idealised seed arrangements in a phantom using MC simulation and MOSFET measurements. The MOSFET measurements are used to validate the MC simulation framework for multiple source arrangements and also to assess the feasibility of using a MOSFET dosimeter in low energy brachytherapy. ISA is measured in symmetrical arrangements of 8 and 36 seeds and compared for the 6711 and 9011 source models.

Section 4 – Clinical ^{125}I MC simulations

In this section MC simulations are investigated for a group of 40 ^{125}I seed implant patients, including the following aspects:

- Comparison of the ISA effect in TRUS based implant plans and CT based post-implant plans.

- Comparison of the ISA effect in clinical plans for 6711 and 9011 sources.
- Investigation of the effects of incorporating tissue models on clinical dose distributions. Comparison of simple structure based and CT based tissue models.
- Modelling of the effects of calcification on dose distributions in CT based post-implant plans.
- Sector based analysis of MC simulation results.

Clinical MC simulations are also investigated for HDR brachytherapy patients and these are included in section 6.

Section 5 – Mp-MRI guided focal boost in HDR prostate brachytherapy

Feasibility of implementing mp-MRI guided focal boost treatments in HDR prostate brachytherapy is investigated in a pilot study of 30 patients. The investigation includes evaluating uncertainties of tumour delineation using mp-MRI and image registration of MRI to TRUS. Dosimetry of focal boost treatments is compared to standard treatments to evaluate the level of boost dose that can be achieved while maintaining the same coverage of the prostate at the prescription dose level and normal tissue dose constraints as for standard treatments.

Section 6 – Dosimetry modeling for LDR and HDR focal therapy

Feasibility of implementing focal therapy treatments is investigated for 9 patients who had been treated using HIFU as part of a focal therapy clinical trial, with comparison of 3 treatment planning approaches: standard whole prostate, hemi-gland focal and ultra-focal (25). Dosimetry is compared for LDR and HDR approaches. MC simulation of focal therapy treatment is performed to assess plan robustness to source position errors and the ISA effect. The ISA effect in focal ^{125}I seed implants was compared for 6711 and 9011 source models.

2 Preliminary validation work

This section describes work to develop and validate a MC simulation and dose calculation framework to allow clinical brachytherapy dose distributions to be simulated. This includes the following:

- Benchmarking MC source models against published data.
- Validating DVH calculation code.
- Investigating phase space source models and lattice MC simulation geometries for tissue models.
- Comparison of statistical uncertainties for simulations with different numbers of histories.

2.1 Background

2.1.1 Monte Carlo modeling approaches

All modeling was done in MCNPX v2.5.0 (101). This is benchmarked for use in brachytherapy dosimetry (3). Only photons were modeled (this means that any energy transferred to secondary electrons is assumed to be deposited at the interaction site, equivalent to assuming that the range of secondary electrons is negligible) with a cut-off energy of 1 keV. These assumptions are valid for ^{125}I photon simulations (102), and for ^{192}Ir >2.5mm from the source (103). The F6 tally (track length estimate of heating), or the mesh tally with the pedep option (101), was used to calculate dose, as this has been shown to be suitable for brachytherapy simulations (102).

2.1.2 TG-43U1 parameter calculations

To verify the accuracy of MC source models, single source simulations were performed with a spherical mesh tally (cells 0.1 mm/0.5°) in a spherical water phantom, radius 20 cm for ^{125}I, 40cm for ^{192}Ir. Results were used to calculate TG-43U1(3) parameters using the line source approximation, assuming an active length of 2.8 mm for 6711 and 9011 sources, and an active length of 3.5mm for the ^{192}Ir mHDR-v2r source.

For S_K the simulations were in a vacuum with a point detector (1 cm diameter air tally cell at 1 m from the seed) (3). A 5 keV cut-off was used to exclude lower energy photons that originate in the seed encapsulation, as recommended in TG-43U1.

Composition and density for water and air were taken from TG-43U1 and are as shown in Table 2. Sufficient particle histories were simulated to reduce the statistical component of uncertainty in individual tally cells below 1% in all cases.

2.1.3 Converting MC simulation results to dose

MCNPX tallies energy deposition as MeV per unit mass per starting particle (F6 tally) or MeV per unit volume per starting particle (mesh tally). Mesh tally results are converted to dose (MeV per unit mass per starting particle) by dividing by the medium density. Results are then converted to Gy as follows (104):

$$Dose = MCDose*((S_K/MCS_K)*1x10^6)*Time*NumSources$$

- MCDose is the MCNPX dose as described above and has units MeV g^{-1} per starting particle.
- The $((S_K/MCS_K)*1x10^6)$ factor converts MCDose to dose rate in Gyh^{-1}.
    - MCSk is the MC simulated value for S_K and has units MeV m^2 g^{-1} $particle^{-1}$.
    - S_K is the source value (activity) at the time of implant and has units µGy m^2 h^{-1}.
    - The $1x10^6$ factor converts from µGy to Gy
- Time is the time in hours that the source is in place. For a permanently implanted source the dose integrated over the lifetime of the source is calculated by setting Time = half life (in hours) divided by ln(2).

- NumSources is the number of sources in a multiple source simulations, this corrects for the fact that MC tally results are per starting particle (so effectively are also per source).

2.2 Single source validation – 6711 and 9011 I-125 seeds

The 6711 and 9011 (ThinSeed™) MC source models from Oncura were validated against published single source data. There are several studies that have modeled these sources. TG-43U1 published consensus source data (average values from earlier published studies based on both MC simulation and phantom dose measurements) for 6711 in 2004. An MC simulation study by Dolan *et al*. in 2006 examined the impact of minor changes in source manufacturing for the 6711 source (105). Two subsequent studies, by Rivard (103) and by Kennedy *et al*. (106) performed MC simulations for both 6711 and 9011 sources, using the source construction data from Dolan *et al*. as the basis for their simulation models. In this section, source modeling results are compared to data from TG-43U1 (for 6711 only) and Kennedy *et al*. (for 6711 and 9011). TG-43U1 is selected because it represents the consensus data that is used in most clinical centres for treatment planning. The Kennedy *et al*. study is chosen because the studies by Dolan *et al*., Rivard and Kennedy *et al*. produced very similar results and the Kennedy *et al*. study is the most complete as it also includes phantom dose measurements alongside MC simulation results.

Source model

Source models (see Figure 3) were based on recently published studies (106) (105) and also verified against technical drawings received from the manufacturer. The silver radio-opaque marker was assumed to be coated in a 1.75 μm thick layer of AgBr and AgI in a 2.5:1 molecular ratio(106). Material composition data is given in Table 2.

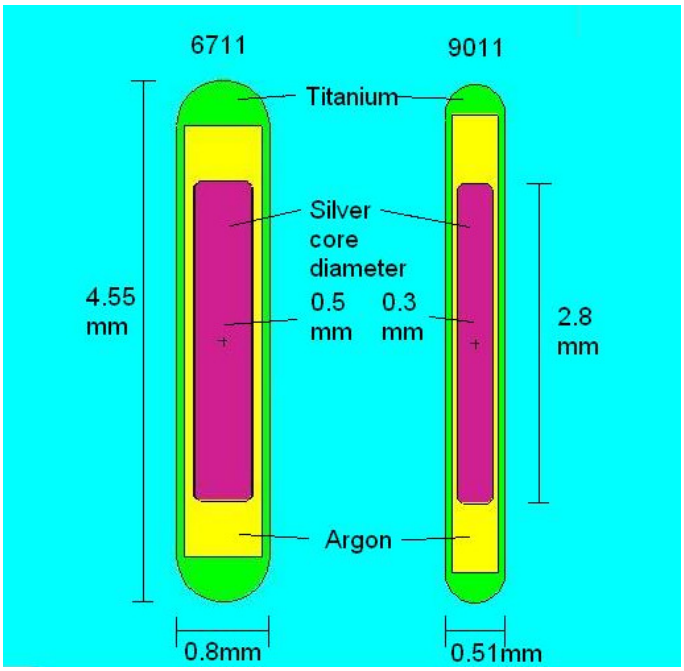

Figure 3 Source models used in the 6711 and 9011 simulations

The I-125 energy spectrum from TG-43U1(3) was used, this has been shown to give equivalent dosimetric results to National Nuclear Data Centre (NNDC) data {Rivard, 2010 #139}, and is shown in Table 3.

Table 2 ^{125}I simulation material composition and density data (3, 105-107)

Component	Material	Density (g cm^{-3})	Atomic number	Relative proportion	Proportion by weight
Source core	Silver	10.5	47 (Ag)	1	
Source coating	AgBr/AgI	6.2	35 (Br)	5	
			53 (I)	2	
			47 (Ag)	7	
Encapsulation	Titanium	4.54	22 (Ti)	1	
Gap inside seed	Argon gas	0.001784	18 (Ar)	1	
Tally for Sk measurement	Air (40% humidity)	0.0019	1 (H)		0.000732
			6 (C)		0.000123
			7 (N)		0.750325
			8 (O)		0.236077
			18 (Ar)		0.012743
Phantom	Water	0.998	1 (H)	2	
			8 (O)	1	

Table 3 125I energy spectrum (3)

Photon energy (keV)	Relative proportion
27.202	40.6
27.472	75.7
30.98	20.2
31.71	43.9
35.492	66.8

Results

Dose rate constant

Table 4 shows the dose rate constant values calculated from MC simulation, compared to Kennedy et al(106) and TG-43U1(3) (note that TG-43U1 does not have values for 9011).

Radial dose function

Table 5 shows a sample of the radial dose function values (g(r)) calculated from MC simulation, compared to values from Kennedy et al(106) and TG-43U1(3) (note that TG-43U1 does not have values for 9011).

Anisotropy function

Table 6 shows example anisotropy function values (F(r,θ)) calculated from single seed MC simulations for both 6711 and 9011, compared to values from Kennedy et al(106) and TG-43U1(3) (note that TG-43U1 does not have values for 9011).

Table 4 Dose rate constant value comparison from this paper (MC), Kennedy et al(106) and TG-43U1(3)

	Source model	MC	Kennedy (diff. from MC)	TG-43U1 (diff. from MC)
Λ (cGy h^{-1} U^{-1})	6711	0.940	0.939 (-0.1%)	0.965 (+2.6%)
	9011	0.926	0.928 (+0.2%)	-

Table 5 Radial dose function (g(r)) values comparison from this paper (MC), Kennedy et al(106) and TG-43U1(3)

	g(r) for 6711			g(r) for 9011	
r (cm)	MC	Kennedy	TG-43U1	MC	Kennedy
0.2	1.094	1.088	1.080	1.084	1.079
0.5	1.074	1.072	1.068	1.073	1.072
0.7	1.046	1.046	1.048	1.047	1.047
1	1	1	1	1	1
2	0.814	0.815	0.814	0.810	0.811
3	0.634	0.635	0.632	0.628	0.629
5	0.362	0.363	0.364	0.356	0.357

Table 6 Anisotropy function values comparison. from this paper (MC), Kennedy et al(106) and TG-43U1(3)

6711	F(r,θ) - MC			F(r,θ) - Kennedy			F(r,θ) – TG-43U1		
r θ	0°	30°	60°	0°	30°	60°	0°	30°	60°
0.5 cm	0.214	0.792	0.996	0.217	0.801	0.998	0.333	0.846	0.991
1 cm	0.283	0.793	0.992	0.296	0.798	0.993	0.370	0.834	0.991
2 cm	0.386	0.814	0.989	0.392	0.816	0.989	0.442	0.842	0.987
5 cm	0.522	0.843	0.985	0.536	0.845	0.986	0.550	0.852	0.987

9011	F(r,θ) - MC			F(r,θ) - Kennedy		
r θ	0°	30°	60°	0°	30°	60°
0.5 cm	0.213	0.792	0.972	0.221	0.800	0.974
1 cm	0.281	0.799	0.971	0.291	0.822	0.972
2 cm	0.386	0.820	0.972	0.390	0.822	0.972
5 cm	0.530	0.850	0.975	0.526	0.852	0.974

Conclusion

Compared to Kennedy et al(106), for 6711 and 9011 seeds, dose rate constant agreed within 0.2%, radial dose function agreed within 0.7% and anisotropy function values agreed within <5% which proves the validity of the MC source model. Compared to TG-43U1(3) consensus data for the 6711 seed, agreement is reasonable - some differences are expected as the consensus data includes experimentally measured data, TG-43U1 values are for a 3 mm active source length whereas this study used an active source

length of 2.8 mm, there have been minor changes in the source specifications from the manufacturer since TG-43U1 (105-107) and because of the impact of updates to the MC code itself (108). The impact of differences between TG-43U1 consensus data and the MC source model on clinical dose distributions is investigated in section 4.

2.3 Single source validation – HDR

The HDR ^{192}Ir mHDR-v2r source was validated against consensus data.

Source model

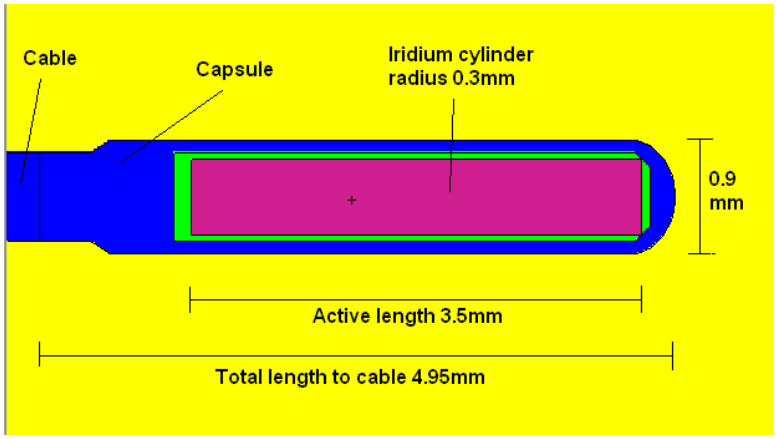

Figure 4 Nucletron HDR ^{192}Ir mHDR-v2r source diagram

The Nucletron HDR ^{192}Ir mHDR-v2r source model was based on the most recent published data, of Granero et al. (103). Figure 4 shows the source model as visualised in the MCNPX visual editor. Detailed dimensions are as in Granero et al. (103). Material composition and density data is given in Table 7. The ^{192}Ir spectrum was taken from NNDC data, vol 113, issues 8-9, p1871-2111 (109). Details are given in Table 8.

Table 7 ^{192}Ir mHDR-v2r simulation material composition and density data (41, 103)

Component	Material	Density (g cm^{-3})	Atomic number	Relative proportion	Proportion by weight
Source	Iridium	22.42	77 (Ir)	1	
Capsule	AISI316L Stainless Steel	8.02	14 (Si)		0.01
			24 (Cr)		0.17
			25 (Mn)		0.02
			26 (Fe)		0.68
			28 (Ni)		0.12
Cable	AISI316L Stainless Steel	4.81	As for Capsule		
Catheter	ANSI 303/304 Stainless Steel	8.02	14 (Si)		0.01
			24 (Cr)		0.19
			25 (Mn)		0.02
			26 (Fe)		0.68
			28 (Ni)		0.1
Gaps inside source/ catheter	Air (40% humidity)	0.0019	1 (H)		0.000732
			6 (C)		0.000123
			7 (N)		0.750325
			8 (O)		0.236077
			18 (Ar)		0.012743
Phantom	Water	0.998	1 (H)	2	
			8 (O)	1	

In addition to modeling the source in a water phantom (to compare to consensus data), the source was modeled inside a steel catheter. The catheters (interstitial bevel needle product number 083.045, Elekta AB) were modeled from Elekta data, verified using autoradiograph, as having outer diameter 1.9mm, inner diameter 1.48mm, a 7mm long plug and 3mm pointed end section, as shown in Figure 5. The end section was modeled as

a cone because in an actual implant the orientation of the bevel is not recorded. The source was placed at the first dwell position (11.5mm from the needle tip).

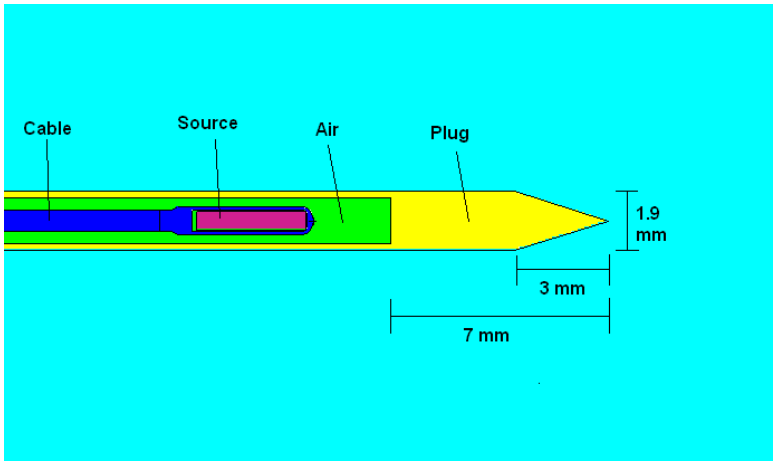

Figure 5 The HDR source and steel catheter model

Table 8 ^{192}Ir energy spectrum (109)

Photon energy (keV)	Relative proportion	Photon energy (keV)	Relative proportion	Photon energy (keV)	Relative proportion
56.71	0.0351	155.16	0.0921	485.5	0.0047
61.49	1.19	177	0.0043	489.1	0.438
63.0	2.02	201.3	0.471	588.6	4.522
63.29	0.176	205.79	3.31	593.6	0.042
64.99	0.3	280.3	0.008	599.4	0.0039
65.12	2.6202	283.3	0.266	604.4	8.216
66.83	4.4403	295.96	28.7119	612.46	5.3404
71.08	0.238	308.5	29.7	703.8	0.0053
71.41	0.46	316.51	82.8694	765.8	0.0013
73.36	0.2645	329.1	0.0173	884.5	0.292
75.4	0.555	374.5	0.727	1061.5	0.0531
75.75	1.0211	416.5	0.67	1089.9	0.0012
77.83	0.364	420.5	0.069	1378.5	0.0014
110.3	0.0127	468.1	47.84		
136.4	0.199	484.6	3.19		

Results

Dose rate constant

The dose rate constant from the MC simulation was calculated as 1.1076, 0.1% less than the consensus data value of 1.109 (110).

Radial dose function

Table 9 shows a sample of the radial dose function values (g(r)) calculated from MC simulation compared to consensus data values (110).

Table 9 Radial dose function (g(r)) values comparison to consensus data (110)

	g(r)		
r (cm)	MC	RPT229	% diff
0.2	0.992	1.001	-0.9%
0.25	0.994	0.995	-0.1%
0.5	0.997	0.997	0.0%
0.75	0.998	0.998	0.0%
1	1.000	1.000	0.0%
1.5	1.004	1.003	0.1%
2	1.006	1.005	0.1%
3	1.009	1.008	0.1%
5	1.004	1.003	0.1%
6	0.997	0.996	0.1%
8	0.975	0.972	0.3%
10	0.942	0.939	0.3%

Anisotropy function

Table 10 shows example anisotropy function values ($F(r,\theta)$) compared to consensus data values(110).

Dosimetric impact of steel catheters

Figure 6 illustrates the dosimetric impact of including a steel catheter in a single source simulation.

Table 10 Anisotropy function compared to consensus data values (110)

6711	F(r,θ) - MC			F(r,θ) - RPT229			%diff		
r θ	0°	30°	60°	0°	30°	60°	0°	30°	60°
0.25 cm	0.778	0.941	0.990	0.787	0.961	0.993	-1.1%	-2.1%	-0.4
0.75 cm	0.644	0.912	0.985	0.619	0.911	0.984	4.1%	0.1%	0.1
1 cm	0.638	0.912	0.985	0.610	0.911	0.985	4.7%	0.1%	0.0%
2 cm	0.641	0.915	0.985	0.625	0.915	0.986	2.6%	0.0%	0.0%
5 cm	0.703	0.926	0.987	0.711	0.926	0.987	-1.1%	0.0%	0.0%
8cm	0.756	0.934	0.988	0.768	0.934	0.988	-1.5%	0.0%	0.0%

Conclusion

Compared to consensus data (110) for the mHDR-v2r source, dose rate constant agreed within 0.1%, radial dose function agreed within <1% and anisotropy function values agreed within <5% which proves the validity of the MC source model. The impact of a steel catheter is small apart from at points along the source longitudinal axis. The greatest area of dose attenuation due to the steel catheter is more than 1cm beyond the last source dwell position, so would not impact clinical prostate dose distributions and may even have a beneficial effect by reducing normal tissue dose. The impact of steel catheters in clinical dose distributions is assessed in section 6.

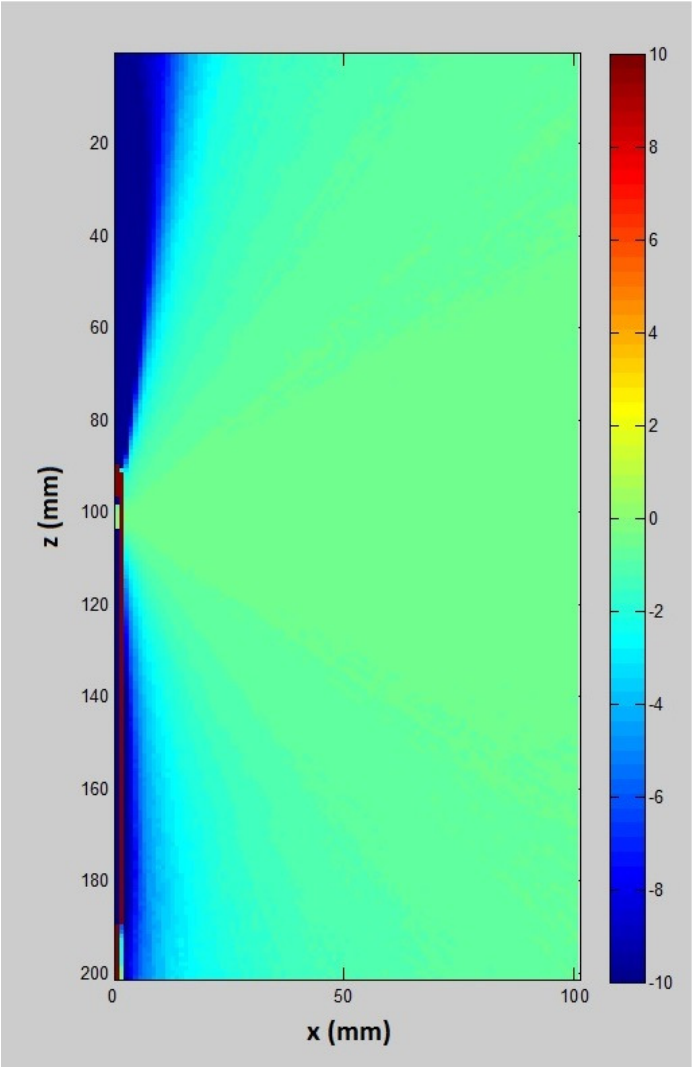

Figure 6 Comparison of dose for a single ^{192}Ir mHDR-v2r source with and without a steel catheter. The x axis is the source transverse axis and the z axis is the longitudinal axis. The source is at z=101 and the needle lies along the z axis. Differences are expressed as %.

2.4 Validation of dose analysis framework

A dose analysis framework was implemented for analysis of MC simulation results, and also to calculate MC superposition dose distributions. MC superposition dose distributions are calculated by superposing single MC source distributions across all source co-ordinates and in many cases in later sections are used instead of TG-43U1 (3) for comparison with full MC simulation. This is so that the comparison is not affected by differences between MC source models and TG-43U1 consensus data, or differences

due to the TG-43U1 line source approximation. This section describes how the framework was implemented and validated.

Method

Source co-ordinates, source activity, source dwell times (HDR only) and structure sets were exported from the TPS (for ^{125}I treatments the TPS is Variseed™ v8.0 (Varian Medical Systems, Inc., Palo Alto, CA, USA) and for ^{192}Ir treatments the TPS is Oncentra Prostate™ v4.0 (Elekta AB)). For some cases (CT tissue based models) the underlying image set was also exported. The dose analysis framework was implemented in Matlab™ R2010a (MathWorks, Natick, MA, USA) and included code to auto-generate MC simulation input files based on the exported patient data.

The dose and DVH calculation framework involved the following steps:

- Extract structure points from DICOM structure data and create 3D masks for all structures in the structure sets (for example prostate, urethra and rectum).
- Calculate a 3D dose distribution. For MC simulated dose, this is the raw dose converted to Gy as described in 2.1.3. For the MC superposition dose, the dose at each point in the distribution was calculated by summing the dose from each source at that point. A single source cylindrical dose distribution calculated using MC simulation, with resolution 1mm and extending 10cm along and 10cm away from the source was used to calculate the contribution from each source. Bi-linear interpolation was used to interpolate between points in the cylindrical dose grid (an inverse-square law correction was applied to the dose grid to smooth the interpolation, and then removed after interpolation). The dose calculation resolution was 1 mm x 1 mm in-plane, with dose calculated on the slices in the original imaging data (2 mm spaced for CT, either 2.5 mm or 5 mm spaced for TRUS).
- For ^{125}I treatments, all sources were assumed to be oriented perpendicular to the plane of the CT/TRUS slices. For ^{192}Ir

treatments, corrections for source orientation were applied using the simplifying assumption that the same rotation could be applied to all sources in a single catheter (Oncentra Prostate™ calculates a separate rotation for each source (111)).

- For dose calculation from MC simulation results of HDR treatments, for voxels that intersect a catheter, dose was interpolated from surrounding voxels to exclude high dose catheter voxels from the DVH analysis.
- Once dose calculation was completed, the 3D structure masks were applied to the 3D dose distributions to calculate DVH statistics.

The resulting DVH calculations were benchmarked by comparing results to DVH statistics calculated by the TPSes. 15 clinical post-implant CT based plans were compared for the 6711 seed model. 5 HDR prostate treatment plans were compared for the ^{192}Ir source model. For the 6711 seed comparison, TG-43 source data calculated from single seed MC simulations was added to Variseed and used instead of 6711 consensus data. This is to remove any effects due to differences between the MC seed model and the consensus data, as noted in 2.2. This was not necessary for validation for the ^{192}Ir source, as MC simulation of that source showed good agreement with consensus data.

Results

Table 11 compares mean DVH parameter values for 15 post-implant 6711 seed implant plans, as calculated by Variseed using the MC source data from 2.2 and the dose analysis framework for the MC superposition dose distribution.

Table 12 compares the mean DVH parameter values for 5 HDR prostate patients from Oncentra Prostate (TG-43U1(3) calculation) and MC superposition dose calculations. Planning target volume (PTV) data is included.

Table 11 Results from benchmarking DVH calculation code comparing Variseed output for the MC simulated source data (MC-SRC) and output from the dose analysis framework MC superposition dose (MC-SUP). All results are mean values for 15 patients using the 6711 seed.

DVH Parameter	Variseed MC-SRC	MC-SUP	Difference Variseed MC-SUP – MC-SRC
Prostate volume	35.1 cm^3	35.2 cm^3	0.3%
Prostate D90	136.6 Gy	137.5 Gy	0.7%
Prostate V100	87.3%	87.6%	0.3%
Prostate V150	56.1%	57.0%	0.9%
Prostate V200	25.8%	26.7%	0.9%
Urethra D10	248.0 Gy	255.4 Gy	3.0%
Rectum D2cm^3	118.3 Gy	119.2 Gy	0.8%

Table 12 Mean DVH parameter values for 5 HDR prostate patients comparing Oncentra Prostate and MC-SUP dose calculations

DVH Parameter	Oncentra Prostate	MC-SUP	Difference Oncp –MC-SUP
PTV volume (cm^3)	46.6	46.9	0.7%
PTV D90 (Gy)	15.5	15.5	-0.2%
PTV V100 (%)	92.4	92.2	-0.3%
Prostate volume (cm^3)	31.9	32.5	1.8%
Prostate D90 (Gy)	17.0	17.0	0.5%
Prostate V100 (%)	99.6	99.5	-0.1%
Prostate V150 (%)	27.0	27.9	0.8%
Prostate V200 (%)	6.87	4.84	-2.0%
Urethra D10 (Gy)	17.2	17.2	0.0%
Rectum D2cm^3 (Gy)	8.86	8.89	0.4%

Conclusion

Small differences are observed between DVH parameters calculated by the DVH calculation framework and the TPSes. These differences are not unexpected as there are differences in the dose calculation resolution and TPSes typically calculate DVH parameters by randomly sampling points within volumes for speed, whereas the DVH calculation framework calculates the DVH using all elements in each structure. The differences

observed are smaller than those that have been observed in a comparison of commercial treatment planning systems (112). Therefore the DVH comparisons demonstrate that the dose and DVH calculation framework is valid.

2.5 Validation of phase space source

MCNPX supports phase space source models: a pre-calculation is used to create a phase space source file that stores information on all particles crossing the source surface. The phase space source file is then used as the source in further simulations. Therefore all absorption and scattering inside a source of particles that originate from the same source is pre-calculated. For seed implants phase space source models have been shown to reduce calculation time by around one half (113). This section describes how phase space models were implemented and validated for the sources used in this study.

Method

The MCNPX ssw (surface source write) card (101) was used to calculate the phase space source model file. This writes all particles that cross the outer surface of the source. For 6711 and 9011 sources the outer surface was defined by the source encapsulation. For the mHDR-v2r source the outer surface was defined by the source encapsulation and extended to include 5cm of source cable. 500 million histories were simulated for the creation of each phase space source file.

For each source, the phase space source files were validated by repeating a single source simulation using a cylindrical mesh tally as described in section 2.2, and comparing tally results to the original simulation that used the full source simulation. In addition, to validate the use of phase space sources in clinical simulations, for 5 ^{125}I patient CT post implant plans MC simulations using both full source model and the phase space source model

for the 6711 source were compared using DVH parameters calculated as described in section 2.4.

Results

Single source simulations

For single source simulations, the mean difference between full source and phase space source simulations for all points up to 10cm along and 10cm away from the source was 0.16% for the 6711 source, 0.09% for the 9011 source and 0.5% for the mHDR-v2r (excluding points inside the source/source cable). At individual points differences were up to ±10% but differences appeared to be statistical (there was no trend in any particular direction) and were less than statistical error in each tally cell (for the reasons explained above, the number of histories used in the phase space validation is considerably less than used in the full source model validation).

Clinical simulations

Table 13 summarizes the comparison of full source and phase space source clinical simulations for 5 CT post implant plans for patients treated with the 6711 source. In clinical simulations use of the phase space source model was found to reduce simulation time by ~55%.

Table 13 Comparison of mean DVH parameter values for full source and phase space source simulations using 6711 source, for 5 patients

DVH Parameter	MC simulation – full source	MC simulation – phase space source	Difference: mean (max)
Prostate D90 (Gy)	133.5	133.4	0.0% (0.3%)
Prostate V100 (%)	86.3	86.3	0.0% (0.2%)
Prostate V150 (%)	50.5	50.6	0.1% (0.5%)
Prostate V200 (%)	24.4	24.5	0.1% (0.8%)
Urethra D10 (Gy)	218.1	218.2	0.0% (0.8%)
Rectum D2cm^3 (Gy)	110.1	110.2	0.2% (0.3%)

Conclusion

Comparison of DVH parameter values calculated from full source and phase space source simulations show that the largest difference observed for any

parameter is <1%, therefore the results confirm that the phase space source models are suitable for use in this study.

2.6 Investigation of statistical variations with number of histories for clinical simulation

MC simulation results are affected by statistical uncertainties that decrease as the number of histories is increased. In a given tally cell, statistical uncertainty is inversely proportional to the square root of the number of histories. This section explores how individual tally cell uncertainties impact DVH parameters uncertainties in clinical simulations.

Method

For the 5 patients described in section 2.5, simulations were performed using 4 million, 1 million and 0.25 million histories per seed. Each reduction in the number of histories by a factor of four approximately doubles individual tally cell uncertainty. Each simulation was repeated 3 times in total using different starting random numbers, to estimate the statistical variation in DVH parameters for a fixed number of histories.

Results

Table 14 shows the uncertainty in DVH parameter values, calculated as the standard deviation/mean of 3 repeat simulations for 5 clinical post-implant plans. The maximum difference from the mean parameter value for 4 million history simulations is also shown.

Conclusion

The analysis of increase in DVH parameter uncertainty as the number of simulation histories is decreased shows that decreasing the number of histories does not increase DVH parameter uncertainty in proportion to tally cell uncertainty. As the simulations used in this study were not particularly time constrained, 2 million histories per seed were used in subsequent simulations as a compromise between levels of uncertainties and simulation

run time, even though adequate results could have been achieved with fewer histories.

Table 14 Uncertainty in DVH parameter values estimated from 3 repeat simulations of 5 clinical post-implant plans, comparing results for different numbers of histories per seed. For 1 and 0.25 million histories the maximum difference from the mean parameter value for 4 million histories is shown in parentheses.

DVH Parameter	4 million histories/seed	1 million histories/seed	0.25 million histories/seed
Prostate D90	0.13%	0.13% (0.45%)	0.17% (0.97%)
Prostate V100	0.06%	0.10% (0.22%)	0.18% (0.30%)
Prostate V150	0.09%	0.14% (0.19%)	0.30% (0.37%)
Prostate V200	0.20%	0.26% (0.23%)	0.35% (0.19%)
Urethra D10	0.21%	0.40% (0.87%)	0.62% (1.8%)
Rectum D2cm^3	0.17%	0.28% (0.64%)	0.56% (1.2%)

2.7 Validation of lattice tissue model

A lattice tissue model was implemented in MCNPX to investigate tissue heterogeneity effects. For the clinical simulations using tissue models in this study an 8cm x 8cm x8cm lattice was defined, centered on the mean source co-ordinate implant. Lattice voxels were 1mm x 1mm x 1mm. MCNPX allows each voxel to be assigned to a particular tissue type. Other geometry can be superimposed on the lattice, for example for ^{125}I simulations, the seeds are defined independently of the lattice and MCNPX automatically removes any parts of lattice voxels that are overlaid by a seed. The lattice model was validated by comparing simulations for identical geometries created with and without the lattice, as described in this section.

Method

For the 5 patients described in section 2.5, simulations were performed firstly using a simple spherical water phantom of radius 15cm and then using the lattice, filled with water, embedded in the same spherical water phantom. Everything else was identical between the simulations, so any

differences in the results would be entirely due to use of the lattice model. Simulations used 2 million histories per seed.

Results

Tally results from the two simulations were not identical, but the average difference in DVH parameter values was <0.1% for prostate D90, V100, V150, V200, urethra D10 and rectum D2cm^3. Analysis of individual tally cell differences showed that inside the prostate, on average (across the 5 patients) 73.2% of cells agreed within 1%, 94.5% of cells agreed within 2% and 100% of cells agreed within 5%. The average difference across all prostate tally cells was <0.1%.

Conclusion

Implementation of the lattice model causes differences in tally results but these appear to be purely statistical in nature, have no impact on DVH parameter values and are assumed to result from details of the MC code implementation.

3 Experimental validation of multi-source MC simulations

This section describes experimental dosimetry work with a phantom which was performed to verify the results of MC simulations using multiple sources and measure ISA independently from the MC simulation. Phantom measurements were performed for 6711 and 9011 sources.

3.1 Introduction

Experimental dosimetry is an accepted method for brachytherapy source characterization (3), and the majority of experimental brachytherapy dosimetry studies are on single source measurements. Although Meigooni et al (114) measured ISA in simple seed arrangements using thermoluminescent dosimeters (TLDs) in a solid water phantom, other studies measuring ISA in phantom and clinical scenarios have used MC simulation without any further validation(43, 115-119). In this study experimental dose rate measurements are performed with a MOSFET in a phantom with the purpose of measuring ISA experimentally and validating the MC simulation framework results for simulations with multiple sources. MOSFET response is energy dependent so to avoid having to apply corrections for energy dependent response, in this study MOSFET calibration was performed using the ^{125}I sources used for the measurements.

Solid phantom materials are not water equivalent for low energy ^{125}I dosimetry (41), so a MC calculated correction is required to convert experimental measurements to dose to water measurements. For this study, this was achieved by comparing measured dose rates to results from MC simulations performed in the phantom material. In addition, as MOSFET response is energy dependent, so would require corrections if the radiation energy spectrum changed with distance from the source, simulations were performed to calculate the energy spectrum at each measurement position.

3.2 Initial ISA modeling

To provide some basic background information for phantom design, the ISA effect was measured for simple two seed arrangements.

Method

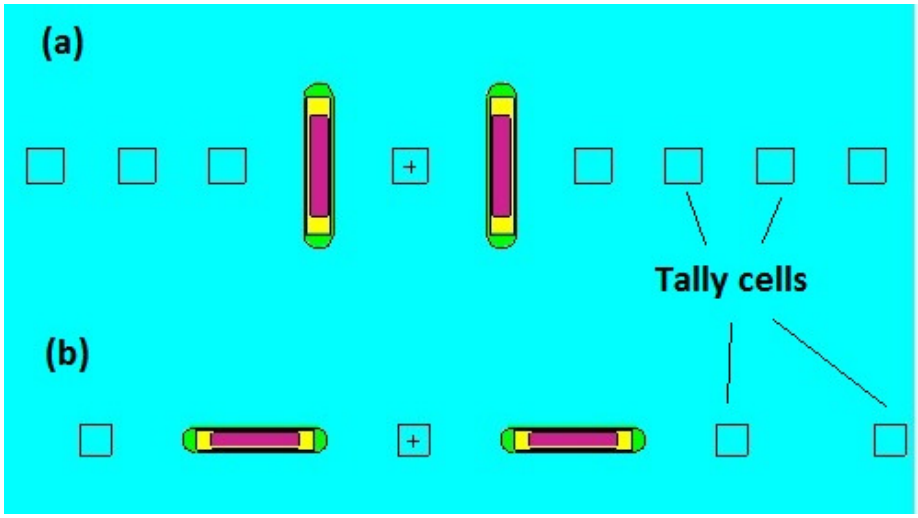

Figure 7 Seed arrangements for two seed ISA MC simulations

Simulations were performed using the methodology described in 2.1 for two seeds placed close to the centre of a 15cm radius water phantom. To measure ISA along the transverse axis, simulations were performed with the transverse source axes aligned, with centre to centre seed separation 0.5cm, 1cm and 1.5cm and dose was tallied in $1mm^3$ cells along the transverse source axes (Figure 7(a)). To measure ISA along the longitudinal axis, simulations were performed with longitudinal axes aligned and centre to centre seed separation 1cm and dose was tallied in $1mm^3$ cells along the longitudinal source axes (Figure 7(b)). Simulations were performed for 6711 and 9011 seeds. The simulation results were compared to dose calculated by superposing dose due to the two seeds individually (from single seed simulations described in 2.2, so ignoring the ISA effect.

Results

For two seeds arranged with transverse axes aligned, Figure 8 (6711 seeds) and Figure 9 (9011 seeds) show how the ISA effect along the source transverse axis varies with source separation and distance (the distance is as measured from either seed, in the direction away from the other seed). For

two seeds arranged with longitudinal axes aligned and separation 1cm, the ISA effect along the source longitudinal axis was between 2-4%, did not vary greatly with distance from the source and was similar for the 6711 and 9011 seed models.

Conclusion

The results show that the ISA effect due to two sources will be easiest to measure if source transverse axes are aligned, if the distance between the sources is decreased and at a distance 1-2cm from the source pair. At smaller distances from the source pair the dose due to the nearest seed dominates so that the ISA effect becomes hard to measure.

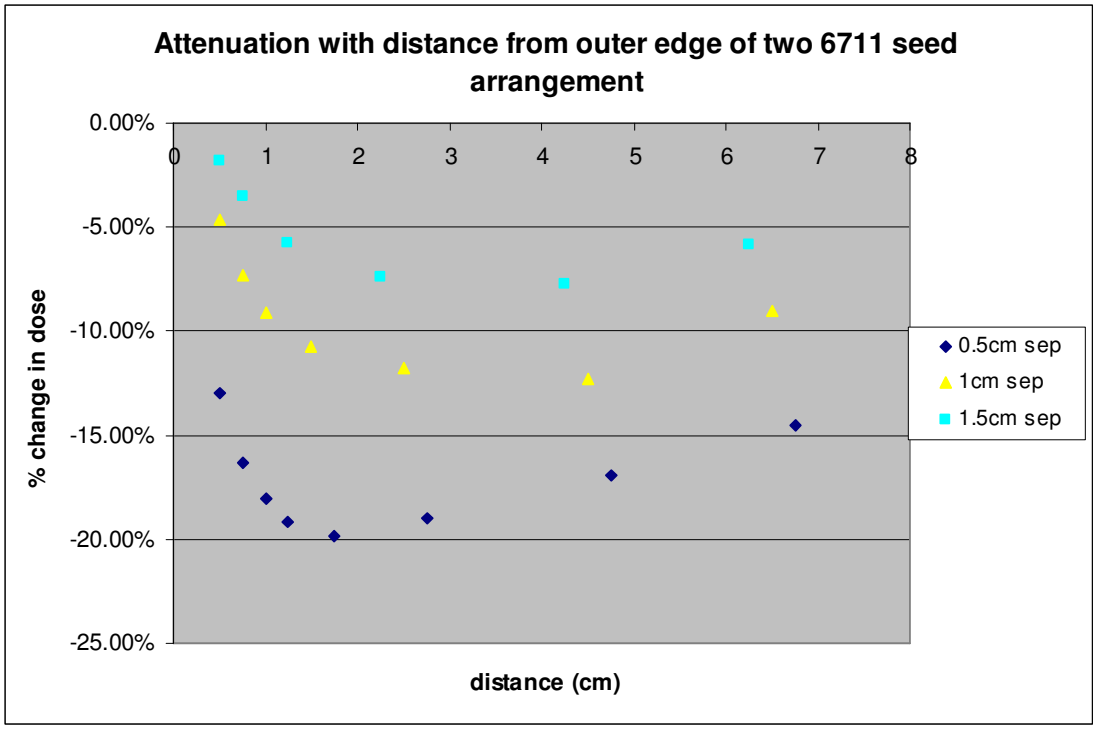

Figure 8 Variation of ISA on the source transverse axis with source separation and distance for two 6711 seeds

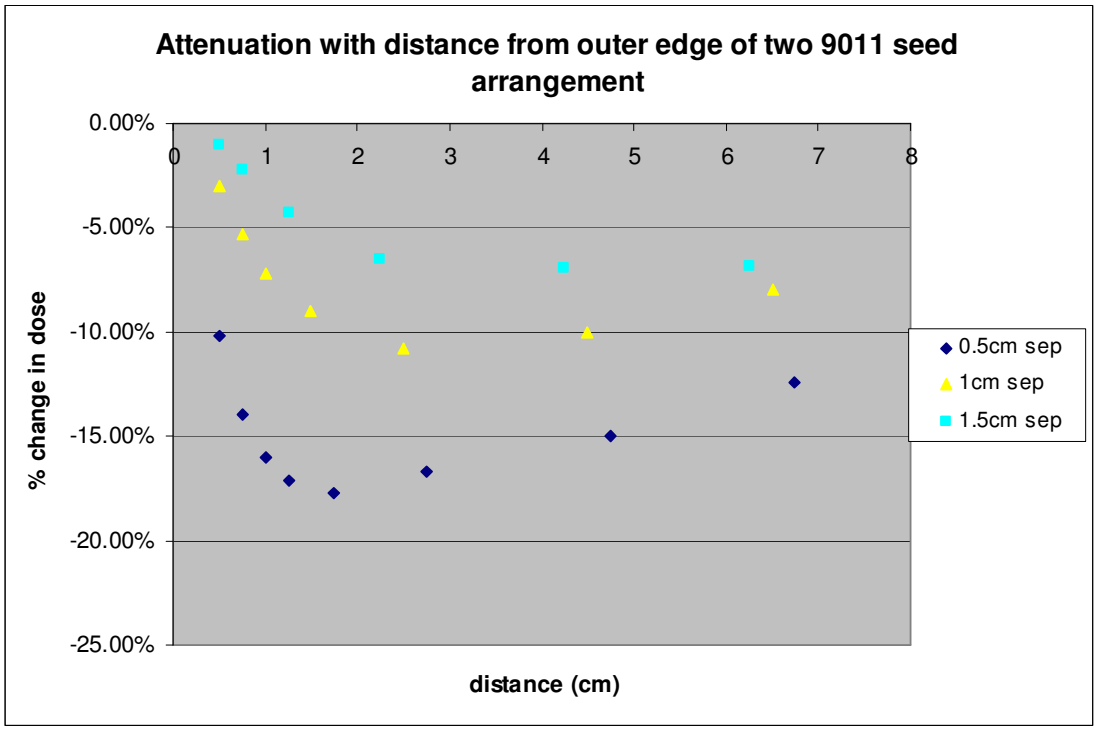

Figure 9 Variation of ISA on the source transverse axis with source separation and distance for two 9011 seeds

3.3 Phantom work

3.3.1 Method

MC simulations

Based on the results described in 3.2, a phantom was designed for experimental ISA measurements, with source positions a compromise between the positions at which the maximum ISA effect can be observed, and the need to reduce the distance between the source and the MOSFET to reduce dose rate related measurement uncertainties. The phantom is described in detail below.

MC simulations of all phantom seed arrangements (described below) were performed using the methodology described in 2.1 and using the complete phantom geometry including all air holes. The composition of polymethyl methacrylate (PMMA) was taken as $C_5H_8O_2$ with density 1.19 g cm^{-3} (41). The expected dose at the MOSFET position was calculated using a 0.5 mm

diameter spherical water cell (MCNPX F6 tally(101)). Energy spectrum calculations used a 1 mm diameter spherical surface (MCNPX F1 tally(101)) at the MOSFET position, with photon energies in the range 0 keV to 40 keV tallied in 2.5 keV bins.

Seed calibration

36 6711 and 36 9011 seeds were first calibrated in a well chamber with calibration traceable to the National Institute of Standards and Technology. Seeds were then stored in separate pots based on the measured S_K and in subsequent measurements the expected dose rate was determined from the mean S_K of the seeds used in that particular measurement.

PMMA phantom design and measurements

A PMMA phantom was designed for MOSFET commissioning and dose rate measurements to assess the ISA effect. The phantom is a 13 cm x13 cm x 13 cm PMMA block with swappable inserts that can be placed at the centre of the phantom to allow different seed configurations to be tested, and a 1.5 mm diameter hole drilled to allow a high sensitivity micro MOSFET dosimeter (Best Medical TN-1002RDM), operated under high bias to increase sensitivity, to be inserted (see Figure 10). Separate inserts were manufactured for 6711 and 9011 seeds. The seed holes are 5 mm deep and 0.9 mm diameter for 6711, 0.6 mm diameter for 9011. In any measurement, the seeds closest to the MOSFET will contribute most to the measured dose rate. This will lead to uncertainties due to small differences in individual seed S_K from the mean S_K and non-uniformities in the distribution of radioactive material on individual seeds. To reduce these uncertainties each MOSFET measurement result presented in this study is the mean of 4 independent measurements (all seeds were removed and randomly replaced). An accumulated dose of ~10 cGy was acquired for each measurement. Dose rate ranged from 2 cGy h^{-1} to 23 cGy h^{-1}. Measurement duration ranged from 25 minutes to 5 hours. All measurements were corrected for source decay and background readings. For all measurements

the MOSFET bulb was oriented towards the front face of the phantom (which was identified by red dot markers – visible in Figure 10).

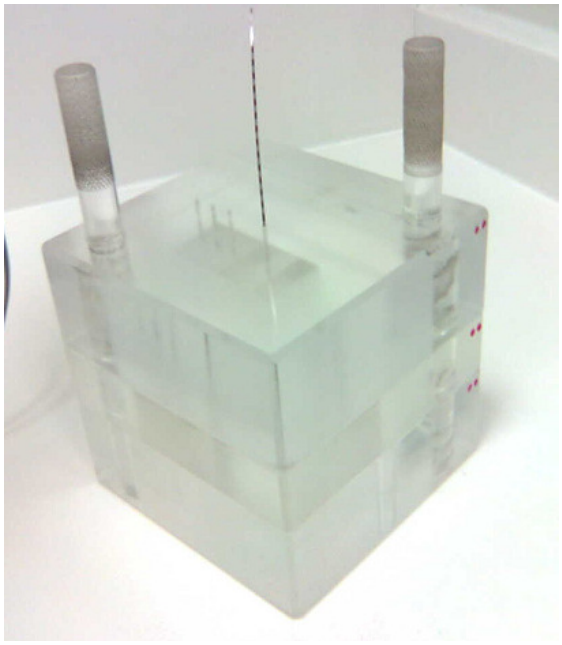

Figure 10 The PMMA phantom used for MC simulation verification, with MOSFET inserted

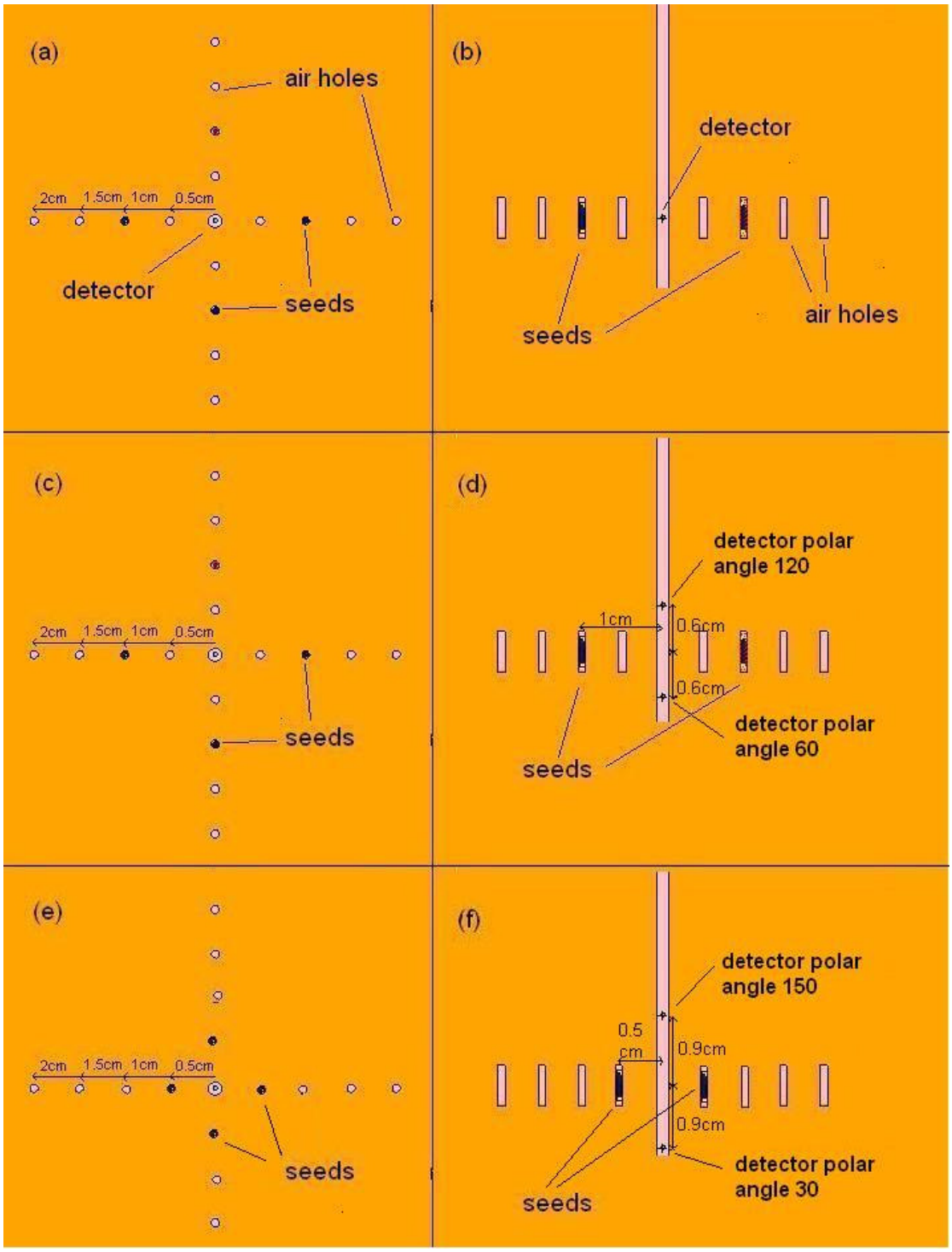

Figure 11 Phantom seed configurations for MOSFET commissioning. The seed configuration for MOSFET calibration is shown in (a) the plane transverse and (b) the plane parallel to the seed longitudinal axis. (c)-(f) show the seed and detector positions for MOSFET polar angle anisotropy measurements.

MOSFET commissioning

(i) For MOSFET calibration, 4 seeds were placed 1 cm from the MOSFET as shown in Figure 11(a) and (b). The dose rate for calibration measurements was ~4 cGy h^{-1}. Calibration was repeated for every 1000 mV increase in MOSFET threshold voltage to assess fade in response. This gave 13 separate calibration measurements in total. Both 6711 and 9011 sources were used in the calibrations.

(ii) Azimuthal anisotropy of MOSFET response was neglected as the phantom seed configurations were designed to negate any anisotropic effects (see below). Polar angle anisotropy was assessed using 4 seeds with the MOSFET placed out of the plane of the seeds to create approximate polar angles of 30°, 60°, 90°, 120° and 150° between the MOSFET and the centre of each seed, as shown in Figure 11(c)-(f). (Polar angle 90° is the calibration position shown in Figure 11(a) and (b).) The measured dose rates were compared to MC simulation results for each detector position.

(iii) As MOSFET response is energy dependent, all measurements including calibration were performed with I-125 seeds. However measured ISA values could still be affected by variations in the energy spectrum due to differences in source-detector distance in the PMMA phantom, or due to the fact that seeds may cause energy spectrum changes as well as dose attenuation. This was assessed using MC simulation to calculate the energy spectrum at the MOSFET position for each measurement configuration.

Phantom dose rate and ISA measurements

Measurements were made in configurations of 8 or 36 seeds arranged symmetrically around the MOSFET in two groups, inner and outer. ISA is measured by comparing the measured dose rate from all seeds together to the sum of the dose rates measured with the inner seed group alone and the outer seed group alone. By this method the scatter between seeds within either group is not accounted for, but is assumed to be negligible compared to seed attenuation at the MOSFET position. The seed configurations are designed to achieve a measurable ISA effect, remove any effects of

MOSFET azimuthal anisotropy, maximize the dose rate and reduce the dose gradient at the MOSFET position.

In the 8 seed configuration there are 4 seeds at 1 cm (inner group) and 4 seeds at 1.5 cm (outer group) from the MOSFET as shown in Figure 12(a) and (b). The 36 seed configuration has 3 blocks, each block having 6 seeds 0.6 cm (inner group) and 6 seeds 1.2 cm (outer group) from the centre, as shown in Figure 12(c) and (d). Blocks are spaced 1 cm apart in the direction of the seed longitudinal axis to replicate seed separation in clinical implants, with the MOSFET at the centre of the middle block.

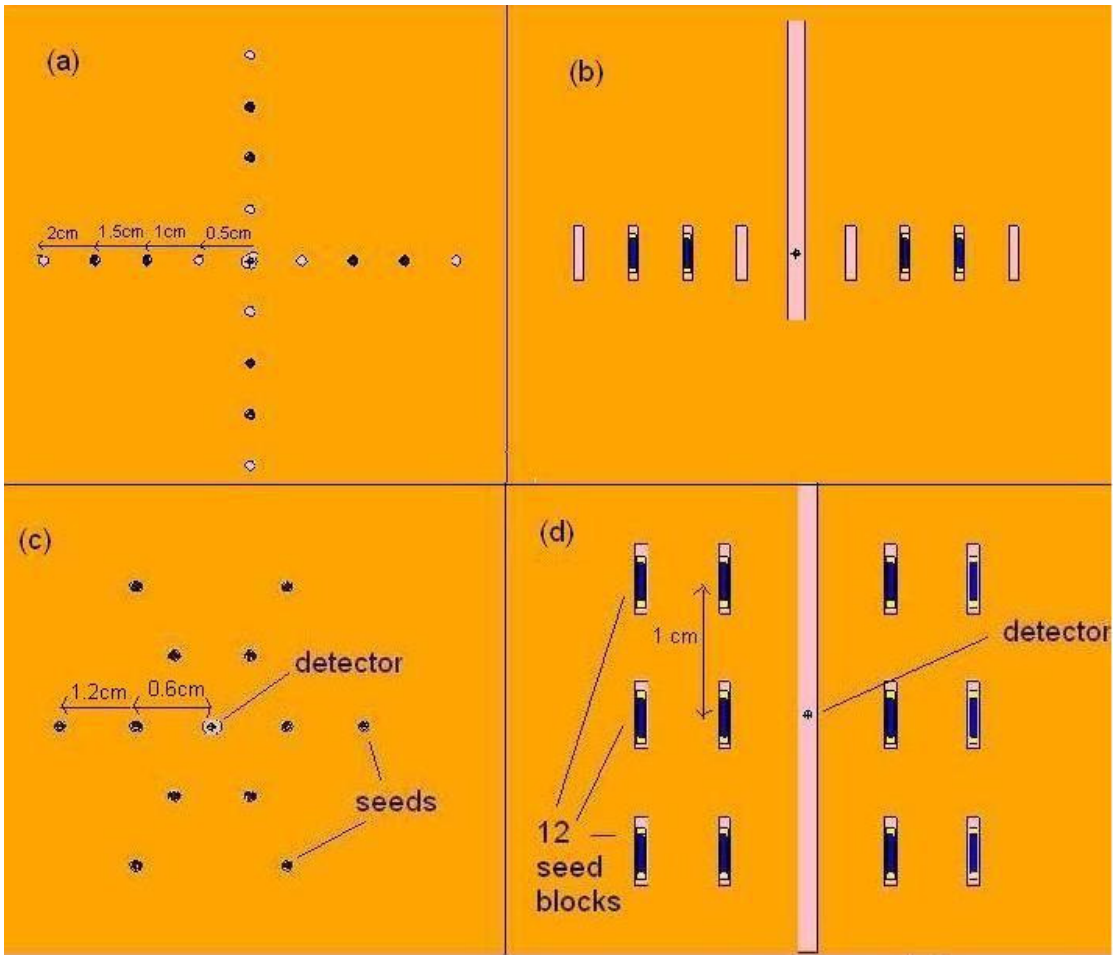

Figure 12 Phantom seed configurations for ISA measurements. The 8 seed measurement configuration is shown in (a) the plane transverse and (b) the plane parallel to the seed longitudinal axis. (c) and (d) show the same views for the 36 seed configuration

3.3.2 Results

Seed calibration

From the well chamber seed calibration, after correction for decay, the mean seed S_K was 0.863 U (range 0.832 U to 0.894 U). The reference S_K provided by the manufacturer was 0.859 U.

MOSFET commissioning

(i) In the calibration seed configuration (Figure 11 (a) and (b)) the expected dose contribution from each of the 4 seeds is the dose rate constant (from TG-43U1(3) for 6711 and from Kennedy et al(106) for 9011) multiplied by the seed S_K and a factor of 1.11 to correct for reduced attenuation in PMMA compared to water (from Luxton et al (120), this was also verified by MC simulation comparing water and PMMA dose rates). This gives a MOSFET sensitivity coefficient of 30.9 mV cGy^{-1} (mean of 13 measurements). Comparison of MC simulation of the calibration seed configuration to measured dose rates gave a sensitivity coefficient of 30.3 mV cGy^{-1}. As the two sensitivity coefficients are in close agreement, the coefficient derived from MC simulation was used for consistency. Fade in response was <1% over the complete set of measurements during which the MOSFET threshold voltage increased from 4000 mV to 17000 mV.

(ii) Polar angle measurements showed that the MOSFET under-responds relative to the MC simulation predicted dose rate by 6.7% at polar angle 30° and by 7.1% at 60°. Response is within 1% of expected values at 90°, 120° and 150°.

(iii) Table 15 shows the calculated energy spectrum in each measurement configuration, compared to reference data from Chen and Nath (121). The mean energy for each configuration is also shown. The results for the 9011 seed were very similar so are not presented - the mean energy in each configuration for the 9011 seed was <1% different from the value for the 6711 seed. As there is no significant spectral variation across the set of measurement configurations, no corrections for MOSFET energy dependent response were applied in this study.

Table 15 The MC calculated energy spectrum and mean energy for each measurement configuration compared to reference data from Chen and Nath (121). Energy bins with <1% of the calculated spectrum are not included. Note the mean energy is taken directly from the MC simulation output and not calculated from the energy spectrum data.

Photon energy bin (keV)	**6711 source reference data** (121)	**Calculated energy spectra**					
		8 seeds			36 seeds		
		inner group	outer group	inner + outer	inner group	outer group	inner + outer
20-22.5	15.3%	13.6%	12.7%	13.3%	13.3%	12.5%	13.0%
22.5-25	4.3%	10.2%	11.7%	12.2%	9.6%	11.8%	10.3%
25-27.5	61.4%	56.5%	55.2%	54.7%	57.2%	55.4%	56.5%
27.5-30	-	3.4%	4.2%	4.2%	3.0%	4.2%	3.5%
30-32.5	15.3%	12.2%	11.6%	11.6%	12.7%	11.8%	12.2%
35-37.5	3.7%	3.3%	3.0%	3.0%	3.5%	3.0%	3.3%
Mean energy 6711 (keV)	26.7	26.9	26.9	26.8	27.0	26.8	26.9

Phantom dose rate and ISA measurements

Table 16 lists the uncertainties of measurements in this study. Sources of uncertainty include the calibration of the well chamber used for seed calibration, the uncertainty associated with repeat MOSFET measurements (for all measurements including calibration), MOSFET position errors resulting in uncertainties due to dose gradients and MC simulation uncertainties. Repeat measurement uncertainties are derived from the standard deviation of each set of measurements and will be caused by inconsistency in MOSFET response, variations in seed construction and seed S_K, variations in distribution of radioactive material within the seed and movement of internal seed components. The repeat measurement uncertainty increased with decreasing dose rate and was lowest (2.5%, k=1) for the full 36 seed configuration and highest (5.2%, k=1) for the outer seed group in the 8 seed configuration. TG-43U1(3) data was used to determine the dose rate uncertainty due to the MOSFET position errors (estimated to be <=0.2 mm); this uncertainty is small as the phantom design reduces the

dose gradient around the measurement position. The MC simulation uncertainty is a combination of statistical uncertainty (<1% in all cases) and uncertainties associated with the MC simulation code (<1% up to 5 cm from a seed (122)). Phantom composition uncertainty will affect calibration and measurement MC simulations equivalently and is assumed to be small relative to the other uncertainties. Uncertainty in the polar angle anisotropy correction was not included as the effect of the correction itself is small (see below).

Table 16 Uncertainty analysis for MOSFET measurements

Description	Uncertainty (k=1)
MOSFET Calibration	
Well chamber calibration certificate uncertainty	1.2%
MOSFET calibration measurement uncertainty	3.6%
Dose rate uncertainty due to MOSFET position uncertainty	<1%
MC simulation uncertainty	2%
MOSFET measurement/comparison to MC simulation	
MOSFET repeat measurement uncertainty (varies with measurement configuration, increasing for lower dose rate configurations)	2.5% to 5.2%
Dose rate uncertainty due to MOSFET position uncertainty	1%
MC simulation uncertainty	2%
Total	5.5% to 7.2%

Table 17 compares MC simulated and MOSFET measured dose rates and ISA values (mean of 4 measurements, normalised to S_K 1U) in each of the phantom seed configurations for 6711 and 9011. A correction for polar angle anisotropy has been applied to the 36 seed MOSFET measurements. The polar angle anisotropy results indicate that the MOSFET will under-respond to the dose contribution of the upper seed block by ~7% (no correction is required for middle and lower seed blocks). The proportion of the total dose (from all 3 blocks) contributed by the upper block at the MOSFET position is 27%, 21% and 17% for outer seed group alone, inner

and outer groups together and inner seed group alone respectively (derived from MC simulations of each block separately). This gives corrections (increase) of 1.9%, 1.5% and 1.2% for these measurements respectively.

Table 17 Comparison of MC simulated (MC) and phantom measured (Expt) dose rates and percentage ISA. ISA is calculated as the ratio of the full seed arrangement dose rate to the sum of the inner and outer seed group dose rates. All dose rates are normalised to S_K 1U.

	Sum of the individual dose rates from Inner and Outer seed groups (cGy h^{-1} U^{-1})			Full seed arrangement dose rate (cGy h^{-1} U^{-1})			ISA	
Measurement	**MC**	**Expt**	**% diff**	**MC**	**Expt**	**% diff**	**MC**	**Expt**
6711 8 seeds	6.27	6.29	+0.3%	5.12	5.06	-1.2%	-18.3%	-19.6%
9011 8 seeds	6.10	6.05	-0.8%	5.08	5.14	+1.2%	-16.7%	-15.0%
6711 36 seeds	31.3	32.0	+2.2%	28.6	28.7	0.3%	-8.63%	-10.3%
9011 36 seeds	30.9	30.8	-0.3%	28.5	28.0	-1.8%	-7.77%	-9.1%

3.3.3 Discussion

Multiple seed MC simulation results agreed with phantom MOSFET measurements in terms of both dose rate and the magnitude of the ISA effect within the estimated level of uncertainty for all seed configurations. This provides additional validation of the MC simulation framework beyond the single seed benchmarking work. The results presented are for the mean of 4 independent measurements; individual measurements show variations up to ±7% from MC values which could be due to inconsistency in MOSFET response, variations in seed S_K across the batch of seeds used, variations in the distribution of radioactive material in individual seeds, and MOSFET positioning errors. The uncertainty analysis shows that uncertainty increases as dose rate decreases. The lowest uncertainty in this study, 5.5% (k=1), was for the mean of 4 measurements at a dose rate of 23 cGy h^{-1}. In a clinical implant dose rates are 7 cGy h^{-1} to 14 cGy h^{-1}, positional uncertainties would be greater and it would not be practicable to perform independent repeat measurements, suggesting that the MOSFET would not be suitable for in-vivo dose rate measurements of this sensitivity.

Fade in MOSFET response with accumulated dose was observed to be insignificant, perhaps because the measurements began after 4000 mV (out of the total MOSFET lifetime of 20000 mV) had already accumulated, as fade has been observed to be most significant early in the lifetime of the MOSFET(123). A small amount of polar angle anisotropy was observed, likely caused by the non-uniform shape of the MOSFET bulb, and the presence of the MOSFET cable and radio-opaque marker above the MOSFET bulb. Azimuthal anisotropy of MOSFET response was neglected due to the geometry of the phantom seed configurations but would need to be investigated and included in the uncertainty budget for in-vivo measurements. Note that all MOSFET commissioning was performed using I-125 sources and the results can not necessarily be applied to higher energy photons due to the energy dependence of MOSFET response. For higher energy photons it would be necessary to correct for spectral variations within the phantom, which were found to be insignificant for the I-125 sources used in this study.

A study by Meigooni et al. (114) used TLDs in a solid water phantom with model 6702 and 6711 seeds and found ISA ranging from 6 % to 12% in non-clinical configurations of either 3 or 18 seeds. Other studies of non-clinical seed arrangements have used MC simulation to evaluate ISA. Burns and Raeside[3] found ISA up to 10% for 2 and 4 seed implants, Mobit & Badragan[7] simulated uniformly spaced implants of 27 seeds and found 10% ISA, and Zhang et al.(119) simulated a spherical prostate gland implanted with 48 symmetrically placed seeds and measured ISA of up to 7.5%. One of the objectives of this study was to measure the ISA effect in a phantom using a MOSFET, so the phantom was designed to maximize the ISA effect; this is why some of the ISA values reported in this study (up to 18.3%) are higher compared to previous studies. The ISA effect is lower for the 9011 seed compared to 6711; this is demonstrated both by MC simulations and the phantom measurements (although for phantom measurements the

difference is smaller than the measurement uncertainty). This is discussed further in 4.1.4.

3.3.4 Conclusion

MOSFET phantom measurements have successfully validated the MC simulation framework in terms of dose measurements and measurements of the ISA effect. The ISA effect is lower for the 9011 seed compared to the 6711 seed. The MOSFET has quite a high uncertainty level for LDR dose rate measurements and it would not be possible to measure the ISA effect in-vivo for LDR seed implants.

4 Clinical I-125 investigations

This section describes an MC simulation investigation to assess the effects of ISA and tissue heterogeneity on clinical ^{125}I implant dose distributions. ISA and tissue effects are compared to other uncertainties in ^{125}I implant brachytherapy, and assessed for both TRUS based implant plans and CT based post-implant plans. Tissue models based on delineated structures are compared to models based on CT density data, and CT based models are applied to patients with calcifications. Dose differences are assessed in terms of DVH parameters and analysed by prostate sector. The ISA effect is compared for 6711 and 9011 sources.

4.1.1 Introduction

The TG-43U1 (3) algorithm used for dose calculation routine clinical I-125 seed implant prostate brachytherapy ignores ISA and tissue composition effects that can cause differences between the true dose distribution and TG-43U1 (39). Several studies have investigated the impact of ISA and tissue effects in phantom and clinical scenarios (43, 113-119, 124-127). However only one study, by Carrier et al. (116), has investigated more than a small number of clinical cases. In this study, the impact of ISA and tissue effects on clinical dose distributions is assessed by comparing MC simulations to TG-43U1 dose calculations for 40 prostate brachytherapy patients. Results are compared for TRUS based implant plans and CT based post-implant plans. Sector analysis is applied to investigate whether ISA and tissue effects are uniform or localised to certain sectors of the prostate. Different tissue models are compared: a water based model (to evaluate ISA alone), a simple contour based tissue model and a model based on CT density data. The ISA effect has been shown to depend on seed design (128) and in this study the 6711 and 9011 models are compared. The 9011 has 0.5 mm diameter compared to 0.8 mm for 6711. Section 2.2 shows the seed models in detail. Chibani et al. (113) investigated the effects of calcifications on prostate dosimetry in a study where 1% - 5% of prostate voxels were randomly assigned to calcified tissue. In this study, the impact of localised

calcifications on dosimetry was assessed for patients with visible calcified regions in post-implant CT data, using a tissue model where calcified regions are assigned to a mixture of prostate and calcification based on CT density values.

4.1.2 Methods

Clinical datasets

Two groups of patients were selected for this study. To allow the effect of calcifications to be assessed separately from other tissue effects, 30 patients were selected from recent consecutive cases excluding patients with visible calcification in the post-implant CT data. Then CT datasets from the last 100 patients treated were reviewed, all visible regions of calcification were segmented and the 10 patients with the largest volume of calcification in post-implant CT data were selected. All patients had been treated by the interoperative preplanned technique, as defined by TG-137 (13). All treatments used stranded 6711 seeds (Oncura, a Unit of GE Healthcare, Chalfont St. Giles, UK) with mean S_K of 0.434 U (range 0.379 U to 0.496 U) and prescribed dose of 145 Gy. At implant, the key planning objectives for the TRUS based plan are prostate V100 > 99.8%, prostate V150 55% - 60%, prostate D90 > 185 Gy, PTV V100 > 95%, rectal D2cm^3 < 145 Gy and urethral D10 < 239 Gy (this is a local dose limit different from GEC-ESTRO recommendations (14)). The TRUS plan PTV is the prostate +3mm (0mm posteriorly) and is equivalent to the clinical target volume (CTV) defined in the GEC-ESTRO recommendations (14). All patients had a post-implant CT scan after 4 - 6 weeks and prostate, urethra and rectum contours were delineated on the CT data by a consultant radiologist.

Overview of dosimetric comparisons

The patient datasets described above were used to perform the following dosimetric comparisons:

Comparison of TRUS implant and CT post-implant TG43 dose distributions

Post-implant dosimetry studies generally show that the dose received by the patient is lower than that planned at implant due to seed migration, prostate

oedema and other uncertainties, discussed further in 4.1.4. To allow ISA and tissue effects on dose to be assessed in the context of these dose differences, DVH statistics calculated using the TG-43U1 (3) algorithm by the TPS from TRUS implant and CT post-implant plans are compared for the 30 patients without visible calcifications.

Impact of differences between MC source models and TG-43U1 consensus data

If MC simulations of clinical implants are compared to TPS TG-43U1 calculations, in addition to ISA and tissue effects, there will be dosimetric differences due to differences between the MC source models and TG-43U1 source consensus data, as discussed in 2.2. Minor differences also exist because of the TG-43U1 line source approximation and differences in the DVH calculation methods used in the TPS and the dose analysis framework, as demonstrated in 2.4. These effects are assessed separately from ISA and tissue effects for the 30 patients without visible calcifications by comparing TG-43U1 dose distributions calculated by the TPS to superposition dose distributions calculated using the MC single source dose distributions.

Assessment of ISA and tissue effects

The magnitude of ISA and tissue effects was evaluated in TRUS based implant plans and CT based post-implant plans for 30 patients without visible calcifications. Plans were simulated in a water phantom to assess ISA alone, and in a structure based tissue model. CT based post-implant plans were also simulated using a CT based tissue model and the results compared to the structure based tissue model simulations.

Assessment of the dosimetric effects of calcifications

To allow the impact of calcifications to be assessed, for the 10 patients with visible calcifications, CT based post-implant plans were simulated using CT based tissue models and structure based tissue models (that ignore calcifications).

Comparison of the ISA effect for 6711 and 9011 seed models

To compare the ISA effect for 6711 and 9011 seed models, CT based post-implant plans were simulated in a water phantom using 6711 and 9011 seed models. This comparison was restricted to the first 15 of the 30 patients without visible calcifications.

Dose distributions

The following describes the dose distributions that were compared in this investigation:

(i) Dose distributions calculated by the TPS using TG-43U1 (3) consensus data and the 2D formalism. The TPS calculates dose on a 0.25 mm x 0.25 mm grid on each slice in the dataset (2mm spacing for CT and 5mm for TRUS).

(ii) A superposition dose calculated by summing across all seed co-ordinates the dose from a single seed MC simulation in a water phantom. This excludes ISA and tissue effects but uses the same source as in MC simulations of implants, so that comparisons are not affected by any differences between the MC source and TG-43U1 consensus data. This dose distribution is referred to as MC-SUP.

(iii) An MC simulation of all the seeds implanted in a uniform water phantom, to investigate ISA and exclude tissue effects. This dose distribution is referred to as MC-ISA.

(iv) An MC simulation of the seeds implanted in a simple prostate tissue model based on delineated structures. This dose distribution is referred to as MC-STR-TISSUE.

(v) An MC simulation of the seeds implanted in a tissue model based on the post-implant CT density data. This dose distribution is referred to as MC-CT-TISSUE.

MC simulation methods

For MC simulation of each plan, the seed coordinates and structure sets were exported from the TPS - Variseed^{TM} v8.0 (Varian Medical Systems,

Inc., Palo Alto, CA, USA). Dose calculation from MC simulation results, DVH parameter calculation and all further analysis described below was performed as described in 2.4.

Monte Carlo framework

MC simulations were performed as described in 2.1, using phase space source models (see 2.5). Typical plan simulation time was ~20 hours on a Windows 7^{TM} (Microsoft Corporation, Redmond, WA) PC with Intel® (Intel Corporation, Santa Clara, CA) i7-2600 CPU @ 3.4 GHz. All seeds were assumed to be oriented perpendicular to the plane of the CT or TRUS slices. For MC-ISA simulations the seeds were placed in a 20 cm radius water phantom centered at the mean seed co-ordinate. For tissue model simulations an 8 x 8 x 8 cm^3 lattice with 1 mm^3 voxels was defined, centered at the mean seed co-ordinate and placed inside a 20 cm radius water phantom. For MC-STR-TISSUE simulations, each lattice voxel inside the prostate contour was assigned to prostate tissue; all other voxels in the lattice were assigned to mean male soft tissue, using the tissue composition and densities recommended in TG-186 (40) Table III (density values are 1.04 gcm^{-3} for prostate and 1.03 gcm^{-3} for mean male soft tissue). A model of the 6711 seed (126) was placed over the lattice at each seed co-ordinate. MCNPX automatically handles partial voxels by removing parts of lattice voxels that are overlaid by a seed.

CT density based simulations

For MC-CT-TISSUE simulations, each lattice voxel was assigned density and tissue composition based on the CT post-implant dataset as follows. First the mean CT Hounsfield unit (HU) value for each voxel was calculated. Voxel physical densities were assigned from HU values using the HU/electron density calibration curve for the CT scanner, with physical density calculated as -0.1746 + 1.176*(electron density) (40). Physical density values were rounded to the nearest 0.02 gcm^{-3} to simplify the MCNPX input model. Inside the prostate contour, voxels with HU less than 200 (density 1.2 gcm^{-3}) were assigned to prostate tissue, voxels with HU

greater than or equal to 200 were assigned to be a mixture of prostate tissue and calcification with the relative proportions determined from the voxel density, assuming prostate tissue density 1.04 gcm^{-3} and calcification density 3.06 gcm^{-3}. Outside the prostate contour, voxels with HU less than 200 were assigned to mean male soft tissue, voxels with HU greater than or equal to 200 were assigned to bone. This HU threshold was determined from visual inspection to achieve accurate segmentation of bone in the CT datasets. Tissue composition and density values recommended in TG-186 (40) Table III were used for prostate, mean male soft tissue and bone. The composition of calcification was taken from values for breast calcification in TG-186 (40) Section IV.B.1.c.

As explained above, the physical MC seed model is overlayed on the tissue lattice at each seed co-ordinate. Therefore the CT HU values associated with each seed were replaced in the tissue model as follows. For each seed co-ordinate in turn, all voxels within 2mm of the seed co-ordinate were replaced with the mean HU value of the immediately surrounding voxels (129). This removes the seed HU values and the CT artifact associated with each seed, although some streaking artifacts remain. Following replacement of the seed HU values, density and composition of the affected lattice voxels were assigned as described above.

Dose calculation

For all MC simulations, dose to the medium used for the simulation (water for MC-ISA and tissue for MC-STR-TISSUE and MC-CT-TISSUE) was calculated over an 8 x 8 x 8 cm^3 cube centered at the mean seed co-ordinate. The MCNPX mesh tally was used with tally results converted to dose using the method described in 2.1.3. Each tally cell was 1 mm^3. DVH calculation was based on the slices used in the original TPS post-implant plan (2mm slice spacing for CT, 5mm for TRUS). 2 million particle histories per seed were simulated to reduce the mean statistical component of uncertainty in individual tally cells below 1% inside the prostate and below 2% inside the rectum in all cases.

Analysis of dose differences

DVH statistics were calculated for the prostate, urethra and rectum, and for the PTV in TRUS plans (13) (14). For CT post implant plans, DVH statistics were also calculated for the volume enclosed by the 100% isodose in the MC-SUP dose distribution (hereafter referred to as 'MC-SUP 100% VOL'). This volume was investigated because a PTV is not added in post-implant plans and poorer contrast between prostate and other tissue in CT compared to TRUS may lead to differences in prostate delineation such that the CT prostate volume may not accurately reflect the intended implant volume (130). A sector analysis of the results was performed using the method devised by Bice et al. (131): the prostate was divided superior-inferior into 3 segments: base, mid-gland and apex. Then each segment was divided into 4 quadrants, anterior, left, right and posterior. V100 values were calculated for each segment and for each dose distribution. In addition the seed density and volume of calcification in each sector were calculated. For the 30 patients without visible calcifications, statistical correlation tests were performed to investigate whether there was any correlation between the magnitude of the ISA and tissue effect on CT post-implant prostate D90, and the following parameters: prostate volume, prostate D90, seed density and the magnitude of the ISA and tissue effect on prostate D90 in the TRUS implant plan.

4.1.3 Results

Across all 40 patients, the mean prostate volume was 34.1 cm^3 (range 14.3 cm^3 to 56.0 cm^3). The mean number of seeds used was 84.2 (range 52 to 112). Mean seed density was 2.6 seeds/cm^3 (range 1.9 seeds/cm^3 to 3.6 seeds/cm^3).

Comparison of TRUS implant and CT post-implant dose distributions

The change in DVH values from the original TRUS implant plans to the values post-implant, for the 30 patients without calcifications, due to differences in seed positions and contoured anatomy, can be seen in Table 18 by comparing the TRUS TG43 and CT TG43 columns. These DVH

values are calculated using TG-43U1 (3) by the TPS, and the results are for the 30 patients without calcifications.

Table 18 Mean DVH values for 30 patients, for dose distributions that ignore tissue and ISA effects. Absolute differences are shown with percentage differences in parentheses.

Structure	DVH Parameter	TRUS TG43	CT TG43	Difference to TRUS-TG43	CT MC-SUP	Difference to CT-TG43
Prostate	Volume (cm^3)	35.0	33.2	-	33.2	-
	D90 (Gy)	185.0	149.8	-35.2 (-19.0%)	144.8	-5.0 (-3.3%)
	D98 (Gy)	170.3	115.2	-55.1 (-32.4%)	111.0	-4.2 (-3.6%)
	V100 (%)	99.9	91.0	-8.9 (-3.0cm^3)	89.6	-1.4 (-0.5cm^3)
	V150 (%)	58.9	61.0	2.1 (0.7cm^3)	57.6	-3.4 (-1.1cm^3)
	V200 (%)	19.5	30.5	11.0 (3.7cm^3)	28.0	-2.5 (-0.8cm^3)
Urethra	D10 (Gy)	214.9	248.1	33.2 (15.4%)	243.6	-4.5 (-1.8%)
Rectum	D2cm^3 (Gy)	95.3	112.5	17.2 (18.0%)	110.0	-2.5 (-2.2%)
PTV	Volume (cm^3)	46.2	-	-	-	-
	D90 (Gy)	175.7	-	-	-	-
	V100 (%)	98.0	-	-	-	-

TRUS-TG43: Trans-rectal ultrasound implant plan TG-43U1 dose distribution.

CT-TG43: CT post-implant plan TG-43U1 dose distribution.

MC-SUP: Single MC source superposition dose calculation (excludes ISA and tissue effects).

Impact of differences between MC source models and TG-43U1 consensus data

The impact of using the MC source model in the dose calculation for the 30 patients without calcifications can be seen in Table 18 by comparing the CT TG43 and CT MC-SUP columns. These results are also affected by use of the line source model in TG43-U1, and differences in the DVH calculation method between the TPS and the dose analysis framework, but these effects were shown to be small in 2.4.

Assessment of ISA and tissue effects

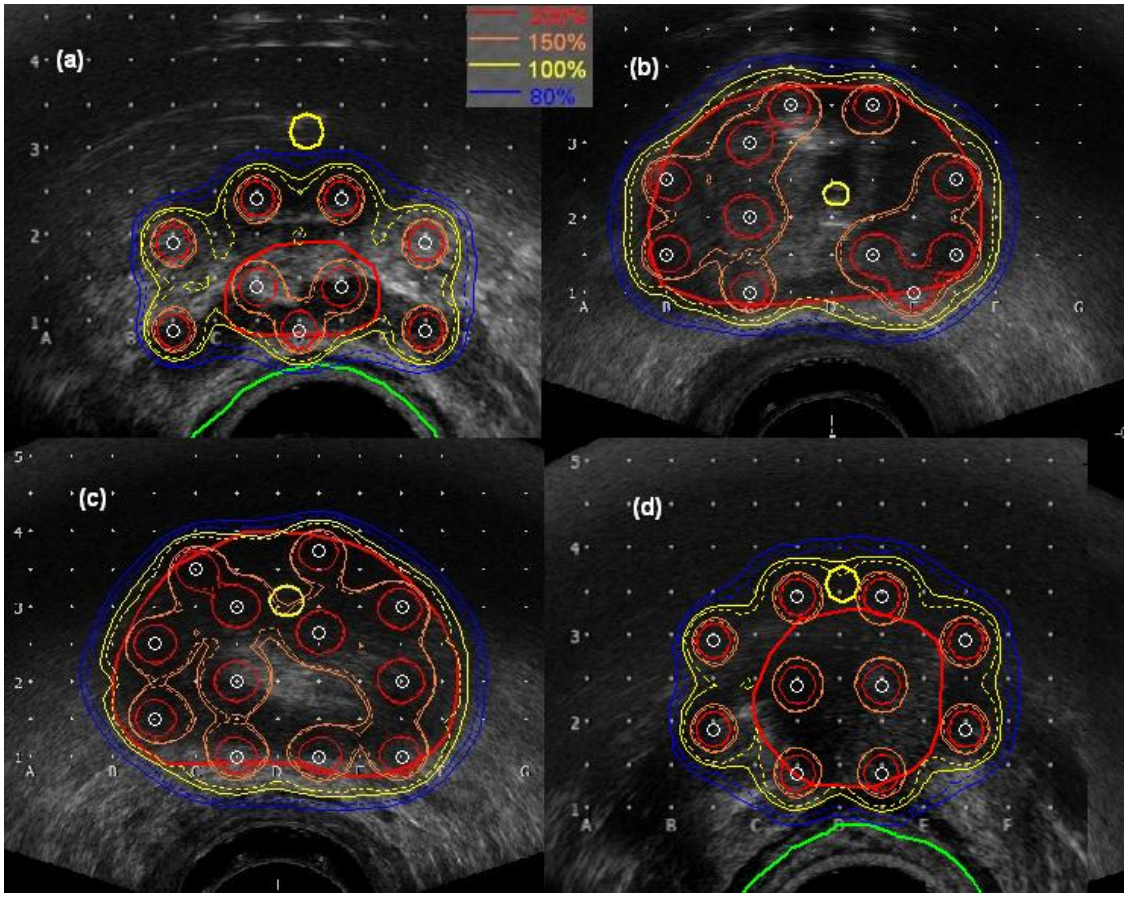

Figure 13 Examples for a single patient comparing superposition dose distribution (MC-SUP) (solid isodoses) and MC simulation dose distribution (dashed isodoses) for the structure based tissue model (MC-STR-TISSUE). Slices are at the base (a), mid-gland (b) and (c) and apex (d). The delineated prostate (red), urethra (yellow) and rectum (green) are also shown.

Table 19 Mean DVH values for 30 patients without visible calcifications, for clinical TRUS implant plans.

Structure	DVH Parameter	DVH Parameter value			Difference from MC-SUP	
		MC-SUP	MC-ISA	MC-STR-TISSUE	MC-ISA	MC-STR-TISSUE
Prostate	Volume (cm^3)	35.0	-	-	-	-
	D90 (Gy)	177.3	173.7	173.1	-3.6 (-2.0%)	-4.2 (-2.4%)
	D98 (Gy)	159.6	156.1	155.7	-3.5 (-2.2%)	-3.9 (-2.4%)
	V100 (%)	99.8	99.5	99.5	-0.3 (-0.1cm^3)	-0.3 (-0.1cm^3)
	V150 (%)	51.4	47.7	47.1	-3.7 (-1.2cm^3)	-4.3 (-1.4cm^3)
	V200 (%)	19.0	17.7	17.7	-1.3 (-0.4cm^3)	-1.3 (-0.4cm^3)
Urethra	D10 (Gy)	216.1	211.4	209.6	-4.7 (-2.2%)	-6.5 (-3.0%)
Rectum	D2cm^3 (Gy)	94.2	91.6	85.9	-2.6 (-2.8%)	-8.3 (-8.8%)
PTV	Volume (cm^3)	46.2				
	D90 (Gy)	163.2	159.2	152.0	-4.0 (-2.5%)	-11.2 (-6.9%)
	V100 (%)	96.4	95.4	92.5	-1.0 (-0.5cm^3)	-3.9 (-1.8cm^3)

MC-SUP: Single MC source superposition dose calculation (excludes ISA and tissue effects).

MC-ISA: Dose from MC simulation in a water phantom (excludes tissue effects).

MC-STR-TISSUE: Dose from MC simulation in a structure based tissue model.

Figure 13 shows examples comparing isodoses for MC-SUP and MC-STR-TISSUE dose distributions from TRUS based implant plans for a single patient. Table 19 summarizes the mean DVH parameter values for these

dose distributions in TRUS based implant plans for the 30 patients without visible calcifications. Across all 30 patients, for TRUS based implant plans the difference between MC-ISA and MC-SUP ranged from -1.5% to -2.8% for prostate D90, 0.0% to -0.8% for prostate V100, -0.4% to -3.6% for urethra D10, -2.0% to -3.7% for rectal D2cm^3, -1.9% to -3.1% for PTV D90 and -0.4% to -2.0% for PTV V100. The difference between MC-STR-TISSUE and MC-SUP ranged from -1.5% to -3.2% for prostate D90, 0.0% to -1.0% for prostate V100, -1.3% to -4.8% for urethra D10, -7.8% to -9.7% for rectal D2cm^3, -4.9% to -8.2% for PTV D90 and -2.3% to -5.8% for PTV V100.

Figure 14 shows examples comparing isodoses for MC-SUP and MC-CT-TISSUE dose distributions from post-implant CT plans for a single patient. The mean density of prostate tissue measured from CT data was 1.03 gcm^{-3}.

Table 20 summarizes the difference in DVH parameter values between the MC simulated dose distributions for these patients. Across all 30 patients, for CT-based post-implant plans the difference between MC-ISA and MC-SUP ranged from -1.7% to -3.9% for prostate D90, -0.7% to -2.1% for prostate V100, -0.8% to -4.0% for urethra D10, -3.3% to -6.3% for rectal D2cm^3, -2.5% to -5.6% for MC-SUP 100% VOL D90 and -3.6% to -5.4% for MC-SUP 100% VOL V100. The difference between MC-CT-TISSUE and MC-SUP ranged from -1.9% to -4.5% for prostate D90, -0.9% to -2.3% for prostate V100, -1.8% to -5.2% for urethra D10, -8.4% to -12.2% for rectal D2cm^3, -6.3% to -10.3% for MC-SUP 100% VOL D90 and -8.3% to -11.5% for MC-SUP 100% VOL V100. For the comparison between MC-STR-TISSUE and MC-CT-TISSUE, in the 30 patients without calcifications all DVH parameters agreed within ±1.5%. The mean density of prostate tissue measured from CT data was 1.03 gcm^{-3}.

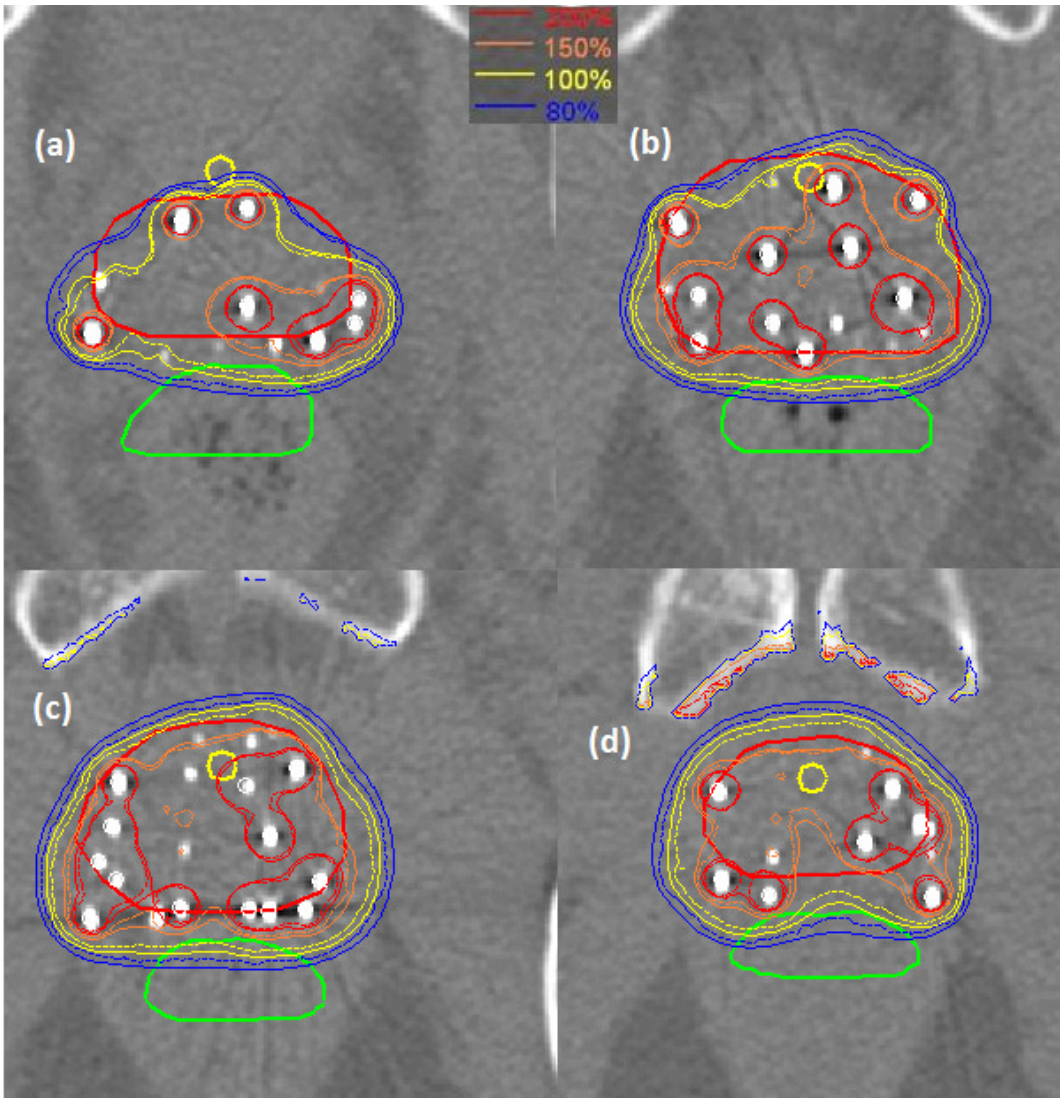

Figure 14 Examples for a single patient comparing superposition dose distribution (MC-SUP) (solid isodoses) and MC simulation dose distribution (dashed isodoses) for the CT density tissue model (MC-CT-TISSUE). Slices are at the base (a), mid-gland (b) and (c) and apex (d). The delineated prostate (red), urethra (yellow) and rectum (green) are also shown.

For the 30 patients without visible calcifications statistical correlation tests showed no statistically significant correlation between the magnitude of the ISA and tissue effect on CT post-implant prostate D90, and any of the following parameters: prostate volume, prostate D90, seed density and the magnitude of the ISA and tissue effect on prostate D90 in the TRUS implant plan.

Table 20 Mean DVH values for MC simulated CT post-implant plans, for 30 patients without visible calcifications.

Structure	DVH Parameter	DVH Parameter value				Difference from MC- SUP		
		MC-SUP	MC-ISA	MC-STR-TISSUE	MC-CT-TISSUE	MC-ISA	MC-STR-TISSUE	MC-CT-TISSUE
Prostate	Volume (cm^3)	33.2	-	-		-	-	-
	D90 (Gy)	144.8	140.9	140.1	140.6	-3.9 (-2.7%)	-4.7 (-3.2%)	-4.2 (-2.9%)
	D98 (Gy)	111.0	107.9	107.2	107.6	-3.1 (-2.8%)	-3.8 (-3.4%)	-3.4 (-3.1%)
	V100 (%)	89.6	88.3	88.0	88.2	-1.3 (-0.4cm^3)	-1.6 (-0.5cm^3)	-1.4 (-0.5cm^3)
	V150 (%)	57.6	54.6	54.2	54.2	-3.0 (-1.0cm^3)	-3.4 (-1.1cm^3)	-3.4 (-1.1cm^3)
	V200 (%)	28.0	25.5	25.4	25.6	-2.5 (-0.8cm^3)	-2.6 (-0.9cm^3)	-2.4 (-0.8cm^3)
Urethra	D10 (Gy)	243.6	236.7	235.4	235.0	-6.9 (-2.8%)	-8.2 (-3.4%)	-8.6 (-3.5%)
Rectum	D2cm^3 (Gy)	110.0	105.1	99.0	98.4	-4.9 (-4.5%)	-11.0 (-10.0%)	-11.6 (-10.5%)
MC-SUP 100% VOL	Volume (cm^3)	48.4	-	-		-	-	-
	D90 (Gy)	158.4	152.7	145.7	145.5	-5.7 (-3.6%)	-12.7 (-8.0%)	-12.9 (-8.1%)
	V100 (%)	100	95.7	90.5	90.3	-4.3 (-2.1cm^3)	-9.5 (-4.6cm^3)	-9.7 (-4.7cm^3)

MC-SUP: Single MC source superposition dose calculation (excludes ISA and tissue effects).

MC-ISA: Dose from MC simulation in a water phantom (excludes tissue effects).

MC-STR-TISSUE: Dose from MC simulation in a structure based tissue model.

MC-CT-TISSUE: Dose from MC simulation in a CT based tissue model.

MC-SUP 100% VOL: The volume enclosed by the 100% isodose in the MC-SUP dose distribution.

Assessment of the dosimetric impact of calcifications

For the 10 patients with calcification, the mean density of the voxels assumed to be mixed prostate/calcification was 1.41 gcm^{-3} (per-patient mean range was 1.32 gcm^{-3} to 1.49 gcm^{-3}, individual voxel range was 1.30 gcm^{-3} to 2.38 gcm^{-3}). The mean volume of calcification for these 10 patients was 0.34 cm^3 (range 0.1 cm^3 to 1.43 cm^3), compared to mean prostate volume of 36.9 cm^3 (range 20.2 cm^3 to 56.0 cm^3).

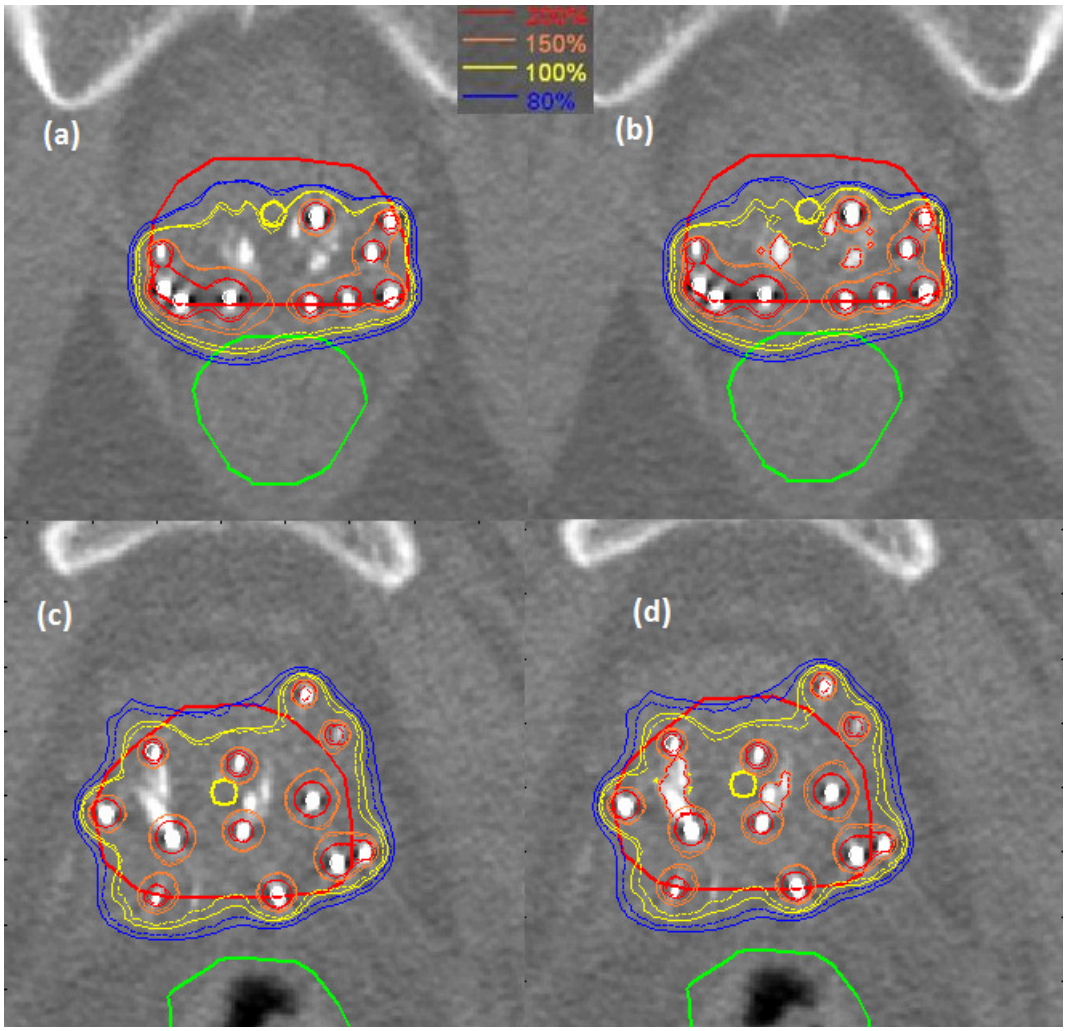

Figure 15 Examples for patients with visible calcifications comparing superposition dose distribution (MC-SUP) (solid isodoses) and MC simulation dose distribution (dashed isodoses). For (a) and (c), MC simulations used the simple tissue model ignoring calcificat ions (MC-STR-TISSUE), (b) and (d) show the same slices with MC simulations using the CT density tissue model accounting for calcifications (MC-CT-TISSUE). The delineated prostate (red), urethra (yellow) and rectum (green) are also shown.

Table 21 Mean DVH values for MC simulated CT post-implant plans, for 10 patients with visible calcifications.

Structure	DVH Parameter	DVH Parameter value			Difference from MC-SUP	
		MC-SUP	MC-STR-TISSUE	MC-CT-TISSUE	MC-STR-TISSUE	MC-CT-TISSUE
Prostate	Volume (cm^3)	36.9	-	-	-	-
	D90 (Gy)	156.0	150.9	149.0	-5.1 (-3.3%)	-7.0 (-4.5%)
	D98 (Gy)	121.5	117.6	116.2	-3.9 (-3.2%)	-5.3 (-4.4%)
	V100 (%)	92.5	91.3	90.6	-1.2 (-0.4cm^3)	-1.9 (-0.7cm^3)
	V150 (%)	59.3	55.7	55.2	-3.6 (-1.3cm^3)	-4.1 (-1.5cm^3)
	V200 (%)	28.7	26.0	26.5	-2.7 (-1.0cm^3)	-2.2 (-0.8cm^3)
Urethra	D10 (Gy)	238.5	230.8	227.9	-7.7 (-3.2%)	-10.6 (-4.4%)
Rectum	D2cm^3 (Gy)	116.4	104.7	104.5	-11.7 (-10.1%)	-11.9 (-10.2%)
MC-SUP 100% VOL	Volume (cm^3)	53.4	-	-	-	-
	D90 (Gy)	158.5	145.4	144.3	-13.1 (-8.3%)	-14.2 (-9.0%)
	V100 (%)	100	90.3	89.5	-9.7 (-4.7cm^3)	-10.5 (-5.1cm^3)

MC-SUP: Single MC source superposition dose calculation (excludes ISA and tissue effects).

MC-STR-TISSUE: Dose from MC simulation in a structure based tissue model (ignores calcifications).

MC-CT-TISSUE: Dose from MC simulation in a CT based tissue model (includes calcifications).

MC-SUP 100% VOL: The volume enclosed by the 100% isodose in the MC-SUP dose distribution.

Figure 15 compares isodoses illustrating the effects of calcifications, where (a) and (b) show an example where the calcification affects the 100% isodose, and (c) and (d) show an example where seed placement means that the calcification has little effect on the 100% isodose. Table 21 summarizes the DVH values from the dose distributions for the 10 patients with calcifications, for CT post-implant plans. MC-ISA results are excluded as these were similar to those shown in Table 2. The difference between MC-CT-TISSUE and MC-SUP ranged from -2.7% to -7.4% for prostate D90, -0.8% to -4.8% for prostate V100, -2.6% to -7.6% for urethra D10, -9.1% to -11.9% for rectal $D2cm^3$, -7.5% to -10.2% for MC-SUP 100% VOL D90 and -8.9% to -12.3% for MC-SUP 100% VOL V100. DVH parameter values were generally lower for MC-CT-TISSUE compared to MC-STR-TISSUE, with maximum difference -3.6% for prostate D90, -2.9% for prostate V100, -4.0% for urethra D10. However prostate V200 values were higher for MC-CT-TISSUE compared to MC-STR-TISSUE, with maximum difference 1.2%.

Sector analysis

Sector analysis of TRUS based implant plans showed that ISA and tissue effects were very similar across all sectors, so results are not included here. Table 22 shows the results of sector analysis of the CT based post-implant plans for 30 patients without calcifications. The maximum reduction in V100 for any one patient in any prostate sector was -9.7% for the base anterior sector. For the 10 patients with calcifications the left, right and posterior base sectors had the highest percentage of calcification by volume with the maximum in any sector being 6.7%. The results of sector analysis for patients with calcifications were similar to those in Table 4 in terms of the pattern of V100 reductions across sectors, so are not included here. Overall each sector showed slightly higher reductions in V100 compared to patients without calcification with the base anterior sector having the highest mean (-6.4%) and maximum (-13.8%) reductions in V100.

Table 22 Sector analysis results (mean values) for 30 CT-based post-implant plans.

Sector	Base Ant	Base Left	Base Right	Base Post	Mid Ant	Mid Left
Prostate						
Sector volume (cm^3)	1.8	2.2	2.2	1.5	3.2	4.1
Seed density (seeds/cm^3)	0.79	1.20	1.18	1.50	1.28	2.35
MC-SUP V100 (%)	54.6	81.0	79.9	87.1	91.1	99.3
MC-ISA V100 (%)	51.4	78.8	77.6	85.2	89.3	99.0
MC-ISA – MC-SUP (%)	-3.2	-2.2	-2.3	-1.9	-1.8	-0.3
MC-CT-TISSUE V100 (%)	50.4	78.5	77.3	85.1	88.7	89.9
MC-CT-TISSUE – MC-SUP (%)	-4.2	-2.5	-2.6	-2.0	-2.4	-0.4

Sector	Mid Right	Mid Post	Apex Ant	Apex Left	Apex Right	Apex Post
Prostate						
Sector volume (cm^3)	4.2	2.7	2.3	3.4	3.3	2.4
Seed density (seeds/cm^3)	2.07	2.09	1.40	2.11	2.08	1.78
MC-SUP V100 (%)	98.6	99.8	91.0	96.8	95.7	95.7
MC-ISA V100 (%)	98.3	99.8	89.4	96.0	94.9	94.9
MC-ISA – MC-SUP (%)	-0.3	0	-1.6	-0.8	-0.8	-0.8
MC-CT-TISSUE V100 (%)	98.2	99.6	89.0	95.9	94.8	94.7
MC-CT-TISSUE – MC-SUP (%)	-0.4	-0.2	-2.0	-0.9	-0.9	-1.0

MC-SUP: Single MC source superposition dose calculation (excludes ISA and tissue effects).

MC-ISA: Dose from MC simulation in a water phantom (excludes tissue effects).

MC-CT-TISSUE: Dose from MC simulation in a CT based tissue model.

Comparison of the ISA effect for 6711 and 9011 seed models

Table 23 compares the ISA effects for 6711 and 9011 seeds, using results from MC simulations in a water phantom, for the CT post-implant plans for the first 15 of the patients without visible calcifications. The range in values for the ISA effect across all 15 patients for 6711 were prostate D90 -2.2% to -3.9%, urethra D10 -2.0% to -13.9% and 100% sup dose volume D90 -3.0%

to -5.8%. For 9011 the range in values for ISA effect were prostate D90 -1.2% to -1.9%, urethra D10 -0.7% to -12.3% and 100% sup dose volume D90 -1.5% to -3.0%.

Table 23 Mean DVH values for 15 clinical cases comparing MC-SUP and MC-ISA to assess the ISA effect for 6711 and 9011 seeds.

Structure	DVH Parameter	6711 seeds			9011 seeds		
		MC-SUP	MC-ISA	ISA effect	MC-SUP	MC-ISA	ISA effect
Prostate	Volume (cm^3)	35.2	35.2	-	35.2	35.1	-
	D90 (Gy)	137.5	133.3	-4.2 (-3.0%)	133.8	131.6	-2.2 (-1.6%)
	D98 (Gy)	101.4	98.3	-3.1 (-3.1%)	98.6	97.0	-1.6 (-1.6%)
	V100 (%)	87.6	86.2	1.4 (-0.5 cm^3)	86.3	85.6	0.7 (-0.3 cm^3)
	V150 (%)	57.0	53.8	3.2 (-1.1 cm^3)	54.1	52.3	1.8 (-0.6 cm^3)
	V200 (%)	26.7	24.1	2.6 (-0.9 cm^3)	24.7	23.2	1.5 (-0.5 cm^3)
Urethra	D10 (Gy)	255.4	244.1	-11.3 (-4.4%)	248.5	240.5	-8.0 (-3.2%)
Rectum	D2cm^3 (Gy)	119.2	113.7	-5.5 (-4.6%)	115.6	112.5	-3.1 (-2.7%)
MC-SUP 100% VOL	Volume (cm^3)	50.6	50.6	-	49.1	49.1	-
	D90 (Gy)	158.8	152.8	-6 (-3.8%)	158.6	155.3	-3.3 Gy (-2.1%)
	D98 (Gy)	147.6	141.7	-5.9 (-4.0%)	147.6	144.4	-3.2 Gy (-2.2%)
	V100 (%)	100	95.5	4.5 (-2.3 cm^3)	100	97.5	2.5 (-1.2 cm^3)

MC-SUP: Single MC source superposition dose calculation (excludes ISA and tissue effects).

MC-ISA: Dose from MC simulation in a water phantom (excludes tissue effects).

MC-SUP 100% VOL: the volume enclosed by the 100% isodose in the superposition dose distribution.

4.1.4 Discussion

This study has investigated the impact of ISA and tissue composition effects in prostate seed implant brachytherapy. The results show that there are differences between TG-43U1 (3) dose calculations and MC simulated dose distributions that take account of seed interactions and tissue composition.

However the differences are small compared to other uncertainties in seed implant brachytherapy. In this study, for 30 patients without visible calcifications, the mean decrease in post-implant prostate D90 due to ISA and tissue effects was -2.9%. Differences between the source model used in this study (which agrees with other recent investigations (106, 107, 126)) and TG-43U1 consensus data produce a reduction in mean prostate D90 of -3.3%, similar in magnitude to the ISA and tissue effect. By comparison the mean reduction in D90 (as calculated by TG-43U1) from the TRUS based implant plan to post-implant was -19%. A study by Kirisits et al. estimated the combined uncertainties for post-implant planning as 11% (k=1), including uncertainty in source calibration, treatment planning reference data, ISA, tissue composition effects, imaging, contouring and anatomy changes from implant to post-implant (38). In that study, ISA and tissue composition effects were estimated to contribute 4% and 5% respectively to the uncertainty budget (38).

This study has also investigated the ISA and tissue effect on the volume defined by the 100% isodose (MC-SUP 100% VOL) in post-implant data. The mean volume in the CT post-implant MC-SUP dose distribution, 48.4 cm^3, closely matched the TRUS implant PTV volume, 46.2 cm^3, underlining the clinical relevance of investigating this volume for post-implant plans - although it is possible that seed placement errors may cause the post-implant 100% isodose volume to be offset from the prostate. The ISA and tissue effects are larger for the MC-SUP 100% VOL compared to the prostate, for example the MC-SUP 100% VOL D90 was reduced by 8.1% and V100 by 9.7%. This illustrates that the effects have most impact at the periphery of an implant. ISA contributes most of the dose reduction for the prostate but ISA and tissue effects are comparable for the 100% isodose volume. This is because ISA and tissue effects act differently on the dose distribution. ISA reduces the dose at all points inside the implant, although differences are more noticeable in lower dose areas which tend to be peripheral. As most prostate tissue models have higher effective atomic number and density than

water, the effect of modeling tissue is to increase absorbed dose inside the implant, but attenuation also generally increases, reducing dose peripherally.

Carrier et al. (116) studied 28 post-implant patients planned with seed strength 0.76 U, mean seed density 1.7 seeds/cm^3 and mean clinical D90 of 169 Gy, prostate D90 was reduced by -6.8 Gy (-4.0%) and -4.1 Gy (-2.4%) by ISA and tissue effects respectively. Their study used the SelectSeed (Nucletron, an Elekta company (Elekta AB)) which is similar in construction to the 6711 seed model. In our study, we used a lower seed activity (0.379 U to 0.496 U) and higher mean seed density (2.6 seeds/cm^3) but found a comparable ISA effect. The tissue effect measured by Carrier et al. (116) is greater than we observed for the prostate but smaller than we observed for the MC-SUP 100% VOL, which could be explained by differences in CT prostate contouring. Other studies that have investigated ISA and tissue effects in clinical implants have only modeled a small number of implants, but have found similar results, with D90 reductions in the range 2% to 6% (113, 117, 118, 124).

This study also investigated ISA and tissue effects in TRUS implant plans. Compared to CT post-implant plans, the overall effect on DVH parameters is very similar. There was no correlation between the magnitudes of the effects in the two plans: it would not be possible to predict the post-implant ISA effect from the TRUS plan.

Comparison of a simple tissue model where composition and density are assigned based on structures and a CT based model with composition assigned based on structures and voxel density assigned from CT data found maximum difference in any DVH parameter of 1.5% for patients without calcifications. This illustrates that a structure-based model would be sufficient to implement advanced dose calculations for TRUS-based implant plans when CT data is not available, at least for patients without calcifications. TRUS can also be used to identify patients with

calcifications, although CT would be required to quantify the calcification density.

Investigation of the effect of calcification on prostate brachytherapy dosimetry is limited by lack of accurate knowledge of the composition of calcified prostate tissue. A study by Chibani et al. (113) assumed that calcification was uniformly and sparsely distributed throughout the prostate and found that 1% calcification lead to a -7.8% reduction prostate D90. In this study, we have modeled localised calcifications using the voxel density determined from CT data to estimate the relative proportion of prostate tissue and calcification in each voxel, and found a maximum D90 reduction of -7.4% with mean -4.5%. Although only 10 patients were modeled for this part of the study, they were selected from a group of 100 as having the largest volume of calcification, illustrating that although calcifications can have significant impact for an individual patient's dosimetry, the expected impact over a group of patients is small.

Sector analysis of CT post-implant plans has shown that ISA and tissue effects cause greatest reduction in 100% isodose coverage in anterior sectors throughout the prostate, and in all sectors at the base. These sectors are the most commonly under-dosed in post-implant plans and the results illustrate that ISA and tissue effects are not uniform but have more impact in lower dose and peripheral areas of an implant. In sector analysis of patients with calcifications, the pattern of dose reduction was the same for patients with calcification as for those without, and there was no correlation between the volume of calcification in a sector and the V100 reduction in that sector. This is because the dose shadow behind a calcification depends on the relative positions of seeds and calcifications and can occur in a sector adjacent to the calcification, particularly as calcifications observed in this study were located centrally in the prostate.

The ISA effect depends on seed design and a study by Afsharpour et al. (128) found that the Selectseed was the most attenuating seed model with an

average 4.8% reduction in prostate D90 for clinical implants compared to an average 1.5% reduction for the least attenuating (IBt Optiseed - this is a ^{103}Pd source with a polymer shell encapsulation). The 6711 seed was not included in that study; it is similar in design to the Selectseed, but has a slightly smaller silver core. In this study the ISA effect is compared for 6711 and the thinner 9011 model. The phantom measurements discussed in 3.3 show that the 9011 is less attenuating in terms of dose at a point. The clinical data show that using the 9011 compared to 6711, the impact of ISA on all DVH parameters is reduced, with ISA effect values being almost half for 9011 compared to 6711. ISA effect for the 9011 is comparable to that for the IBt Optiseed. This benefit of reduced ISA effect using the 9011 seed must however be seen in the context of overall uncertainties in seed implant brachytherapy as discussed above.

Previous investigations into ISA and tissue effects (113, 116-118, 124) have noted that, because the existing dose prescription is sufficient to achieve good patient outcomes, it might be necessary to reduce the prescribed dose if advanced dose calculation methods were routinely implemented in prostate seed implant brachytherapy. This study has shown that any such change would need to take account of the variations in ISA and tissue effects between sectors of the prostate, and between patients, for example due to calcifications.

This study has some limitations. For the investigation of ISA, all seeds were assumed to have the same orientation. Tissue composition models are assumed and more accurate dosimetric results would be achieved if the composition of soft tissues and calcifications could be measured directly. Dose results are sensitive to CT artifact correction methods. In this study artifacts were corrected by replacing each a small volume around each seed with the mean HU of immediately surrounding voxels. This will not completely remove all artifacts as there are some streak artifacts that run across the CT data. However the close agreement between CT based and structure based models illustrates that these artifacts have minimal impact

on dose. Another limitation is that the artifact correction would remove any regions of calcification that are obscured by the seed CT image, so that the volume of calcification may have been underestimated.

4.1.5 Conclusion

Advanced dose calculation methods that take account of ISA and differences in tissue composition from water, show that the dose delivered in clinical I-125 seed implants is different from that calculated by TG-43U1. These differences lead to reduced DVH parameter values especially for patients with calcifications. Dose reductions particularly affect peripheral dose and areas of the implant with relatively poorer coverage, the impact on the volume encompassed by the 100% isodose is more significant that the impact on the prostate. However dose reductions are less significant compared to other uncertainties in post-implant dosimetry such as seed placement errors, anatomy changes and imaging and contouring uncertainties.

5 Multi-parametric MRI guided focal boost in HDR prostate brachytherapy

This section describes work done to investigate the feasibility of incorporating mp-MRI in HDR prostate brachytherapy to deliver focal boost treatments, in a pilot study of 30 patients. The investigation includes evaluating uncertainties of tumour delineation using mp-MRI and image registration of MRI to TRUS. Dosimetry of focal boost treatments is compared to standard treatments to evaluate the level of boost dose that can be achieved while maintaining the same normal tissue dose constraints as for standard treatments. The first part of this section describes the pilot study using MRI scans acquired specifically for tumour delineation to incorporate into brachytherapy treatment planning. On completion of the pilot study, an investigation into incorporating staging MRI scan data for focal boost treatment planning was performed, as funding for further pre-treatment MRI scans was not available. This work is described in the second part of this section.

5.1 Initial feasibility study

5.1.1 Introduction

In radiotherapy for prostate cancer, it is standard practice to prescribe one dose level to the whole prostate, as prostate cancer is known to be a multi-focal disease. Tumour control probability may be improved by delivering a focal boost dose to a DIL (98), as these lesions are the most common site of recurrence (11). Previous studies have investigated focal boost in radiotherapy. A study by Gauder et al. (132) of sextant biopsy guided dose escalation in permanent seed implant prostate brachytherapy treatments achieved 95% DIL coverage with 150% of the 144Gy prescription dose with no difference in acute and late toxicities compared to a group of patients who did not receive the dose escalation. Focal boost doses of up to 150% of prescription dose have been achieved in HDR prostate brachytherapy planning studies for DILs identified using MRI and MRSI (96) (95). Focal

boost dose has also been investigated for IMRT and volumetric modulated arc therapy (VMAT) treatments with DIL volumes identified using MRSI and DCE-MRI (97, 133, 134).

Focal boost techniques require accurate methods for tumour delineation. Mp-MRI techniques such as T2W MRI, MRSI, DCE-MRI and DWI in combination**,** improve sensitivity and specificity of prostate cancer detection (56) (57) (58) (59). Prostate radiotherapy patients often receive neo-adjuvant hormone therapy, and this has been shown to reduce the conspicuity of tumour tissue using mp-MRI in the prostate (135, 136).

This study investigates the feasibility of using mp-MRI for tumour delineation and HDR prostate brachytherapy to deliver focal boost dose, in a group of patients who are being treated using HDR prostate brachytherapy in combination with external beam treatment. The majority of HDR prostate brachytherapy patients are given hormone therapy, so one aspect of the study is to investigate if tumour delineation for treatment planning is possible for these patients. The study also investigates how the achievable focal boost dose is affected if a margin is added to the tumour region, to account for delineation and image registration uncertainties.

This pilot study of 30 patients does not have sufficient patient numbers to determine whether focal boost doses improve prostate cancer control however the patients in the study are followed up to assess whether there is any increase in normal tissue toxicities resulting from the focal boost treatment. This follow up was done by the clinical oncology consultants and registrars working with the patients but a summary of the results is included here for completeness.

5.1.2 Method

Patients

30 patients (ages 57-77 years, mean 66 years) with biopsy proven prostate cancer, scheduled for prostate HDR brachytherapy between February 2011 and November 2013, were recruited to the study. Informed consent was

obtained from all patients and the local ethics review committee approved the study. Patient prostate staging data is presented in Table 24. MRI scans took place in the week before HDR brachytherapy, 2.5 - 5 months (mean 4 months) after biopsy. Of 30 patients, 27 had received neo-adjuvant hormone therapy for between 2 and 5 months (mean 3 months) prior to the MRI scan. For the first 15 patients in the study, MRI data was analysed retrospectively and patients received the standard treatment (15Gy to the whole prostate in a single fraction of HDR brachytherapy, followed by 37.5Gy in 15 fractions of external beam therapy to the prostate and seminal vesicles) (35). For the remaining 15 patients, a focal boost treatment was given if tumour could be identified in the mp-MRI data. Gastro-intestinal and genitourinary toxicity was recorded using CTCAE v4.0 (137) at 6 weeks and then 3 monthly intervals following treatment.

MRI acquisition

The mp-MRI techniques used were T2W MRI, DWI and DCE-MRI. MRSI was not used as it was thought this would make the scan time uncomfortably long and DCE-MRI is preferred over MRSI for prostate cancer localization according to a recent European consensus meeting (138). Scans were performed on an Avanto (Siemens AG, Munich, Germany) 1.5T scanner, using phased-array pelvic and spine coils for signal reception. Endo-rectal coils were not used as phased-array coils are adequate for prostate cancer detection (139) and because of the need to reduce distortion in the MRI images for treatment planning use. All MRI images were acquired in transverse-oblique planes such that slice-by-slice the posterior edge of the prostate remains in as consistent a position as possible. This is designed to assist matching of prostate position in MRI to TRUS image registration for treatment planning. T2W MRI used a turbo-SE sequence with repetition time (TR) 4970ms, echo time (TE) 87ms, echo train length 13, 0.7mm pixel size, slice thickness 2.5mm (no slice gap), 28 slices, field of view (FOV) 220mm. DWI MRI used a single shot SE-EPI sequence with TR 3000ms, TE 77ms, 1.4mm pixel size, slice thickness 4.5mm (0.5mm gap), 14 slices, FOV 220mm, b-values 0, 150, 500 s/mm^2 (first 15 patients) or 0, 150, 500,

750 s/mm^2 (subsequent patients). ADC maps generated by the scanner from all 3 b-values were used for subsequent analysis. DCE MRI used a 3D spoiled gradient echo sequence with TR 4.4ms, TE 1.2ms, flip angle 21°, 2x2x5mm pixel size, FOV 320mm and 20 slices (the superior 6 slices were added to the imaging volume for the purpose of reducing in-flow effects (140)). 200 acquisitions were acquired with 2s time resolution. A bolus injection of 0.1mmol/kg Dotarem® (Guerbet Group, Villepinte, France) was administered at 3ml/s after 10s scan time. A patient specific AIF was measured in the iliac artery, and pixel maps of K^{trans} were generated by fitting a Tofts (76) 1-compartment model to concentration-time data (approximated using relative change in signal intensity (141)) obtained from the DCE acquisition, using Platform for Research in Medical Imaging (142).

Tumour delineation

A manual rigid registration was applied to align the DWI ADC and DCE K^{trans} maps to the T2W images, to account for differences in prostate position due to patient movement or, for the DWI ADC map, distortion resulting from EPI susceptibility artefacts. The registration was evaluated from baseline images (the b=0 image for DWI, the first DCE acquisition for DCE). The focal gross tumour volumes (F-GTVs) for the treatment planning study were delineated based on having low intensity on T2W MRI, low ADC map values and high K^{trans} map values, by one of two consultant radiologists, who had 18 years and 11 years experience of prostate MRI. To allow quantitative comparison of MRI data values, normal tissue regions were delineated when regions with high intensity on T2W MRI, high ADC map values and low K^{trans} map values, contra-lateral to the tumour regions, could be identified.

Treatment planning study

The HDR prostate brachytherapy procedure involves the following steps, using the Oncentra Prostate™ v4.0 (Elekta AB) treatment planning system. HDR needles are inserted under TRUS guidance, a TRUS volume is acquired with the needles in position, the prostate, urethra and rectum are

contoured on the TRUS volume and a 3mm margin (0mm at the posterior boundary of the prostate), to encompass potential microscopic spread of disease, is added to create a PTV. This follows GEC-ESTRO recommendations although the terminology used here is different: the delineated prostate structure may be expanded to include any macroscopic extracapsular disease and/or seminal vesicle involvement, and the PTV is equivalent to the CTV defined by the GEC-ESTRO recommendations (15). Needles are reconstructed, a treatment plan is created using DVH-based inverse optimization (111) to achieve prostate V100>95% and PTV V100>90% (100% isodose = 15Gy). Note this study was completed before the recent GEC-ESTRO update which recommends PTV V100>95% (15). If necessary, small manual adjustments to dwell times are made to refine the treatment plan. The dose constraints for OARs are urethra D10 <17.5 Gy and rectum $D2cm^3$ <11.8Gy, V100 = 0%.

For the treatment planning study, T2W MRI was registered to the TRUS images acquired after needle insertion using the manual rigid registration function in Oncentra Prostate™ (Elekta AB). To allow for uncertainties in tumour delineation and image registration, a margin (determined from the uncertainty estimation work described below) on each F-GTV was used to generate a focal PTV (F-PTV) structure. F-PTV(s) were not allowed to intersect the urethra or extend beyond the prostate capsule. No margin is applied to account for microscopic tumour spread as prostate tissue outside the F-PTV is still prescribed the standard 15Gy treatment.

For each patient in the study two treatment plans were generated: a standard plan prescribing the same dose to the whole prostate and a focal boost plan. For the first 15 patients in the study, standard plans were delivered and focal boost plans were generated retrospectively after treatment. For the remaining 15 patients in the study, focal boost plans were delivered (unless no tumour was visible in mp-MRI data) and standard plans were generated retrospectively after treatment. Focal boost plans were optimised to maximize dose to the F-PTV(s), but used the same dose objectives and

constraints for prostate, PTV, urethra and rectum as in the standard plans. For focal boost plans produced retrospectively, up to 2 additional HDR needles were added to target the F-PTV(s). Dose optimization was performed using DVH-based inverse optimization (111) with small manual adjustments to dwell times where necessary to improve the treatment plan. The objective for the optimizer was set to give 150-200% of the prescription dose to the F-PTV.

Estimation of margin for uncertainty in tumour delineation and image registration

The margin required for uncertainty in tumour delineation and image registration was investigated as follows. For tumour delineation, the MRI datasets of five patients, selected randomly from first 15 patients, were contoured four times in total, three times by the same consultant radiologist, with at least 4 weeks gap between each contouring session, and one time by another consultant radiologist, to give four different contours for each F-GTV. The four contours were used to estimate a margin for tumour delineation uncertainty by incrementally applying a margin (increasing the margin size one pixel at a time) to each contour until it completely covered each other contour for that F-GTV. The margin calculation was performed separately for each anatomical direction. To illustrate the method, Figure 16 shows how the calculation would work for an idealised pair of contours, labeled as CTR1 and CTR2, on a single slice. In this example the margin would be 2mm anterior, 5mm left, 0mm posterior (as CTR2 is inside CTR1) and 0mm right (as CTR1 and CTR2 match). The method was also applied to superior and inferior directions. Results for all F-GTVs across the 5 patients were combined, and the 90th percentile value was taken as the margin required for tumour delineation error, as this represents the margin where one contour would cover another 90% of the time (90% was chosen as this matches the criterion often applied in external beam radiotherapy margin derivation (143)).

To assess inter and intra-observer variability in image registration, for the same five patients, the MRI-TRUS image registration was repeated five times in total by three physicists. A rigid registration has six parameters: a translation and an angle of rotation in each of 3 imaging planes (left-right, anterior-posterior and superior-inferior). Differences in image registration were assessed as follows. For each patient the standard deviation from five registration attempts was calculated for each of the six registration parameters. The margin was taken as two times the mean of the standard deviation values for the five patients, in each direction. Rotation values were converted to distances by calculating the distance corresponding to the rotation at the surface of a sphere of radius 2cm (to represent the prostate). The estimated margin was then applied to all 30 patient's F-GTVs to generate F-PTVs for the treatment planning study as described above.

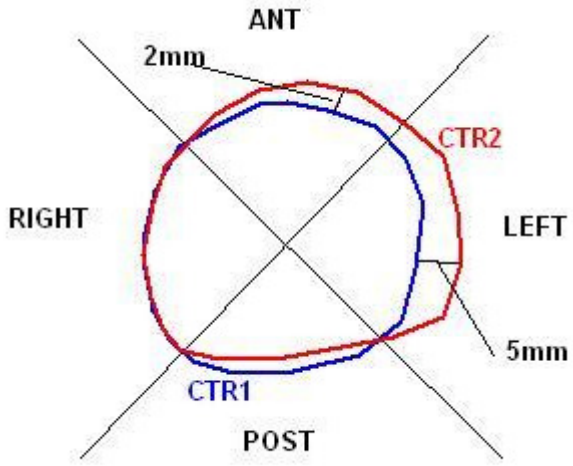

Figure 16 Idealised example of margin calculation method for tumour delineation uncertainty study

Margin consistency test

The combined margin was tested for consistency on a further 5 patients. For these patients tumour delineation was repeated separately by each of the two radiologists, and the resulting F-GTVs were registered to TRUS treatment planning images. The F-PTV used in the treatment planning study was overlaid on the F-GTVs and the effectiveness of the margin was assessed by

calculating the percentage of the F-GTVs (from the repeat delineations) covered by the original F-PTV.

5.1.3 Results

Patient logistics

Two patients were unable to have MRI scans for logistical reasons so were not included in the study. 2 patients were determined to be unfit for surgery after the MRI scan, however standard and focal boost treatment plans were produced for these patients and their results are included in the dosimetric results for this study.

Tumour delineation

In most cases small rigid registration shifts were required to align the mp-MRI datasets. The median shift was 2.1mm (range 0-10mm). F-GTVs were identified in 25 of the 28 patients who had an MRI scan. The three patients in whom tumour tissue could not be identified were all in the second group of 15 patients considered for prospective treatment. F-GTVs had median volume 0.8 cm^3 (range 0.1-23.0 cm^3). Two F-GTVs (bi-lateral) were identified in 8 patients, giving a total of 33 F-GTVs in the 28 patients. Of these, 3 were in anterior central gland tissue, 4 involved peripheral zone and central gland tissue and 26 were confined to the peripheral zone. All F-GTVs were in areas positive for prostate cancer at biopsy. Normal tissue regions were identified in 13 patients and all normal regions were in areas testing negative for prostate cancer at biopsy. Table 24 lists the F-GTV volumes for each patient. Figure 17 shows an example of tumour delineation for one patient from the study.

Table 24 Clinical details, volumes and dosimetry results for the 30 patients included in the study. The F-PTV D90 and V150 are for the plan optimised for focal boost with additional needles added to target the F-PTV. 15Gy is 100% dose. Patients 8 and 28 were not scanned so are not included.

Patient	Clinical Stage	PSA (ng/ml)	Gleason score	Prostate Volume (TRUS) (cm^3)	Volume of F-GTVs (cm^3)	Volume of F-PTV (cm^3)	F-PTV D90 (Gy)	F-PTV V150 (%)
1 *	T1c	5	3+4	24.3	4.1	9.0	20.7	77.5
2	T2c	31	4+3	29.7	0.4	2.7	20.5	75.9
					0.2	1.3	19.9	68.9
3	T1c	4	3+4	29.7	3.7	9.5	20.2	70.6
					0.2	1.1	20.9	75.8
4	T3a	39	4+4	29.2	0.9	4.0	18.9	61.6
5	T2c	11	4+3	58.3	0.2	1.4	25.0	99.4
6	T2c	10	4+3	38.7	1.9	6.2	19.3	54.9
7 *	T3a	7	3+4	44.0	4.0	9.8	22.8	91.2
					0.8	3.5	22.7	91.9
9	T3a	3	3+4	23.7	1.1	4.9	20.4	66.5
					0.3	1.6	22.8	91.6
10	T3b	27	3+4	50.9	23.0	36.0	18.0	41.9
11	T3a	35	3+4	31.4	2.6	7.6	20.5	73.7
					0.2	1.2	24.4	97.7
12	T3a	30	4+3	23.6	4.0	10.2	19.5	67.0
13	T3a	21	4+5	19.0	0.4	2.4	20.1	74.2
14	T3a	6	4+3	23.1	0.5	2.5	22.8	91.2
					0.3	2.4	23.6	97.4
15	T2c	5	4+3	24.2	0.4	3.0	23.0	92.8
16 *	T2c	8	3+4	29.7	5.5	12.6	21.1	81.6
17	T1c	11	3+3	31.3	-	-	-	-
18	T3a	4	3+4	22.1	0.2	1.5	23.8	96.4
					0.8	3.6	23.5	94.5

Patient	Clinical Stage	PSA (ng/ml)	Gleason score	Prostate Volume (TRUS) (cm^3)	Volume of F-GTVs (cm^3)	Volume of F-PTV (cm^3)	F-PTV D90 (Gy)	F-PTV V150 (%)
19	T3a	8	4+4	29.2	0.1	0.5	23.6	94.3
					0.8	4.6	17.5	29.1
20	T3a	15	4+3	22.0	1.1	4.6	23.2	93.1
21 **	T3a	6	5+4	47.9	2.6	8.7	21.9	85.6
22	T2c	5	4+3	19.8	1.8	5.8	19.7	71.9
23	T3a	4	3+4	24.6	-	-	-	-
24 **	T3a	4	3+4	13.2	0.2	1.6	21.9	87.0
25	T3a	7	3+4	34.7	1.4	6.1	20.1	70.7
26	T3a	11	3+3	31.0	-	-	-	-
27	T3b	14	3+4	32.3	3.3	9.2	21.4	82.2
29	T3a	21	3+4	59.3	0.8	2.9	24.6	97.5
30	T2c	8	3+4	25.1	0.2	1.6	23.6	94.5

* Did not receive neo-adjuvant hormone therapy. All other patients had undergone between 2-5 months hormone therapy at the time of the MRI scan.

** Not treated as unfit for surgery.

The mean ADC values in F-GTV and normal tissue regions were 1.19 $x10^{-3}$ mm^2/s and 1.74 $x10^{-3}$ mm^2/s respectively. There was considerable inter-patient variation with per-patient mean ADC values 0.87 - 1.48 $x10^{-3}$ mm^2/s for the F-GTV and 1.49 - 2.05 $x10^{-3}$ mm^2/s for normal tissue. For the patients where it was possible to delineate a normal tissue region, the difference between F-GTV and normal tissue ADC values was significant ($p<0.0001$). The mean K^{trans} values in F-GTV and normal tissue regions were 0.16 min^{-1} and 0.07 min^{-1} respectively. Again there was considerable inter-patient variation with per-patient mean K^{trans} values 0.09 - 0.48 min^{-1} for the F-GTV and 0.01 - 0.22 min^{-1} for normal tissue. In spite of this overlap in ranges, for the patients where it was possible to delineate a normal tissue region, the difference between F-GTV and normal tissue K^{trans} values was significant ($p<0.005$).

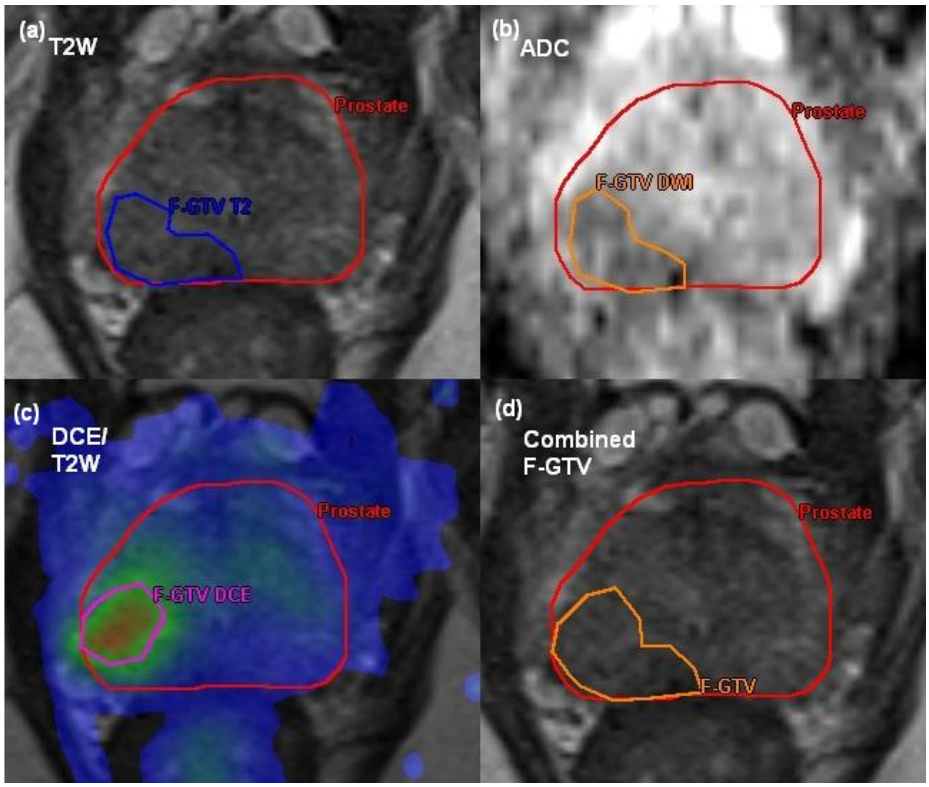

Figure 17 Example of tumour delineation on (a) T2 weighted MRI (b) DWI MRI ADC map (c) DCE-MRI Ktrans map superimposed on T2W MRI. (d) shows the F-GTV derived from (a), (b) and (c)

Assessment of variability in tumour delineation and image registration

In the tumour delineation uncertainty analysis a total of eight F-GTVs were delineated. An example of four separate delineations (each represents the F-GTV combined from T2, DWI and DCE-MRI) for a single slice is shown in Figure 18. The margins for tumour delineation uncertainty were left 3.7mm, right 3.4mm, anterior 4.9mm, posterior 2.1 mm, inferior 3.8mm and superior 3.8mm. The margins for image registration uncertainty were left-right 1.6mm, anterior-posterior 1.6mm, superior-inferior 2.8mm. The overall margin was determined by combining the tumour delineation and image registration uncertainties in quadrature giving left 4.0mm, right 3.8mm, anterior 5.2mm, posterior 2.6 mm, inferior 4.7mm and superior 4.7mm. The mean of these values is 4.2mm. Although some directional dependence was observed anterior-posterior for tumour delineation uncertainty, this is likely due to the majority of F-GTVs being close to the posterior border of the prostate. For these F-GTVs a large posterior margin

would not apply anyway as the F-PTV is restricted to the prostate capsule. For this reason and to simplify treatment planning, it was decided to use a single margin of 4.5mm in all directions. Table 24 lists the F-PTV volumes for each patient.

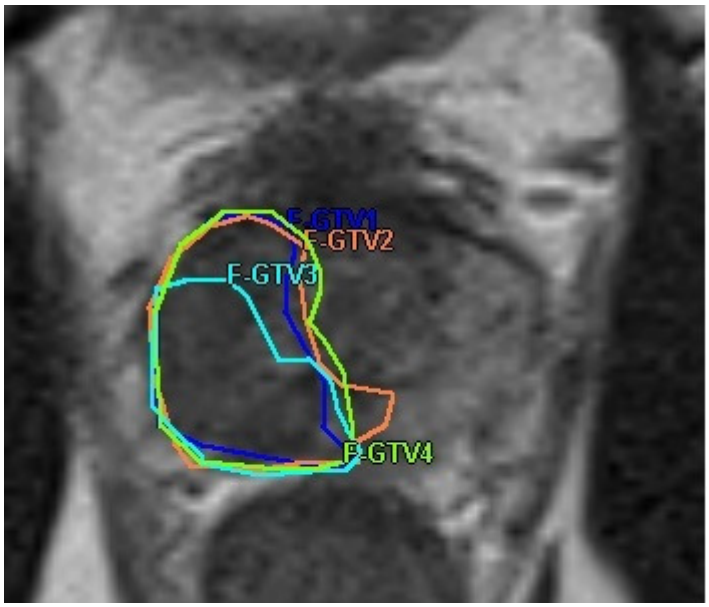

Figure 18 Example of four separate delineation attempts for one F-GTV (for each F-GTV, contours are combined from all mp-MRI data)

Margin consistency test

In the margin consistency test, the F-PTVs created using the 4.5mm margin in the treatment planning study covered 91.2% (mean for 5 patients, range 74.1% - 100%) of the F-GTV volumes from repeat delineations by the two radiologists.

Treatment planning study

Table 24 shows the dose achieved in the focal boost optimised plan with additional needles for each tumour region. The median (range) volumes for F-PTV, prostate and PTV were 3.6 cm^3 (0.5 cm^3 – 36.0 cm^3), 29.2 cm^3 (13.2 cm^3 – 59.3 cm^3) and 43.0 cm^3 (21.6 cm^3 – 81.3 cm^3) respectively. Table 25 shows DVH statistic values for the 28 patients, comparing the delivered treatment plans to the plans optimised for focal boost. Focal boost coverage was comparable in the retrospective and prospective phases of the study, with median F-PTV D90 20.7 Gy and V150 75.9% in the retrospective focal

boost plans for the patients who received the standard treatment, and median F-PTV D90 22.5 Gy and V150 90.1% in the delivered focal boost plans for the patients who received the focal boost treatment. The slightly better coverage in the latter group is probably due to the retrospective group containing the majority of patients with bi-lateral F-PTVs. Figure 19 shows an example comparing standard and focal boost plans for one patient. Figure 20 shows a comparison of V150 values for each F-PTV for the treatment plans. From patient follow up assessments, in the patients treated with F-PTV boost no Grade 3 toxicities were seen, 3 of 8 patients had Grade 2 toxicity in the first 3 months, with median follow up 12 months.

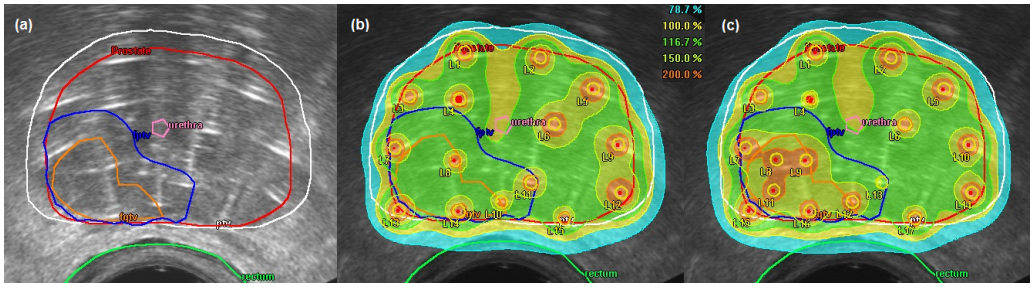

Figure 19 (a) MRI F-GTV registered to TRUS and used to generate F-PTV (b) isodoses from the standard plan (c) isodoses from the focal boost plan

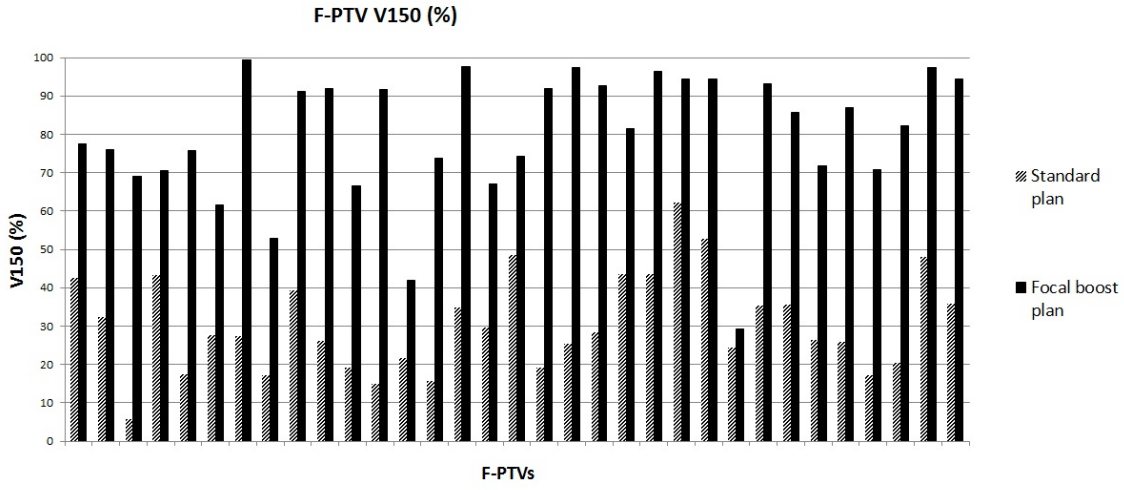

Figure 20 Comparison of V150 values for standard and focal boost plans for all F-PTVs in the study

Table 25 DVH parameter values from the dose optimization study. Values shown are the median for 30 patients with the range of values shown in parentheses.

	Plan	D90 (Gy)	V100 (%)	V150 (%)	V200 (%)
Prostate*	STD	17.1 (16.6 - 17.6)	99.6 (98.2 -100)	27.8 (18.4 – 39.1)	6.2 (4.0 – 11.1)
	FBOOST	17.1 (16.2 - 17.7)	99.5 (98.0 - 99.9)	39.9 (23.4 – 52.3)	9.9 (5.3 – 16.7)
PTV	STD	15.6 (14.5 - 16.5)	93.4 (87.3 – 96.6)	23.3 (16.3 – 32.0)	5.8 (3.9 – 9.3)
	FBOOST	15.7 (14.5 – 16.9)	93.6 (87.4 - 97.6)	33.0 (20.0 – 42.6)	8.5 (4.3 – 13.5)
F-GTV	STD	18.2 (16.3 – 22.2)	100 (98.7 - 100)	26.2 (0 – 88.5)	5.3 (0 – 35.3)
	FBOOST	24.0 (17.9 – 37.5)	100 (-)	97.3 (17.5 – 100)	41.9 (1.6 - 100)
F-PTV	STD	17.8 (16.7 - 19.3)	100 (98.6 - 100)	27.5 (5.7 – 62.1)	5.4 (0.1 – 20.0)
	FBOOST	21.4 (17.5 - 25.0)	100 (-)	82.2 (29.1 - 99.4)	25.6 (6.5 – 62.9)
		D10 (Gy)	**D2cm^3 (Gy)**	**V100 (cm^3)**	
Urethra	STD	17.2 (17.0 – 17.5)	-	-	
	FBOOST	17.3 (17.0 – 17.5)	-	-	
Rectum	STD	-	8.1 (6.3 – 10.8)	0 (-)	
	FBOOST	-	9.0 (6.6 – 10.8)	0 (-)	

STD – standard plan delivering 15Gy to the whole prostate

FBOOST – focal boost plan delivering 15Gy to the whole prostate and escalating dose to the F-PTV

* Prostate is the whole prostate including F-GTV and F-PTV.

5.1.4 Discussion

This study has investigated the feasibility of mp-MRI-guided focal boost, using HDR prostate brachytherapy with TRUS based treatment planning. 25 of 28 patients had undergone hormone therapy at the time of their MRI scan. Hormone therapy has been shown to reduce the contrast between tumour and normal tissue in mp-MRI techniques (92, 135, 136). Although use of staging MRI acquired before hormone therapy might avoid this problem, hormone therapy also causes a reduction of 30-40% in prostate volume and the % volume reduction can vary between central gland and peripheral zone (88), so that staging MRI might be less suitable for image fusion to plan HDR treatments. Use of staging MRI to plan focal boost treatments is investigated separately in 5.2. Tumour volumes were identified

in 25 out of 28 patients scanned in this study. For comparison, a study by Groenendaal et al (92) found that longer duration of hormone therapy was associated with reduced tumour conspicuity but identified tumour volumes in 18 out of 21 IMRT and I-125 seed implant patients who had received >3months hormone therapy. The majority of F-GTVs were in the peripheral zone. This may be biased by the fact that central gland tumours are less easily identifiable on DWI and DCE-MRI but in any case urethral dose constraints would limit the level of boost dose that could be achieved in central gland regions.

When using mp-MRI for tumour delineation the question arises how to deal with areas of the prostate that are suspicious for tumour on some but not all of the mp-MRI datasets in an individual study. Differences could reflect the fact that DWI and DCE-MRI techniques probe different tissue characteristics or be caused by image registration errors between the mp-MRI datasets (58), particularly as the EPI sequence used for DWI can cause artifacts that deform the prostate shape (although these are reduced by using right-left rather than anterior-posterior phase encoding). In this study the union of suspicious areas was taken as the F-GTV; this seems the safest approach given that the reasons for the inconsistencies are not fully understood. For example, a study by Alonzi et al (135) concluded that reduction in tumour K^{trans} values caused by hormone therapy (that might cause a tumour to not be considered suspicious in DCE-MRI) can be associated with hypoxic areas of tumour, that would benefit from a higher radiation dose. In spite of these inconsistencies there was still a significant difference in both ADC and K^{trans} values between F-GTV regions and normal tissue regions. The tumour ADC values were at the high end compared to other published studies (for example Groenendaal et al (58) quotes values from 4 different studies ranging from 0.9 - 1.38 $x10^{-3}$ mm^2/s). This could be an effect of hormone therapy, but may also be because the acquisition protocol did not include any b-values higher than 500 s/mm^2, and our acquisition protocol has been adjusted for subsequent patients to

include b = 750 s/mm^2. The tumour K^{trans} values are low compared to other studies, which could again be a consequence of hormone therapy.

A limitation of this study is that tumour delineation and image registration procedures were not validated. Tumour delineation could be validated with template biopsy procedures and image registration could be validated by inserting markers into the prostate, but this would require additional invasive procedures for the patient. Instead uncertainties were estimated by looking at variability in repeat attempts using multiple observers. Image registration uncertainty was largest in the superior-inferior direction which is not surprising as matching the base and apex of the prostate on MRI and ultrasound is difficult. Image registration accuracy is also limited by use of a rigid registration to register MRI to TRUS, when TRUS is acquired with the patient in a different position from MRI and with the ultrasound probe deforming the prostate to some extent. For tumour delineation it was found that uncertainty was largest in the anterior direction. This could be because many peripheral zone tumours are located close to the prostate capsule, which provides a clearly defined posterior boundary. Also tumours tend to be more easily recognizable in the peripheral zone, compared to the central gland where there is overlap of signal characteristics between benign and malignant tissue. There are no published studies that have estimated prostate tumour margin in this way, but a study by Groenendaal et al (144) determined that a margin of 5mm accounted for errors in mp-MRI based tumour delineation, when compared to pathology results. As this is a focal boost study, an additional margin is provided by the fact that the whole prostate continues to receive the standard prescription dose. For focal therapy (treating just the tumour) larger margins would need to be considered.

The size of the F-PTV and its proximity to the urethra and rectum determines how large a boost dose can be achieved. The boost doses achieved in this study are comparable to other retrospective planning studies and were achieved without changes to urethra and rectal dose constraints,

specific to a single fraction HDR treatment regime (145). For comparison, Kim et al. (96) retrospectively planned treatments and achieved focal boost V150 values of 82.4% on average for 13 patients with slight adjustment of dose constraints, although this level of boost could not be achieved for 2 other patients in their study. Pouliot et al. (95), found boost dose of 120% could be achieved without affecting dose to surrounding normal tissue or the urethra, and boosts up to 170% were feasible with slightly increased urethral and rectal dose. In this study the median V150 coverage was 97.3% for the F-GTV (comparable to the studies mentioned above as these did not add a margin to the MRI delineated tumour regions) and 82.2% for the F-PTV. This demonstrates that focal boost techniques could be improved if better techniques for tumour localization and image registration can be developed.

5.1.5 Conclusion

The study has shown that mp-MRI-guided HDR prostate brachytherapy focal boost is feasible. Mp-MRI techniques can be used to define tumour regions in spite of the fact that the majority of patients have undergone hormone therapy. Increased focal boost dose can be achieved without violating urethral and rectal dose constraints and maintaining standard prostate/ptv coverage. No increases in the level of treatment related toxicities were observed in patients treated with the focal boost treatment. The level of dose boost is lower for larger tumour regions or tumour regions close to either the urethra or rectum.

5.2 Retrospective investigation of focal boost planning based on staging scan sectors

5.2.1 Introduction

Following completion of the pilot study described in 5.1, it was decided to bring focal boost treatments into routine clinical practice. However due to resource constraints it was not possible to request pre-treatment MRI scans, so an additional investigation was performed into the feasibility of HDR focal boost planning based on staging MRI scans. This work is described in this section

Two aspects were investigated. Firstly any differences in tumour delineation between staging and pre-treatment MRI scans were assessed. Secondly focal boost optimization was compared for prostate sector and F-PTV based boost. This comparison was performed because of concerns that, for patients who receive hormone therapy, changes in prostate volume and morphology may mean that an F-GTV delineated in a staging scan cannot be accurately transposed to treatment planning TRUS. Focal boosting all involved sectors would effectively increase boosted volume and provide additional confidence that uncertainties in tumour delineation and image registration are accounted for.

5.2.2 Method

Tumour delineation

For the tumour delineation part of this investigation, all patients from the pilot study described in 5.1 who had received a staging MRI scan in our centre were selected. This was 10 patients in total, and included one patient for whom it had not been possible to delineate tumour in the pre-treatment scan. All 10 patients had received hormone therapy for between 2 and 4 months (mean 3 months).Patients who had been staged at other centres were not included because differences in the MRI protocols used in those centres meant that we did not feel that a comparison to the pre-treatment scans would be valid for those patients. F-GTVs were delineated on the staging scan sequences by the same consultant radiologists who had performed the pre-treatment scan delineations. At least one year had elapsed since the radiologists delineated the pre-treatment scans. The prostate was delineated to assess the effects of hormone therapy on prostate volume from staging to pre-treatment scan.

The staging scan sequences that were reviewed were T2W and DWI MRI, as the staging scan protocol did not include DCE-MRI at the time these patients were scanned. MRI sequences were acquired using protocols as described in 5.1.2, except that the T2W MRI used a slice thickness of 3mm (and 0.3mm gap) as opposed to 2.5mm.

The sectors intersected by the F-GTVs in the scans were recorded. For this the prostate was divided into 12 sectors by dividing into three equal length sections superior-inferior, then dividing each of these sections into four sectors. Figure 21 illustrates the sector divisions and the sector numbering scheme used to refer to individual sectors in the analysis below.

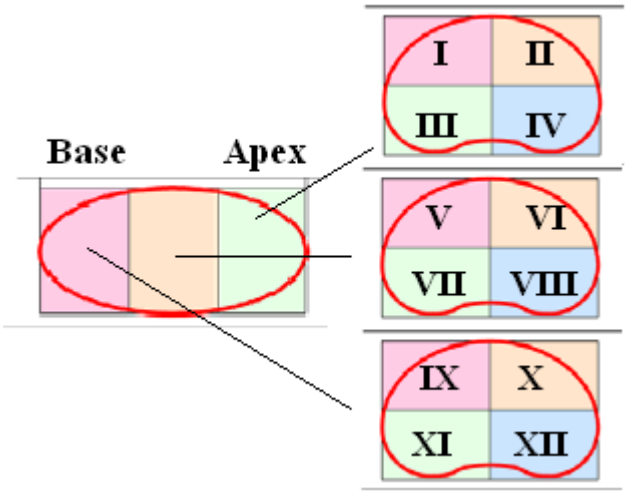

Figure 21 Prostate sector divisions and numbering scheme

Optimisation

Additional patients were randomly chosen from the pilot study to increase the number of patients in the optimization part of the study to 15 patients in total. To exclude the effect of any differences between F-GTV delineation in staging and pre-treatment scans, and to allow for uncertainties in tumour delineation and image registration, the sectors included in optimization were selected based on the F-PTVs used in the original focal boost study. All sectors that contained part of the F-PTV were included.

Table 26 Comparison of prostate volume, F-GTV volume and tumour sectors between staging and pre-treatment scans. Patient numbers refer to those in Table 24. Sector numbers refer to sectors as illustrated in Figure 21. Staging and pre-treatment scans were compared for the first 10 patients shown in this table.

Patient	**Staging scan**			**Pre-treatment scan**			**TRUS F-PTVs**	
Patient	**Prostate volume (cm^3)**	**F-GTV volume (cm^3)**	**Involved sectors**	**Prostate volume (cm^3)**	**F-GTV volume (cm^3)**	**Involved sectors**	**F-PTV volume (cm^3)**	**F-PTV sectors**
9	24.5	0.6	III, VII	21.2	0.9	III, VII		III, VII, VIII, XI
					0.2	VIII		
18	32.4	0.2	VII	22.6	0.2	VII	1.1	VI, VII, VIII
		1.1	VI, VIII		0.9	VI, VIII	3.0	
20	29.7	3.0	VII, IX	16.2	1.3	VII, IX	4.6	VII, IX
22	31.0	0.5	III, VII	16.3	1.9	V, VII, IX, XI	5.8	III, V, VII, IX, XI
		0.6	IV, VIII		-	-		
23	23.2	0.2	VIII	22.3	-	-	-	-
24	29.2	1.4	IV, VIII	13.5	0.4	VIII, XII	1.6	VIII, XII
25	44.2	2.0	VII, VIII	24.9	1.5	VII, VIII	6.1	VII, VIII, XI, XII
27	34.8	2.5	III, VII, VIII	27.3	3.8	VII, XI, XIII	9.2	VII, XI, XII
29	48.4	1.5	VIII, XII	36.4	0.9	VIII, XII	2.9	VIII, XII
30	29.7	0.8	VII, XI	19.3	0.3	VII, XI	1.6	VII, XI
1	-	-	-	21.3	4.6	III, V, VII, IX, XI	9.0	I, III, V, VII, IX, XI
3	-	-	-	24.0	3.8	VII, XI, XII	9.5	VII, VIII, XI, XII
	-	-	-		0.2	VIII	1.1	
7	-	-	-	44.5	3.9	VII	9.8	VII, VIII, XI
	-	-	-		0.9	VIII	3.5	
12	-	-	-	21.9	3.6	III, IV, VIII, XII	10.2	III, IV, VI, VIII
13	-	-	-	11.4	0.5	V, IX	2.4	V, IX
15	-	-	-	21.9	0.4	VIII	3.0	VIII

For each patient, 3 plans were produced. Standard and focal boost plans optimised to the F-PTV were produced by the method described in 5.1.2, and sector focal boost plans were produced using the sector based optimization feature of Oncentra Prostate™ v4.0 (111). All plans used the same dose objectives and constraints for prostate, PTV, urethra and rectum. These were as detailed in 5.1.2 except that the PTV V100 dose objective was increased to 95%, due to a recent update to guidelines (15) (note this change means that the standard and F-PTV focal boost plans produced were slightly different from those created in 5.1.2). Sector focal boost plans were optimised to maximize dose to the involved sectors. Sector and F-PTV based focal boost plans used the same needle configurations, which in some cases included additional needles compared to the standard plans added to target the tumour volume. Dose optimization was performed using DVH-based inverse optimization (111) with small manual adjustments to dwell times where necessary to improve the treatment plan. The objective for the optimizer was set to give 150-200% of the prescription dose to the F-PTV/involved sectors.

Table 27 Median DVH values for the 15 patients in the optimisation study. For F-GTV, F-PTV and sectors, the values shown are the median (range) of the combined values (for both F-GTVs/F-PTVS or all sectors) for each patient

	Plan	D90 (Gy)	V100 (%)	V150 (%)	V200 (%)
Prostate*	STD	17.2 (16.6 - 17.5)	99.9 (99.3 -100)	33.3 (28.1 – 43.2)	10.1 (5.5 – 13.5)
	FBOOST	17.3 (16.6 - 17.8)	99.9 (99.0 - 99.9)	42.1 (32.1 – 52.5)	12.1 (8.7 – 20.5)
	SBOOST	17.3 (16.6 - 17.7)	99.8 (99.2 - 100)	43.4 (32.5 – 57.2)	12.3 (8.6 – 17.5)
PTV	STD	16.2 (15.5 - 16.6)	92.8 (87.3 – 97.2)	28.8 (26.2 – 36.7)	8.9 (5.4 – 11.5)
	FBOOST	16.3 (15.3 – 16.8)	91.6 (87.4 - 97.1)	35.0 (28.0 – 44.5)	10.1 (7.6 – 16.4)
	SBOOST	16.1 (15.3 – 16.8)	91.6 (87.4 - 97.1)	35.9 (28.5 – 45.3)	10.9 (8.0 – 13.7)
F-GTV	STD	18.3 (16.1 – 21.8)	100 (99.6 - 100)	35.8 (9.1 – 85.1)	6.1 (0.6 – 32.2)
	FBOOST	24.3 (20.5 – 30.4)	100 (-)	95.4 (73.1 – 100)	46.9 (14.5 – 91.4)
	SBOOST	22.3 (19.9 – 25.8)	100 (-)	88.7 (66.3 – 100)	29.9 (12.3 – 59.9)
F-PTV	STD	17.5 (15.8 - 19.3)	100 (97.5 - 100)	33.7 (16.0 – 56.5)	8.9 (2.5 – 16.7)
	FBOOST	21.0 (18.8 – 24.1)	100 (-)	77.2 (64.7 – 96.9)	30.2 (12.3 – 54.1)
	SBOOST	19.8 (18.9 – 24.2)	100 (-)	75.6 (49.7 – 96.7)	23.4 (10.1 – 48.1)
Sectors	STD	17.7 (16.8 - 18.3)	100 (99.0 - 100)	37.8 (14.4 – 49.4)	9.8 (3.3 – 18.6)
	FBOOST	19.0 (18.0 – 21.5)	100 (99.6 - 100)	62.2 (53.1 – 82.7)	20.9 (14.4 – 31.7)
	SBOOST	20.3 (18.7 – 22.8)	100 (-)	74.7 (56.9 – 91.1)	27.5 (16.1 – 38.7)

		D10 (Gy)	D2cm^3 (Gy)	V100 (cm^3)
Urethra	STD	17.1 (17.1 – 17.2)	-	-
	FBOOST	17.2 (17.1 – 17.5)	-	-
	SBOOST	17.2 (17.1 – 17.5)	-	-
Rectum	STD	-	8.4 (6.5 – 9.7)	0 (-)
	FBOOST	-	8.9 (6.6 – 10.4)	0 (-)
	SBOOST	-	8.9 (6.8 – 10.6)	0 (-)

STD – standard plan delivering 15Gy to the whole prostate

FBOOST – focal boost plan delivering 15Gy to the whole prostate and escalating dose to the F-PTV(s)

SBOOST – focal boost plan delivering 15Gy to the whole prostate and escalating dose to the involved sector(s)

* Prostate is the whole prostate including F-GTV and F-PTV/sectors.

5.2.3 Results

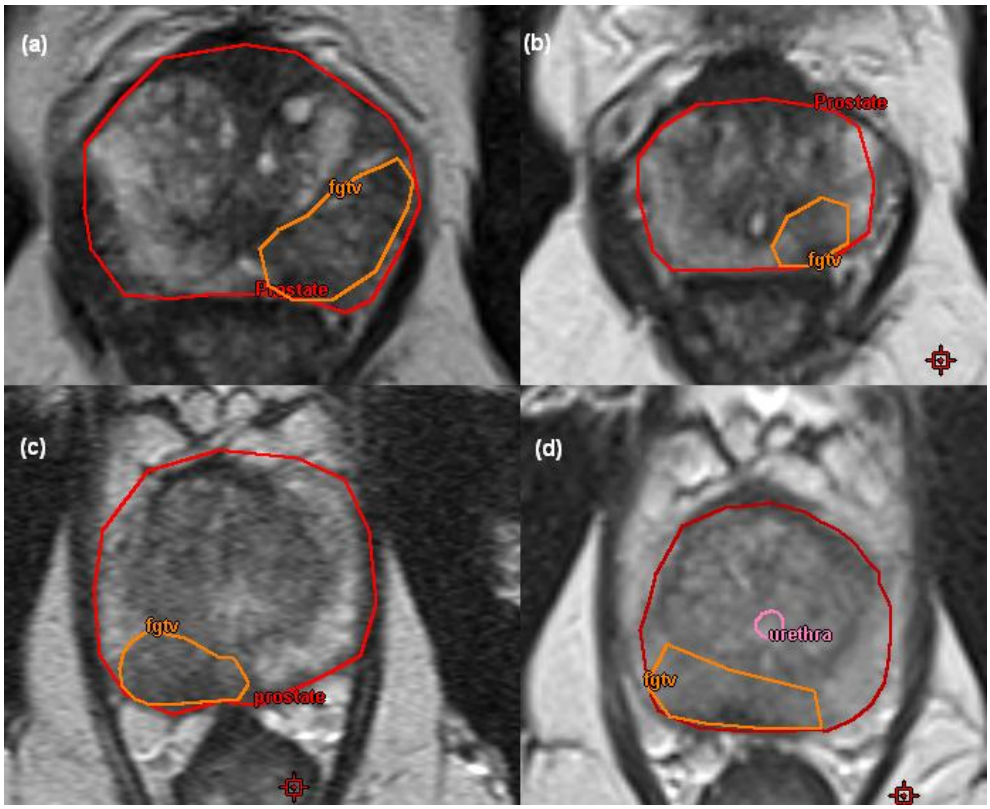

Figure 22 Staging and pre-treatment MRI . (a) and (b) are from staging and pre-treatment MRI s respectively for the same patient illustrating prostate and tumour shrinkage. (c) and (d) are from staging and pre-treatment MRIs respectively for a different patient and illustrate that tumour can be more difficult to distinguish in the pre-treatment MRI (post hormone therapy). Note in all cases the delineated tumour volumes were based on mp-MRI data, not just on the T2 weighted images shown.

Tumour delineation

Results for the 10 patients for whom staging and pre-treatment scan tumour delineations were compared are shown Table 26. For these 10 patients, the median prostate volume was 30.4 cm^3 in the staging scan and 21.8 cm^3 in the pre-treatment scan, corresponding to a median reduction in volume of 28.3% (range 3.9% - 53.8%). Table 26 shows the sectors intersected by the F-GTVs in the scans for each patient. The following explains these results in overview:

- For 5 patients (18, 20, 25, 29, 30) the sectors corresponded exactly.

- For 3 patients (9, 24, 27) the sectors overlapped but did not exactly match. In two cases this was due to delineation variation and in one case (patient 24) due to the large change in prostate volume between the two scans.
- For patient 22, the tumour outlined in the pre-treatment scan did not correspond to the tumour outlined in the staging scan, although there was one sector in common.
- For patient 23, for whom no tumour has been observed in the pre-treatment scan, a small tumour was visible in the staging scan.

Optimisation

The sectors and F-PTV volumes are shown in Table 26. The results of the optimization study are shown in

Table 27. The per-patient median volume of the boosted F-PTVs and sectors were 5.8 cm^3 and 9.8 cm^3 respectively. Median prostate conformal index (146) values were 0.624, 0.616 and 0.612 in standard, F-PTV boost and sector boost plans respectively. Median PTV conformal index values were 0.867, 0.846 and 0.842 in standard, F-PTV boost and sector boost plans respectively. Figure 23 shows an isodose comparison for one patient in the study.

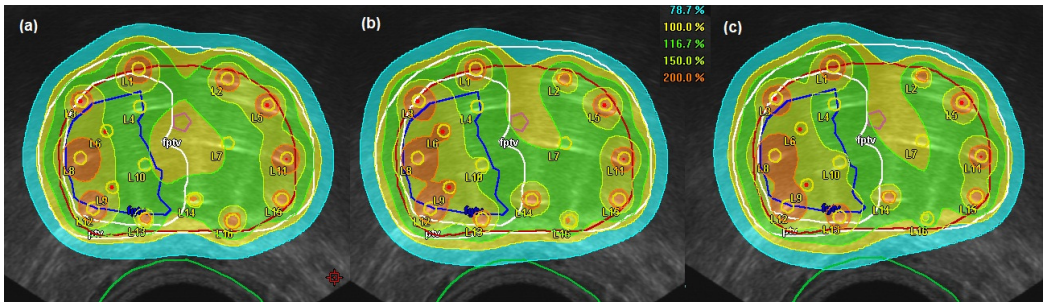

Figure 23 Comparison of isodoses for a patient with F-PTV in the right anterior and right posterior mid-gland sectors (V and VII). (a) no boost plan (b) F-PTV boost plan (c) sector boost plan.

Table 28 compares the DVH values that were achieved in each sector of the prostate across all patients for standard and sector boost plans. In total 10 anterior sectors and 38 posterior sectors were boosted. The median D90 and V150 for anterior sectors (I, II, V, VI, IX, X) was 18.4 Gy and 53.3%. For posterior sectors (III, IV, VII, VIII, XI, XII) the values were 21.0 Gy and 80.6%.

5.2.4 Discussion

This study has investigated the feasibility of focal boost planning using staging MRI scans in terms of differences in tumour delineation between staging and pre-treatment scans and focal boost optimization using sectors and F-PTVs. All 10 patients for whom staging scans were available had received several months hormone therapy at the time of the pre-treatment scan and this resulted in reductions in prostate volume which varied for individual patients from a few percent to a reduction by more than half the initial volume. As well as reduced volume the relative proportions of central gland and peripheral zone can change (88) and this was observed for some patients in this study with the peripheral zone shrinking much more significantly than the central gland. As discussed in 5.1.4, differences in tumour delineation occur even when the same images are delineated on separate occasions and hormone therapy will reduce the contrast between normal and cancerous prostate tissue. It is therefore not surprising that there were differences in tumour delineation and in the sectors selected as involved in the tumour, between staging and pre-treatment scans. These

differences between pre-treatment and staging scans underline the importance of using mp-MRI to improve confidence in tumour delineation. A limitation of this study is that DCE-MRI was not available for the staging scans which may contribute to the differences observed compared to pre-treatment scans. DCE-MRI is likely to be used in staging scans for future patients treated in our centre.

Table 28 Median DVH values per sector across all patients in the study, comparing standard and sector boost plans. The sector numbers are explained in Figure 21.

Sector	Number of times boosted	Standard plans		Sector boost plans	
		D90 (Gy)	V150 (%)	D90 (Gy)	V150 (%)
I	1	17.5 (-)	27.7 (-)	18.3 (-)	52.8 (-)
II	0	-	-	-	-
III	4	18.0 (17.1- 18.3)	31.5 (22.6 – 38.4)	20.8 (19.0 – 22.5)	76.8 (57.0 – 90.2)
IV	1	18.3 (-)	35.9 (-)	20.7 (-)	80.3 (-)
V	3	17.3 (17.2 – 17.5)	38.7 (34.1 – 39.4)	18.5 (18.4 – 19.1)	58.1 (53.8 – 60.3)
VI	2	17.4 (17.3 – 17.5)	42.0 (32.3 - 51.7)	17.9 (17.8 -18.1)	51.2 (45.4 – 56.9)
VII	10	17.3 (15.8 – 18.2)	28.8 (14.4 – 44.8)	21.3 (18.4 – 24.0)	82.0 (48.5 – 95.7)
VIII	9	16.9 (16.2 – 18.1)	25.6 (12.4 - 41.4)	19.8 (18.3 – 22.1)	74.7 (49.2 – 87.8)
IX	4	17.4 (16.8 – 18.2)	42.1 (38.6 – 60.2)	18.9 (17.8 – 19.5)	66.4 (61.2 – 74.6)
X	0	-	-	-	-
X1	8	18.4 (17.1 – 19.2)	47.5 (23.6 – 57.8)	22.7 (19.0 – 23.8)	90.5 (69.8 – 95.3)
X11	6	18.3 (17.2 – 18.6)	52.3 (37.6 – 68.0)	20.8 (19.9 – 21.6)	79.5 (77.2 – 86.7)

For the dosimetric part of this study, focal boost sectors were determined from the F-PTVs that had been boosted in the original study. This was to allow direct comparison of boost doses that can be achieved, not taking into account tumour delineation variations. The TRUS based F-PTVs in some cases included sectors that were adjacent to the sectors that were involved in the pre-treatment MRI F-GTVs. This is because of the margin applied when generating the F-PTVs, and illustrates that if sectors are selected based on staging scans, it is important to consider including sectors adjacent to those

sectors which contain visible tumour, to allow for the uncertainties discussed above.

There are no published studies of sector based focal boost planning in HDR prostate brachytherapy. Optimising to the involved sectors rather than F-PTVs was possible without compromising prostate and PTV coverage, and without exceeding OAR tolerances. Sector boost plans were similar to F-PTV boost plans, although with slightly lower F-PTV boost dose. Because the involved sectors represent a higher proportion of the prostate volume than F-PTVs, the overall volume of the prostate that receives a boost dose is higher in sector boost plans Sector boost doses were higher for posterior sectors than for anterior sectors – generally the anterior sectors are closer to the urethra and smaller than the posterior sectors. Similar results were seen in the previous study for F-PTVs with lower boost doses achieved for F-PTVs located closer to the urethra.

5.2.5 Conclusion

Although use of a pre-treatment MRI scan is preferable, focal boost planning based on involved sectors determined from staging scan data is feasible and can achieve focal boost doses comparable with the pre-treatment MRI based F-PTV focal boost plans. Future HDR prostate brachytherapy patients in our centre will receive treatments planned this way.

6 Dosimetry modeling for focal prostate brachytherapy

This section describes a dosimetric investigation into the feasibility of focal prostate brachytherapy treatments using LDR ^{125}I permanent seed implants and HDR ^{192}Ir monotherapy. Focal treatments using hemi-gland and ultra-focal approaches are compared to standard whole gland plans. Plan robustness to source position errors is assessed. MC simulations are used to compare ISA effects for 6711 and 9011 sources in LDR ^{125}I focal treatments and to assess attenuation by steel catheters in HDR ^{192}Ir focal treatments.

This section includes results from an LDR focal brachytherapy treatment planning study that was performed by another physicist. This work is included to allow comparison between LDR and HDR approaches and is clearly indicated in the text below.

6.1.1 Introduction

Both LDR and HDR brachytherapy treatments routinely target the whole prostate gland (13, 15). Prostate brachytherapy patients may suffer some side effects in terms of urethral, rectal and sexual function (15, 25). In focal prostate brachytherapy the aim is to reduce dose to the OARs by targeting treatment to areas of the prostate known to contain tumour, with reduced dose to the prostate gland as a whole (25). The objective is to achieve equivalent rates of tumour control as whole-gland treatments while reducing treatment related toxicities. There are few papers in the literature describing focal therapy treatment planning. Cossett et al. (24) describe a pilot study treating focal tumour volumes for 21 patients with an LDR technique. Kamrava et al. (27) completed a retrospective planning study for 10 patients comparing whole-gland and hemi-gland treatments for HDR. Todor et al. (147) describe a planning study for a focused LDR treatment using mixed isotopes to achieve two different dose levels, with a focal tumour volume receiving the higher dose level and the whole prostate treated to a reduced level. Nguyen et al. (28) describe a focal treatment targeting the peripheral

zone of the prostate. In addition, several groups have investigated or implemented HDR focal boost treatments, including our own study described in section 5. In focal boost treatments the whole prostate is treated, but the focal tumour volume is boosted to a higher dose level (93, 95, 96, 148-150) – an approach intended to improve tumour control rates while keeping toxicities at a similar level.

This study investigates three aspects of treatment planning for LDR and HDR focal prostate brachytherapy. Firstly it compares target and OAR doses for different treatment planning approaches: whole prostate, hemi-gland and ultra-focal treatments. Secondly plan robustness is assessed to determine whether focal treatments are more sensitive to source position errors than standard treatments. Finally MC simulation of the treatment plans is performed to assess whether focal therapy plans are more sensitive than standard plans to dosimetric errors introduced by differences between TG-43U1 (3) and advanced dose calculation methods. For LDR treatments, the ISA effect is assessed for 6711 and 9011 seed models. For HDR treatments attenuation of dose due to delivering treatment through steel catheters is measured.

6.1.2 Methods

Patient selection and tumour delineation

Treatment planning for this dosimetric modeling study was based on MRI data from a group at University College London Hospital performing clinical trials of focal therapy using HIFU (23), for 14 patients who were considered candidates for focal therapy according to the patient characteristics defined by a recent consensus report (25) for LDR focal therapy. Patients were aged 52 - 77 years and had low or intermediate risk disease. Patients were evaluated based on clinical data, T2W and DWI MRI, and template mapping biopsy data. MRI data was acquired on an Avanto (Siemens AG, Munich, Germany) 1.5T scanner using phased-array pelvic and spine coils for signal reception. T2W MRI used a turbo-SE sequence with slice thickness 3 mm and 0.7 mm pixel size. DWI MRI used a single shot SE-echo planar imaging sequence with slice thickness 5 mm, 1.5 mm

pixel size and b-values 0, 150, 500 and 1000 s/mm2. The MRI volumes were rotated so that the position of the prostate approximated that used in TRUS based treatment planning (flat posterior prostate capsule), as is practiced in our centre. A consultant radiologist with 18 years experience of prostate MRI delineated F-GTVs where suspicious regions in the MRI data agreed with tumour locations from template biopsy data. The prostate, urethra, rectum and bladder were delineated based on the T2W MRI.

Target definition

For both LDR and HDR treatments, three treatment plans were created for each patient: a standard whole-gland treatment (WG), a hemi-gland treatment treating the half of the prostate containing the tumour volume (HEMI) and an ultra-focal treatment treating the tumour volume plus a margin (UF). These target definitions were taken from an LDR focal therapy consensus report (25). For WG plans a 3mm margin was applied to the prostate (0mm posteriorly) to create a PTV (15). For HEMI plans the same margin was applied to the hemi-prostate, excluding the urethra, to create a hemi-PTV (H-PTV). For UF plans a margin of 6mm was applied to the F-GTV to create an F-PTV, constrained to avoid the urethra and to remain within the PTV defined for whole-gland plans.

Treatment planning - LDR

The LDR treatment planning part of this study was performed by another physicist (Bashar Al-Qaisieh), as follows:

Plans were created using Variseed^{TM} v8.0 (Varian Medical Systems, Inc., Palo Alto, CA, USA) and the 6711 source. Stranded seeds were used (with 10 mm seed spacing) and seed positions were constrained to template grid positions. The prescribed dose was 145 Gy for all plan types. Plans were manually generated and the planning objective was to achieve as close as possible to 100% coverage of the prostate (WG plans), hemi-prostate (HEMI plans) or F-PTV (UF plans) with the prescription isodose. Dose constraints for OARs were the same for all plans: rectal $D2cm^3 < 145$ Gy

and urethral D10 < 239 Gy (this is a local dose limit different from GEC-ESTRO recommendations (14)).

All other work described in this section was performed by the author.

Treatment planning - HDR

The TPS used was Oncentra Prostate™ v4.0 (Elekta AB). All treatment plans assumed a single fraction monotherapy treatment with 19Gy prescribed to the prostate/hemi-prostate/F-PTV. This dose prescription has been used for single fraction whole-gland treatments in recent studies (151, 152) and has been shown by modelling studies to be a suitable dose for single fraction treatments (153). For WG plans, virtual catheters were placed using our standard clinical approach - approximately 1cm apart around the periphery of the target as visualised at mid-gland, with 2-5 additional catheters (depending on the size of the prostate) to cover the central regions, prostate apex and prostate base. For HEMI plans, catheter placing was similar with additional catheters near the urethra to try and cover the hemi-gland without increasing urethral dose. For UF plans catheter density was increased on the assumption that this would improve dose conformality for a small target. Catheters were spaced approximately 0.75 cm apart across the full mediolateral and anteroposterior extent of the F-PTV as visualized on multiple transverse slices. The 0.75 cm spacing was achieved by placing catheters alternately 0.5 cm or 1 cm apart in the template grid and tracking the catheters to the desired position. This tracking is clinically realistic as we routinely steer catheters in this manner during clinical implants. DVH-based inverse optimization was used to generate the treatment plan, with small manual adjustments to dwell times if necessary. Dose constraints for OARs were the same for all plans: urethra D10 <22 Gy, D30 < 20.8 Gy and rectum $D2cm^3$ <15Gy, V100 = 0% (151). Planning objectives were to aim for 100% prescription dose coverage of the prostate in WG plans, hemi-prostate in HEMI plans and F-PTV in UF plans.

Plan robustness

Plan robustness to source position errors in focal therapy treatments was assessed as follows. For each patient and each plan (WG, HEMI and UF), DVH parameters were recalculated after applying random or systematic shifts to all source co-ordinates. For random source displacements, a different random shift was applied to each component (x, y and z) of each source co-ordinate, based on a Gaussian distribution of random numbers with mean zero and standard deviation varied to test different ranges of shifts. For systematic source displacements, a systematic shift was applied to move each source in a single direction only. For these calculations, source positions, structure sets and dwell times (HDR only) were exported from the TPS, shifts were applied and DVH parameters re-calculated using the dose calculation framework described in 2.4.

For LDR plans random and systematic shifts were investigated. For random shifts, the standard deviation of the random number distribution was increased from 2mm to 5mm in 1mm steps. For systematic shifts, shifts of 2mm and 4mm were applied separately to each anatomical direction (superior, inferior, right, left, anterior and posterior).

For HDR plans only systematic shifts were investigated. Shifts of 2mm and 4mm were applied separately in each anatomical direction. Random source position errors were not investigated as it was felt that for HDR prostate brachytherapy, random errors are likely to be small compared to systematic errors.

Monte Carlo simulation - LDR

MC simulation was performed for each plan to assess the effects of ISA, performed as described for clinical ^{125}I simulations in 4.1.2. The same number of particle histories, 2 million per seed in the WG plan, was simulated for WG, HEMI and UF plans, to maintain similar levels of statistical uncertainty in the OAR DVH statistics for each plan type. All simulations were performed in a water phantom.

Monte Carlo simulation – HDR

MC simulations were performed for each treatment plan to assess the dosimetric effect of steel catheters on delivered dose. Source positions, structure sets and dwell times were exported from the TPS and used to create input files for simulations in MCNPX v2.5.0 (101). The HDR ^{192}Ir mHDR-v2r source and steel catheters were modeled as described in 0. A phase space model of the source was used in the treatment plan simulations to match the treatment setup, where the physical source occupies only one dwell position at any time. For all plans it was assumed that the catheters were inserted 1cm beyond the prostate base to account for the dead end space (this applied even to the UF plans where depending on the tumour location, insertion to a shorter depth may have been possible). The treatment was modeled in a 40cm radius water phantom. Dose was calculated over an 8 x 8 x 8 cm^3 cube centered at the mean source co-ordinate, using the MCNPX mesh tally. Each tally cell was 1 mm^3. 100-200 million particle histories were simulated, depending on the number of source positions, to reduce the mean statistical component of uncertainty in individual tally cells below 1% inside the target volume in all cases. The dose analysis framework is described in 2.4.

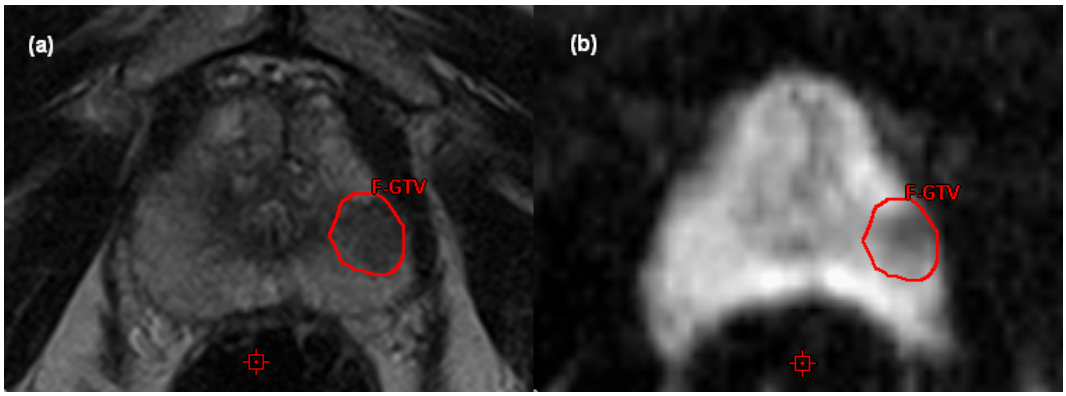

Figure 24 Example of F-GTV delineation on (a) T2 weighted and (b) DWI MRI

RESULTS

Tumour delineation

Five patients where MRI data was inconsistent with template biopsy results were excluded from the dosimetric study as it was felt that whole gland

treatments would be more suitable for those patients. Of the nine patients included, two had low risk disease and Gleason score 3+3 and seven had intermediate risk disease and Gleason score 3+4. Mean PSA at diagnosis was 7 ng/ml (range 1.5 ng/ml – 15.2 ng/ml). On average 14% (range 6% - 27%) of transperineal mapping biopsy cores were positive. The delineated F-GTV volumes ranged from 0.1 cm^3 to 1.5cm^3. F-GTVs were located in the peripheral zone for seven patients and in the central gland for two patients. Figure 24 shows an example of tumour delineation for one patient in the study.

Treatment planning

Figure 25 and Figure 26 compare isodoses for WG, HEMI and UF treatment plans for LDR and HDR treatments respectively.

Table 29 and Table 30 summarize the mean DVH values for the 9 patients in the study, for LDR and HDR plans respectively. The range of values for each DVH parameter is also shown.

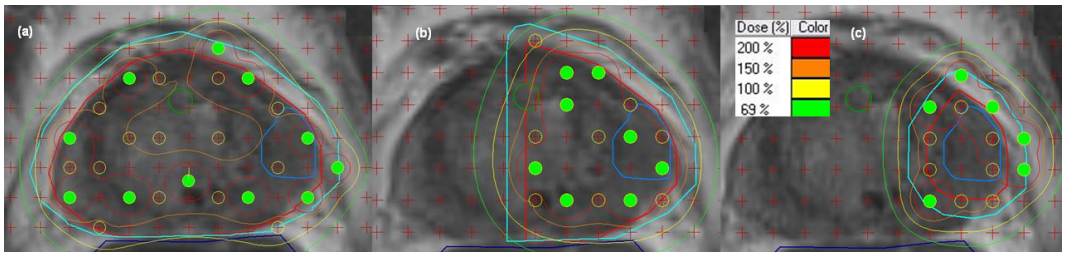

Figure 25 Isodose comparison for LDR treatment plans showing (a) whole-gland treatment plan, (b) hemi-gland treatment plan and (c) ultra-focal treatment plan. The 100% isodose corresponds to 145Gy. Prostate and hemi-prostate are shown in red, F-GTV (focal-gross tumour volume) is shown in blue, PTV (planning target volume), H-PTV (hemi-PTV) and F-PTV (focal-PTV) are shown in light blue, the urethra is shown in green and the rectum is shown in dark blue.

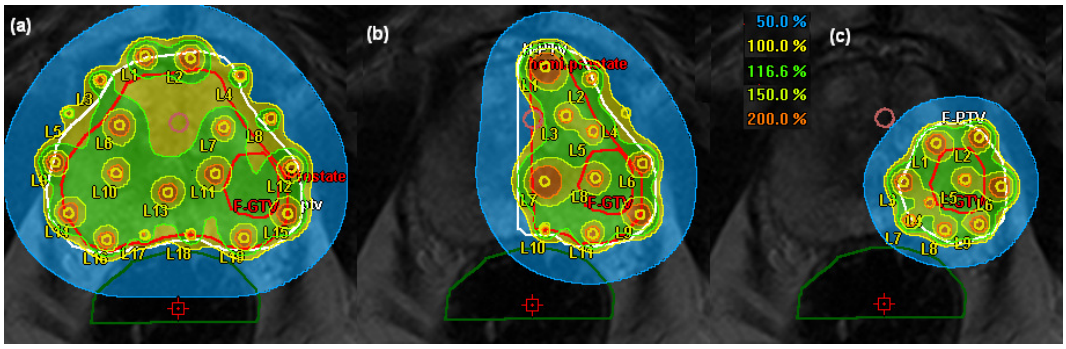

Figure 26 Isodose comparison for HDR treatment plans showing (a) whole-gland treatment plan, (b) hemi-gland treatment plan and (c) ultra-focal treatment plan. The 100% isodose corresponds to 19Gy. Prostate, hemi-prostate and F-GTV (focal-gross tumour volume) are shown in red, PTV (planning target volume), H-PTV (hemi-PTV) and F-PTV (focal-PTV) are shown in white, the urethra is shown in pink and the rectum is shown in green.

Table 29 Comparison of plan and DVH parameters for LDR focal therapy treatments: whole-gland (WG), hemi-gland (HEMI) and ultra-focal (UF). Values are the mean (range) for 9 patients. Seed density is measured for the prostate in WG plans, hemi-prostate in HEMI plans and F-PTV in UF plans.

Plan	WG	HEMI	UF
No. of needles	27.8 (20 – 37)	17.2 (12 – 21)	11.8 (10 – 15)
No. of seeds	81.1 (61 – 106)	55.6 (37 – 72)	24.6 (20 – 31)
Seed density (seeds/cm^3)	2.2 (1.8 – 2.7)	3.1 (2.5 – 4.0)	5.5 (3.8 – 7.2)
Prostate			
Volume (cm^3)		37.8 (22.7 – 58.6)	
D90 (Gy)	181.3 (177.9 – 188.6)	42.9 (33.2 – 54.7)	14.1 (10.7 – 17.9)
V100 (%)	99.8 (99.1 – 100)	54.7 (41.2 – 62.8)	19.9 (15.4 – 24.9)
Urethra			
D10 (Gy)	205.9 (183.8 – 236.8)	191.4 (161.6 – 215.6)	92.4 (47.9 – 194.4)
Dmax (Gy)	294.4 (189.6 - 570.2)	229.7 (177.4 - 250.7)	134.3 (55.5 - 391.1)
Rectum			
D2cm^3 (Gy)	107.5 (85.0 – 131.6)	77.0 (39.2 – 105.1)	42.7 (13.7 – 86.7)
Bladder			
D2cm^3 (Gy)	80.5 (18.5 – 116.3)	54.7 (13.2 – 87.2)	17.6 (2.5 – 69.5)
PTV			
Volume (cm^3)		49.4 (30.4 – 76.0)	
D90 (Gy)	172.2 (165.4 – 176.8)	35.4 (27.4 – 45.5)	11.7 (9.2 – 15.2)
V100 (%)	98.1 (96.1 – 99.2)	53.0 (42.1 – 59.8)	18.9 (14.0 – 23.9)

Plan	WG	HEMI	UF
Hemi-prostate			
Volume (cm^3)		18.4 (11.1 – 28.0)	
D90 (Gy)	183.6 (177.6 – 193.8)	195.7 (140.8 – 222.5)	31.8 (18.6 – 45.9)
V100 (%)	99.9 (99.6 – 100)	97.8 (88.4 – 99.8)	40.5 (31.2 – 46.9)
H-PTV			
Volume (cm^3)		28.0 (17.4 – 41.5)	
D90 (Gy)	174.2 (168.0 – 182.6)	152.9 (102.1 – 176.4)	26.1 (16.5 – 39.5)
V100 (%)	98.7 (97.2 – 99.8)	90.9 (74.9 – 96.4)	32.9 (24.7 – 40.2)
F-GTV			
Volume (cm^3)		0.7 (0.2 – 1.7)	
D90 (Gy)	241.1 (210.0 – 277.7)	267.0 (235.3 – 312.3)	272.4 (221.1 – 310.6)
V100 (%)	100 (–)	100 (–)	100 (–)
F-PTV			
Volume (cm^3)		4.8 (2.8 – 8.2)	
D90 (Gy)	199.3 (182.8 – 215.3)	218.2 (176.8 – 241.2)	218.3 (199.0 – 243.3)
V100 (%)	99.7 (97.9 – 100)	99.5 (96.5 – 100)	99.8 (98.7 – 100)

Table 30 Comparison of plan and DVH parameters for HDR focal therapy treatments: whole-gland (WG), hemi-gland (HEMI) and ultra-focal (UF). Values are the mean (range) for 9 patients.

Plan	WG	HEMI	UF
Needles	17.3 (14 – 19)	10.3 (9 – 11)	6.8 (6 – 9)
TRAK (cGy@1m)	0.690 (0.508 – 0.932)	0.487 (0.351 – 0.654)	0.205 (0.147 – 0.270)
Prostate			
Volume (cm^3)		37.1 (22.3 – 57.3)	
D90 (Gy)	20.4 (19.9 - 20.9)	6.7 (5.8 – 8.0)	2.1 (1.6 – 2.8)
V100 (%)	97.9 (96.5 – 98.5)	52.4 (43.2 – 59.7)	14.3 (10.7 – 17.5)
Urethra			
D30 (Gy)	19.9 (19.5 - 20.5)	18.6 (17.1 - 19.7)	7.5 (4.0 - 12.9)
D10 (Gy)	20.3 (19.8 – 20.8)	19.7 (18.5 – 20.5)	9.2 (4.5 – 16.0)
Dmax (Gy)	20.7(20.1 – 21.6)	21.2 (19.9 – 22.1)	11.7 (4.5 – 21.9)
Rectum			
$D2cm^3$ (Gy)	12.5 (9.5 – 14.1)	9.8 (6.6 – 11.5)	4.6 (2.3 – 8.0)
Bladder			
$D2cm^3$ (Gy)	9.8 (3.2 – 14.9)	7.3 (2.3 – 11.4)	2.6 (0.4 – 9.2)

Plan	WG	HEMI	UF
PTV			
Volume (cm^3)		48.2 (29.9 – 74.0)	
D90 (Gy)	19.9 (19.4 – 20.2)	5.8 (5.0 – 6.9)	1.8 (1.4 – 2.5)
V100 (%)	94.8 (93.4 – 96.2)	50.3 (43.3 – 55.2)	13.6 (10.0 – 16.5)
Hemi-prostate			
Volume (cm^3)		18.0 (10.8 – 27.4)	
D90 (Gy)	20.6 (19.9 – 21.0)	22.2 (21.1 – 23.4)	4.0 (2.7 – 4.9)
V100 (%)	98.3 (96.7 – 99.0)	98.1 (96.0 – 99.2)	29.7 (22.7 – 39.3)
H-PTV			
Volume (cm^3)		27.3 (17.0 – 40.4)	
D90 (Gy)	19.7 (19.2 – 20.0)	18.6 (15.6 – 19.9)	3.4 (2.5 – 4.4)
V100 (%)	94.3 (92.6 – 96.0)	88.6 (78.8 – 93.1)	24.1 (18.0 – 31.0)
F-GTV			
Volume (cm^3)		0.6 (0.1 – 1.5)	
D90 (Gy)	24.3 (21.2 – 30.1)	24.9 (21.1 – 28.6)	29.6 (24.7 – 34.0)
V100 (%)	100 (99.7 – 100)	99.9 (99.4 – 100)	100.0 (99.8 – 100)
F-PTV			
Volume (cm^3)		4.4 (2.5 – 7.5)	
D90 (Gy)	21.4 (20.3 – 23.0)	21.9 (20.2 – 24.0)	23.0 (21.1 – 23.9)
V100 (%)	98.0 (95.4 – 99.9)	97.3 (94.7 – 100)	98.2 (95.4 – 100)

TRAK – Total reference air kerma

Plan robustness - LDR

Table 31 summarizes the changes in DVH parameter values for prostate, hemi-prostate, F-PTV, urethra and rectum with random shifts of 2mm to 5mm. The target D90 and V100 values compared are for prostate in WG plans, hemi-prostate in HEMI plans and F-PTV in UF plans, as these are the structures in each plan where planning objectives aimed to achieve 100% coverage. Note that the DVH values in
Table 29 were taken from the TPS, whereas the baseline DVH values in Table 31, Table 32 and Table 34 were taken from dose analysis framework. This is to remove the effects of differences due to the TG-43U1 (3) line source approximation and differences between MC source model and TG-43U1 consensus data from the robustness and ISA analysis, as discussed in 2.2.

Table 31 Impact on DVH parameters of random shifts in source dwell positions. All entries are mean values for 9 patients. The 0mm shift corresponds to the baseline (planned) values. Results are shown for whole-gland (WG), hemi-gland (HEMI) and ultra-focal (UF) plans. The target D90 and V100 values are for the prostate for WG plans, hemi-prostate for HEMI plans and F-PTV (focal-planning target volume) for UF plans.

Shift	Target D90			Target V100			Urethra D10			Rectum D2cm^3			Bladder D2cm^3		
	WG	HEMI	UF	WG	HEMI	UF	WG	HEMI	UF	WG	HEMI	UF	WG	HEMI	UF
0mm	175.6	187.4	206.8	99.6	97.1	99.6	205.3	186.7	90.4	106.3	76.2	42.6	90.8	63.4	18.9
2mm	167.7	172.0	176.6	98.2	95.5	97.4	223.7	202.2	95.9	107.8	77.3	43.2	91.2	64.1	19.1
3mm	159.9	160.3	157.7	95.9	93.2	93.3	238.3	221.8	97.6	109.4	78.6	43.8	91.2	64.5	19.2
4mm	151.0	149.0	140.8	92.4	90.0	86.2	253.4	232.6	101.9	110.8	80.5	44.7	91.6	65.5	19.6
5mm	142.6	138.6	125.8	87.9	85.6	76.0	262.7	246.2	104.3	113.7	82.0	45.4	91.1	66.7	20.8

Table 32 Impact on DVH parameters of systematic shifts in source dwell positions. All entries are mean values for 9 patients. The 0mm shift corresponds to the baseline (planned) values. Results are shown for whole-gland (WG), hemi-gland (HEMI) and ultra-focal (UF) plans. Target D90 and V100 values are for prostate for WG plans, hemi-prostate for HEMI plans and F-PTV (focal-PTV) for UF plans.

Shift	Target D90			Target V100			Urethra D10			Rectum D2cm^3			Bladder D2cm^3		
	WG	HEMI	UF	WG	HEMI	UF	WG	HEMI	UF	WG	HEMI	UF	WG	HEMI	UF
0mm	175.6	187.4	206.8	99.6	97.1	99.6	205.3	186.7	90.4	106.3	76.2	42.6	90.8	63.4	18.9
2mm inf	173.0	179.0	189.5	98.8	96.1	99.0	200.1	186.0	91.7	105.9	75.9	42.3	79.9	55.9	16.7
2mm sup	174.5	187.1	201.4	99.0	97.0	98.7	205.2	185.1	88.2	105.8	76.0	42.5	102.8	70.8	21.1
2mm post	173.2	186.9	190.0	98.9	96.5	98.0	206.7	181.9	81.5	130.2	94.2	52.7	76.6	53.6	16.2
2mm ant	172.5	174.9	194.4	98.5	95.5	98.5	206.8	199.6	98.4	87.7	62.4	34.8	107.8	75.0	22.1
2mm left	175.3	178.6	192.4	99.6	94.8	98.2	229.5	192.6	96.6	106.2	75.9	41.8	90.4	61.8	18.4
2mm right	174.0	183.2	196.3	99.3	96.6	98.1	206.8	196.2	96.3	105.9	76.0	43.2	90.7	64.5	19.3
4mm inf	162.3	159.4	146.2	94.3	92.1	90.1	198.1	186.8	92.4	105.3	75.0	41.5	69.8	49.0	14.8
4mm sup	169.2	177.1	162.7	96.4	95.1	92.8	204.3	185.3	85.3	104.9	75.3	42.0	113.6	77.6	23.5
4mm post	166.1	174.1	152.4	96.4	94.4	91.5	210.7	185.7	72.2	161.6	118.3	65.8	65.1	45.5	13.9
4mm ant	161.1	152.8	161.3	94.3	91.0	92.5	211.4	229.1	105.8	73.0	51.7	28.7	126.8	89.1	25.9
4mm left	172.2	159.8	162.2	98.6	90.3	92.9	350.7	295.2	130.5	105.9	75.1	41.0	89.7	60.0	17.9
4mm right	170.1	165.7	162.3	98.0	92.8	93.0	237.3	231.3	116.7	105.2	75.4	43.7	90.2	65.2	19.7

Figure 27 and Figure 28 illustrate the variation of D90 and V100 values for planning targets with increasing random shift.

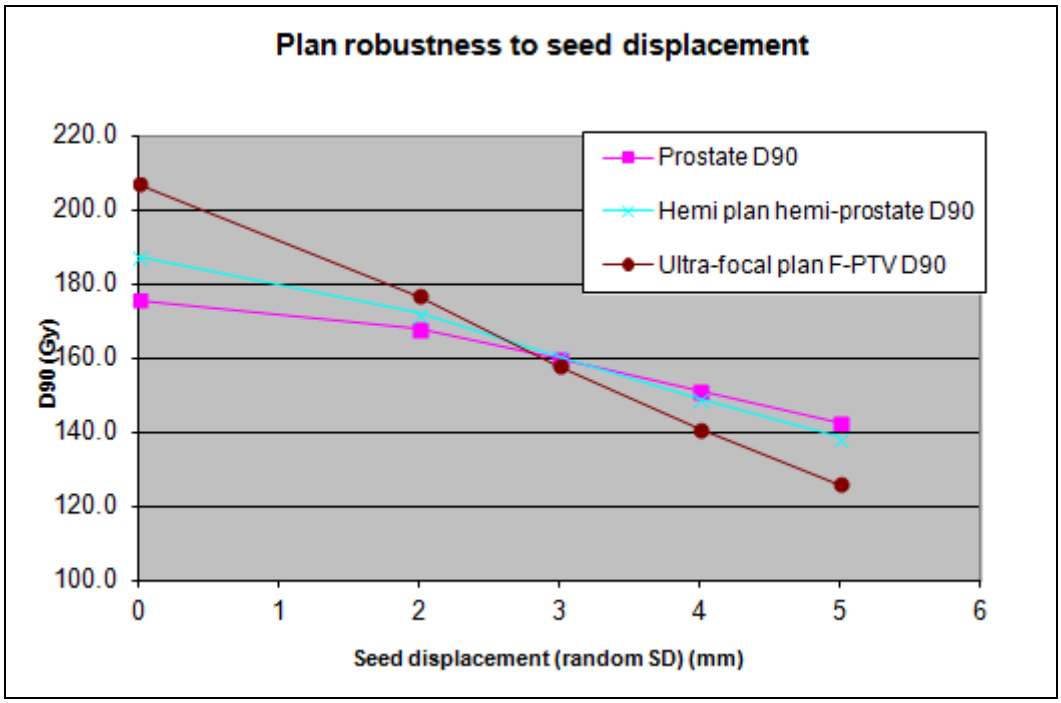

Figure 27 LDR plan robustness to random seed displacement - target D90 values

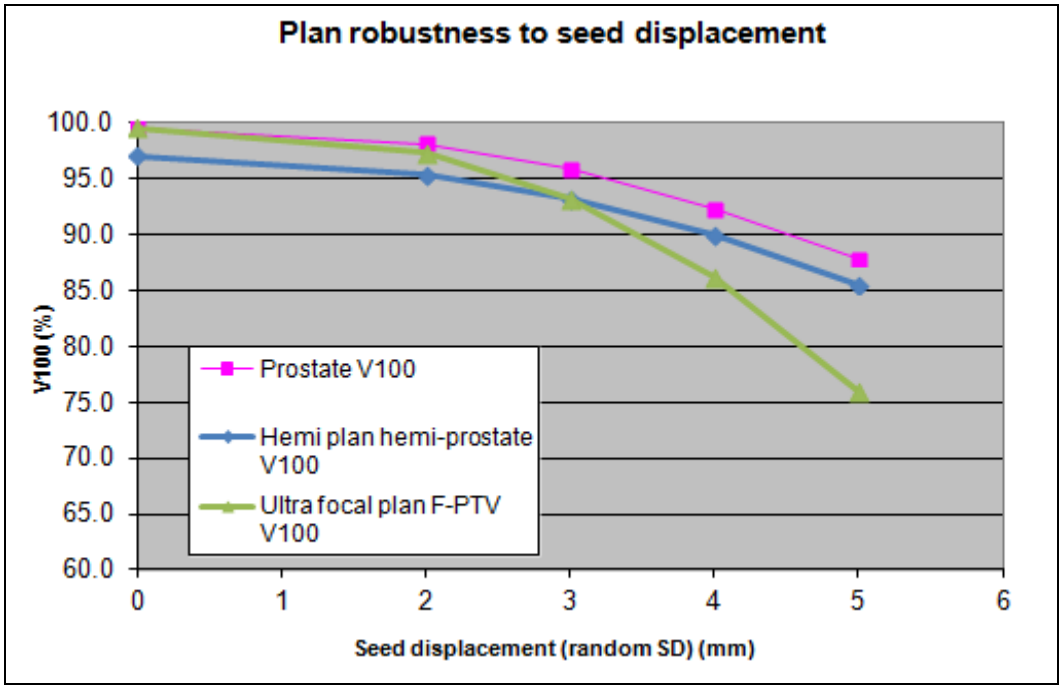

Figure 28 LDR plan robustness to random seed displacement - target V100 values

Table 32 summarizes the changes in DVH parameter values for prostate, hemi-prostate, F-PTV, urethra and rectum with systematic shifts of 2mm and 4mm applied in each anatomical direction.

Plan robustness - HDR

Table 33 shows the impact on key DVH parameters of the systematic shifts tested in the robustness analysis (mean values for 9 patients). The target D90 and V100 values compared are for prostate in WG plans, hemi-prostate in HEMI plans and F-PTV in UF plans, as these are the structures in each plan where planning objectives aimed to achieve 100% coverage.

Table 33 Impact on DVH parameters of systematic shifts in source dwell positions. All entries are mean values for 9 patients. The 0mm shift corresponds to the baseline (planned) values. Results are shown for whole-gland (WG), hemi-gland (HEMI) and ultra-focal (UF) plans. The target D90 and V100 values are for the prostate for WG plans, hemi-prostate for HEMI plans and F-PTV (focal-planning target volume) for UF plans.

Shift	Target D90			Target V100			Urethra D10			Rectum D2cm^3			Bladder D2cm^3		
	WG	HEMI	UF	WG	HEMI	UF	WG	HEMI	UF	WG	HEMI	UF	WG	HEMI	UF
0mm	20.5	22.3	23.2	97.9	98.2	98.3	20.2	19.8	9.2	12.6	9.9	4.6	10.6	7.9	2.8
2mm inf	20.3	22.0	21.6	97.0	97.6	96.3	20.2	19.8	9.1	12.5	9.8	4.6	10.2	7.6	2.7
2mm sup	20.3	21.8	22.4	96.9	97.1	97.4	20.2	19.9	9.2	12.6	9.9	4.6	8.6	6.4	2.3
2mm post	20.4	22.2	21.4	96.7	97.3	94.7	20.3	19.9	8.5	14.8	11.8	5.4	8.3	6.2	2.2
2mm ant	20.1	21.2	20.7	95.2	95.5	93.4	20.8	21.2	9.8	10.9	8.4	3.9	10.8	7.9	2.8
2mm left	20.4	21.5	21.0	97.7	95.6	94.0	20.6	19.6	9.9	12.6	9.9	4.5	9.4	6.9	2.4
2mm right	20.4	21.6	20.5	97.7	96.7	93.0	20.5	20.1	9.4	12.6	9.9	4.7	9.4	7.0	2.5
4mm inf	19.9	21.0	18.2	94.0	95.0	87.0	20.3	19.9	9.0	12.4	9.7	4.6	11.0	8.2	2.9
4mm sup	19.7	20.3	19.6	93.2	93.3	91.1	20.4	20.0	9.1	12.6	9.8	4.5	7.9	5.9	2.1
4mm post	19.8	21.0	16.7	93.3	94.2	84.7	21.0	21.1	7.8	17.6	14.3	6.4	7.3	5.5	2.0
4mm ant	18.7	18.8	16.0	89.6	89.6	82.2	22.3	25.3	10.4	9.6	7.3	3.4	12.5	9.0	3.2
4mm left	20.2	19.2	16.5	96.5	89.3	83.2	22.0	20.1	11.5	12.6	9.8	4.4	9.3	6.9	2.4
4mm right	20.2	19.5	15.5	96.4	91.0	81.2	22.1	21.2	10.7	12.6	9.8	4.7	9.3	7.0	2.5

Monte Carlo simulation - LDR

Table 34 summarizes the impact of ISA on key DVH parameter values in each focal therapy plan, for plans using 6711 and 9011 seeds.

Monte Carlo simulation - HDR

Table 35 compares the mean baseline DVH values from the robustness analysis with corresponding results from the MC simulation study - any differences will be purely down to taking account of the steel catheters in the MC simulation. Note that the baseline DVH values in Table 30 were calculated using the TPS so are slightly different from those in Table 33 and Table 35 which were calculated using the DVH analysis framework described above. These differences are particularly noticeable for the bladder; this is most likely caused by differences in how the DVH calculations handle contour interpolation, as the bladder contour varies rapidly from slice to slice at the prostate base.

6.1.3 Discussion

This study has investigated the dosimetry of focal prostate brachytherapy for a group of patients who met the clinical characteristics defined for focal therapy by a consensus report for LDR focal brachytherapy (25). Two focal treatment approaches, hemi-gland and ultra-focal, as defined by the consensus report (25), were compared to standard whole-gland planning approaches. Cossett et al. (24) reported from a pilot study on LDR focal therapy treatments. 21 patients were treated with an ultra-focal approach with the treated volume covering on average 34% of the prostate or 13.7 cm^3. 145Gy was prescribed to the treatment volume achieving a mean D90 of 183.2Gy and mean V100 of 99.3%. OAR doses were not reported. In this study higher F-PTV D90 values were achieved (mean 218.3 Gy) however this may be because the volumes were smaller (mean 4.8cm^3).

Table 34 DVH parameter value differences between planned and MC simulation.

		6711			9011	
	Planned value	**MC simulation**	**Difference**	**Planned value**	**MC simulation**	**Difference**
Standard plan						
Prostate D90 (Gy)	175.9	173.1	-2.8 (-1.6%)	170.8	169.6	-1.2 (-0.8%)
Prostate V100 (%)	99.6	99.4	-0.2	99.3	99.2	-0.1
Prostate V150 (%)	54.4	51.7	-2.7	50.2	48.9	-1.3
Urethra D10 (Gy)	202.7	199.9	-2.8 (-1.4%)	196.6	196.0	-0.6 (-0.3%)
Rectum D2**cm^3** (Gy)	106.2	103.6	-2.6 (-2.5%)	102.9	101.7	-1.2 (-1.2%)
Hemi-gland plan						
Hemi-prostate D90 (Gy)	188.0	183.9	-4.1 (-2.2%)	183.2	181.0	-2.2 (-1.2%)
Hemi-prostate V100 (%)	97.1	96.7	-0.4	96.7	96.5	-0.2
Hemi-prostate V150 (%)	78.1	76.1	-2.0	75.5	74.4	-1.1
Urethra D10 (Gy)	185.4	180.9	-4.5 (-2.3%)	180.0	178.2	-1.8 (-1.0%)
Rectum D2cm^3 (Gy)	76.3	74.2	-2.1 (-2.7%)	73.9	72.8	-1.1 (-1.4%)
Ultra-focal plan						
F-PTV D90 (Gy)	207.5	203.3	-4.2 (-2.0%)	202.9	201.2	-1.7 (-0.8%)
F-PTV V100 (%)	99.7	99.6	-0.1	99.6	99.5	-0.1
F-PTV V150 (%)	84.8	83.5	-1.3	82.5	81.9	-0.6
Urethra D10 (Gy)	90.3	88.1	-2.2 (-2.5%)	87.6	86.6	-1.0 (-1.1%)
Rectum D2cm^3 (Gy)	42.7	41.6	-1.1 (-2.8%)	41.3	40.7	-0.6 (-1.5%)

Table 35 DVH parameter value differences between planned and MC simulation.

	Planned value	**MC simulation**	**Difference (%)**
Standard plan			
Prostate D90	20.5	20.2	-1.3
Prostate V100	97.9	97.4	-0.5
Prostate V150	23.5	22.2	-1.4
Urethra D10	20.2	19.9	-1.1
Rectum D2cm^3	12.6	12.4	-1.4
Hemi-gland plan			
Hemi-prostate D90	22.3	22.0	-1.4
Hemi-prostate -CTV V100	98.2	97.8	-0.4
Hemi-prostate -CTV V150	38.3	35.8	-2.4
Urethra D10	19.8	19.5	-1.5
Rectum D2cm^3	9.9	9.7	-1.7
Ultra-focal plan			
F-PTV D90	23.2	22.8	-1.6
F-PTV V100	98.3	98.0	-0.3
F-PTV V150	61.8	58.9	-3.0
Urethra D10	9.2	9.0	-1.8
Rectum D2cm^3	4.6	4.5	-2.0

HDR hemi-gland treatments were previously modeled by Kamrava et al. (27), who found similar target coverage to whole-gland treatments, but with urethral D2cm^3 reduced from 95.2% to 69.3% of the prescription dose. In the current study, for hemi-gland treatments, hemi-prostate D90 and V100 were slightly higher than whole-gland treatment prostate D90 and V100, and the mean urethral D10 reduced from 20.3 Gy to 19.7 Gy. This much smaller reduction in urethral dose is explained by two factors. Firstly the current study evaluated urethra D10 and D30, these have similar values to D0.1cm^3 in the patients studied, and Kamrava et al. did observe a smaller reduction in D0.1cm^3, from 106.7% to 97.7% (27). Secondly the current study attempted to cover the entire hemi prostate whereas Kamrava et al. (27) deliberately excluded the most anterior part of the hemi-prostate and a 2mm margin around the urethra. This second point also explains why the H-PTV coverage (mean V100 88.6%) is lower than PTV coverage in standard plans (mean V100 94.8%). These results illustrate that for hemi-gland treatments there is a compromise to be reached between treating the whole hemi-gland and achieving a reduced urethral dose. For some patients in the current study, urethra Dmax (maximum point dose) was higher for hemi-gland plans than for whole-gland (although overall the mean difference was not statistically significant). A comparable urethral dose in hemi-gland treatments may still be acceptable if the objective of focal therapy is to spare the contra-lateral neuro-vascular bundle. Hemi-gland plans did achieve 20% - 30% reductions in mean rectum and bladder doses compared to whole-gland plans for both LDR and HDR plans.

There are no published studies reporting dosimetry for ultra-focal HDR brachytherapy treatment planning. The results of this study show that it is possible to deliver a high D90 to an ultra-focal target (mean dose 23 Gy or 121% of the prescription dose for the F-PTV) while achieving significant reductions to OAR doses. Mean reductions from hemi-gland to ultra-focal plans for HDR were 53% for urethra D10, 53% for rectum D2cm^3 and 64% for bladder D2cm^3. The small size and irregular shape of ultra-focal targets mean that some over-treatment is inevitable if the objective is to achieve

100% coverage of the F-PTV. For ultra-focal plans in this study the mean volume of the whole-gland PTV receiving 100% dose was 13.6% for HDR plans and 18.9% for LDR plans, while the mean F-PTV volume was 9% of the PTV. This over-treatment may be beneficial providing an additional safety margin around the tumour.

A limitation of this study is that the dosimetric results for ultra-focal planning depend partly on the size of the margin applied to the F-GTV. A margin of 4.5mm was estimated in 5.1.3 to account for tumour delineation and MR-TRUS image registration uncertainties in focal boost treatment planning and a study by Groenendaal et al (144) estimated a margin of 5mm for MR tumour delineation error, by comparison to pathology results. In focal boost treatments the whole prostate is treated to the prescription dose, which provides an additional safety margin compared to ultra-focal treatments. For this reason a 6mm margin was used in this study, constrained to the whole-gland PTV and to avoid the urethra. Results for ultra-focal plans also depend on the location and size of the target. In this study lesions were small and the majority of lesions were located in peripheral zone tissue. In two cases lesions were in the central gland close to the urethra. This did not impact F-PTV coverage but did lead to increased urethral dose; this is reflected in the wide range of ultra-focal plans urethra D10 values. If larger lesions were treated this would also lead to increased urethral dose, however patients with large lesions are less likely to be considered suitable for focal therapy. Further limitations of this study are that the prostate position and shape from the MRI data used for treatment planning will not be exactly as would be expected for TRUS based planning and that a treatment planning study can use ideal catheter positions that may not be achieved in practice.

The results for plan robustness show that source position errors will have a greater effect on target dosimetry for focal therapy targets than for whole-gland treatments. For LDR treatments random and systematic errors were simulated. In clinical implants these errors could be caused by errors in

source placement, prostate oedema and source migration after implantation. A study by Bues et al (154) estimated post implant source position shifts could be simulated using random shifts with standard deviation 4mm. In our study this level of random shift reduces whole-gland plan prostate D90 by 14% but reduces ultra-focal plan F-PTV D90 by 32%. These are significant differences in the context of overall LDR prostate brachytherapy uncertainties, which were estimated as 11% (k=1) in a review by Kirisits et al. (38).

For HDR plans, as our study assumes a single fraction treatment, inter-fraction catheter movement does not need to be considered. However source position errors can still occur within a single fraction and the magnitude of these errors depends on the treatment protocol. For example, for CT based treatment planning, Whitaker et al. (155) observed a median caudal shift of 7.5mm between planning scan and treatment delivery with any shift 5mm or greater being corrected before treatment delivery. That means a shift of 4mm would not be corrected. On average for the patients in our study, a caudal shift of 4mm for all catheters would reduce whole-gland treatment prostate D90 by 2.8% and V100 by 4.0%, hemi-gland treatment hemi-prostate D90 by 5.8% and V100 by 3.3% and ultra-focal treatment F-PTV D90 by 21.4% and V100 by 11.5%. For TRUS based treatment planning there is no need to move the patient between planning scan and treatment delivery, so shifts should be smaller. A study by Milickovic et al. (156) compared treatment planning TRUS scans to scans taken immediately before and immediately after treatment delivery, and measured mean catheter displacement of 1mm and mean prostate displacement of 0.57mm. Our results show that 1mm shifts have negligible impact on whole-gland and hemi-gland treatments, whilst ultra-focal treatment F-PTV D90 is reduced by 2.2% (mean for all directions). However a 2mm shift (the maximum shift observed in the study by Milickovic et al. (156) reduces ultra-focal treatment F-PTV D90 by 8.3% (mean for all directions), illustrating the sensitivity to source position errors. These results should be considered in the context of overall uncertainties in HDR prostate

brachytherapy - a review by Kirisits et al. (38) estimated that catheter shifts contributed 2% to overall (k=1) uncertainty of 5% in TRUS based treatment planning.

MC simulation results for LDR plans show that there is little difference in the magnitude of the ISA effect for focal therapy treatments compared to whole gland treatments. This is in spite of the seed density in ultra-focal plans being on average 2.5 times greater compared to whole gland plans. Achieving 100% coverage of a small target results in a higher target D90 compared to whole gland plans, so that the ISA effect remains at the same level in percentage terms even though the absolute dose that is attenuated increases. Comparison of the ISA effect for 6711 and 9011 seed models shows that the 9011 source approximately halves the ISA effect compared to 6711, as was seen for clinical whole gland plans in 4.1.3.

There are no published studies of MC simulation of prostate dosimetry for HDR brachytherapy. Our results have shown that the presence of steel catheters in the implant has only a small impact on dose for whole-gland plans, reducing key DVH parameters by <1.5%. For focal therapy plans the impact is slightly increased, but still $\leq 2\%$, except for F-PTV V150 which is reduced by 3%. Therefore we conclude that there are no special considerations for focal therapy in terms of the differences between TG-43U1 (3) and advanced dose calculations methods.

This study has assessed LDR and HDR treatment planning for a single group of patients. LDR and HDR focal therapy treatment plans are very similar in terms of dosimetry. The greater flexibility in plan optimization that can be achieved in HDR treatment planning by varying source dwell times results in OAR doses in HDR focal therapy plans that are lower as a percentage of the prescription dose than can be achieved for LDR plans. Source position errors are less likely in HDR treatments so the greater sensitivity of focal therapy plans to position errors demonstrated in this study will have less impact for HDR focal therapy. However this is a purely

dosimetric investigation which does not take into account the impact on the radiobiology of the treatments given the very different dose prescriptions and dose rates. An additional factor in favour of LDR treatments is that the 145Gy prescription dose is very well established for monotherapy whereas the 19Gy monotherapy prescription dose for HDR has only been used in clinical trials to date.

6.1.4 Conclusion

Hemi-gland and ultra-focal treatment options can achieve higher D90 values compared to standard whole-gland treatments and also give reduced dose to OARs. Focal therapy treatment plans are more sensitive to systematic source position errors than standard whole-gland treatments and this will have a bigger impact for LDR treatments compared to HDR. There are no special considerations for focal therapy in terms of the differences between TG-43U1 (4) and advanced dose calculations methods.

7 Conclusion

This research has investigated whether clinical prostate brachytherapy treatments can be improved through use of advanced dose calculation algorithms to better understand dose distributions, and more accurate targeting of dose to the prostate tumour using advanced imaging techniques. Prostate brachytherapy treatments using both LDR permanent implants and HDR temporary implants in combination with external beam have an excellent record in terms of patient outcomes. Nonetheless some patients do relapse after treatment and some patients suffer complications in terms of urinary and sexual function. Better patient outcomes may be possible with a better understanding of the relationship between dose and response which requires more accurate dosimetry and more accurate identification and targeting of tumour tissue within the prostate.

Advanced dose calculation methods using MC simulation have been applied to LDR ^{125}I permanent prostate implants and to HDR ^{192}Ir implants to explore the impact of assumptions made in the TG-43U1 (3) dose calculation algorithm that is widely used in clinical practice. Experimental phantom work using a MOSFET based dosimeter has successfully validated results of MC simulations. The feasibility of incorporating mp-MRI tumour delineation into prostate brachytherapy treatment planning has been assessed, and dosimetry of focal boost and focal treatments based on MRI data has been investigated. The following outlines key conclusions from this work and ideas for clinical implementation and/or further research work in each area.

Advanced dose calculations - LDR

This study has shown that ISA and tissue heterogeneities do have an effect on dose distributions in LDR prostate brachytherapy. These differences lead to reduced DVH parameter values especially for patients with calcifications. Dose reductions particularly affect peripheral dose and areas of the implant with relatively poorer coverage, the impact on the volume encompassed by

the 100% isodose is greater than the impact on the prostate. Dose reductions are smaller than other uncertainties in post-implant dosimetry such as seed placement errors, anatomy changes and imaging and contouring uncertainties. The ISA effect can be reduced by using a thinner seed model.

Clinical implementation and future work

Application of advanced dose calculations in LDR seed implant brachytherapy is limited by the time taken to calculate dose for a clinical implant - it is not possible to use MC simulation or other advanced dose calculation methods for real-time treatment planning, although methods to use pre-calculated MC simulation results are under development (157). Another limitation is that for the low energy sources used in LDR brachytherapy, dosimetric accuracy is sensitive to tissue composition which cannot be determined from standard CT data. Tissue composition determination using dual energy CT is under investigation (158).

MC simulations can be applied in post implant dosimetry, and could also be used for patients whose treatment is pre-planned (TRUS planning images acquired and treatment delivered in separate operating theatre sessions), although this is only a small proportion of cases in Leeds. Future work could include developing the MC simulation framework so that it becomes a routine part of post implant dosimetry. CT post implant data allows accurate density information to be incorporated into the simulation, although tissue composition (which has a larger impact on dosimetry than density) must still be assumed. This would be most likely to show an impact for patients with calcifications, and could allow a more accurate knowledge of dose-response relationships to be developed. The results in this study also show that advanced dose calculations would provide useful dosimetric information at the implant stage if the limitations discussed above can be overcome with advances in technology.

MC simulations naturally calculate dose to the medium that the simulation is performed in (tissue), whereas TG-43U1 (3) calculates dose to water.

Future work could investigate methods of converting between dose to medium and dose to water to provide a better understanding of the differences between simulation results and TG-43U1 dose calculations. This conversion is uncertain for low source energies (40) and is still under investigation (159-161).

Advanced dose calculations - HDR

The impact of TG-43U1 (3) assumptions in HDR prostate brachytherapy is less than for LDR. This is due to the higher energy of ^{192}Ir compared to ^{125}I. Tissue is water equivalent at ^{192}Ir energies (39), therefore dosimetric differences are due to dose attenuation by the steel catheters used to deliver the HDR source.

Clinical implementation and future work

Although the dosimetric impact would be small compared to other uncertainties, it would be straightforward to approximate the impact of these catheters in commercial treatment planning systems, as the impact of the catheter containing the source could easily be pre-calculated using MC simulation.

Advanced imaging - MRI guided brachytherapy

This study has investigated the use of mp-MRI techniques for prostate tumour delineation, to allow dose to the tumour to be escalated (focal boost) or treatment to target the tumour to reduce treatment related toxicities (focal therapy). The results show that mp-MRI-guided HDR prostate brachytherapy focal boost is feasible. Focal boost treatments planned on involved sectors determined from staging scans have comparable dosimetry to pre-treatment MRI based F-PTV focal boost plans, although differences in tumour delineation between staging and pre-treatment scans were observed. Mp-MRI techniques can be used to define tumour regions even in patients who have undergone hormone therapy. Increased focal boost dose can be achieved without violating urethral and rectal dose constraints and maintaining standard prostate/ptv coverage. No increases in the level of

treatment related toxicities were observed in patients treated with the focal boost treatment. The level of dose boost is lower for larger tumour regions or tumour regions close to either the urethra or rectum.

The dosimetric investigation of focal therapy has demonstrated that hemi-gland and ultra-focal treatment options can achieve higher D90 values compared to standard whole-gland treatments and also give reduced dose to OARs. Focal therapy treatment plans are more sensitive to systematic source position errors than standard whole-gland treatments and this will have a bigger impact for LDR treatments compared to HDR. There are no special considerations for focal therapy in terms of the differences between TG-43U1 (4) and advanced dose calculations methods.

Clinical implementation and future work

Focal boost treatments are now being implemented in Leeds. A key area for future work is to improve confidence and reduce variation in mp-MRI tumour delineation. For focal boost treatments a safety margin is provided because the whole prostate is still treated to the prescribed dose level, however for focal therapy treatments template biopsy validation of MRI results would be required. For ultra-focal approaches that target just the visible lesion, further investigation is required to determine the appropriate margin to account for uncertainties in tumour delineation, image fusion, and treatment source position errors.

Studies have investigated the use of software based automatic tumour segmentation for tumour delineation in these scenarios (144, 162, 163). Although this approach would remove the variability in tumour delineation, it has not been demonstrated that these approaches are more accurate than radiologist delineation. A possible future approach would be to develop better software to present mp-MRI data to radiologists and incorporate some kind of automatic segmentation based on radiologist delineations. More advanced quantitative MRI techniques may also help, for example DWI MRI using models that take account of incoherent motion (164) and the

ability to apply advanced tissue models on a voxel basis in DCE-MRI. Addition of MRSI to the mp-MRI protocol would further aid tumour delineation but using all three of DWI, DCE-MRI and MRSI would require a scan time of at least 40 minutes. For three out of thirty patients it was not possible to delineate tumour using the mp-MRI data. Improved MRI techniques would also help in these cases, an alternative would be to perform template mapping biopsy to determine the tumour location. Techniques for using TRUS for tumour delineation, based on ultrasound elastography or contrast enhanced ultrasound are also under investigation (165, 166). These would be more convenient for brachytherapy treatment planning as the brachytherapy procedure is already based on TRUS.

Image fusion of MRI delineated tumour volumes to treatment planning TRUS is a source of uncertainty in MRI targeted treatments. The presence of the TRUS probe in the rectum deforms the prostate. The prostate may also be deformed in the MRI scan depending on how much air is in the rectum at the time of the scan. The use of deformable image registration to increase the accuracy of fusion in these scenarios should be investigated. Treatment planning TRUS has low image contrast and mutual information based approaches to image fusion would be difficult to implement. However fusion could be calculated based on delineated prostate contours (167). Alternatively implanted markers could be used to assist image fusion. If staging scans are used for tumour delineation for patients treated after hormone therapy, changes in the prostate morphology may make image fusion unfeasible. In that case, as demonstrated in this study, sector based treatment planning may be a means of dealing with these uncertainties.

The focal boost patients treated in this study also receive external beam therapy. The MRI delineated tumour volumes could be registered to the external beam planning CT scan and used to deliver a focal boost during the external beam treatment. An investigation into delivering focal boost stereotactic ablative radiation therapy using VMAT for 10 patients from the HDR prostate MRI pilot study concluded that this was technically feasible

although radiobiologically the tumour control probability increase that could be achieved depended on the alpha-beta ratio assumed for prostate cancer (168).

Conclusion

This research has investigated whether clinical prostate brachytherapy treatments can be improved through better understanding of dose distributions through use of advanced dose calculation algorithms, and more accurate targeting of dose to the prostate tumour using advanced imaging techniques. Source interactions and tissue effects have been shown to reduce the dose that is delivered to patients in LDR treatments, particularly for patients with calcifications, however the dosimetric impact is small compared to other uncertainties in LDR seed implant brachytherapy. For HDR treatments attenuation by steel catheters has only a small impact on dose distributions. Feasibility of mp-MRI guided focal boost HDR prostate brachytherapy has been demonstrated in terms of tumour delineation and the ability to dose escalate the DIL without increased dose to normal tissues. The dosimetric feasibility of LDR and HDR focal therapy treatments has been demonstrated. Focal therapy treatments have been shown to be more sensitive to source position errors than whole gland treatments. MC simulations of focal therapy treatments show that there are no additional concerns in terms of dosimetric accuracy compared to standard whole gland treatments. Advanced dose calculation and imaging techniques can improve clinical prostate brachytherapy treatments.

8 References

1. National Institute for Health and Care Excellence. Prostate cancer: diagnosis and treatment, January 2014
2. KOUKOURAKIS, G., N. KELEKIS, V. ARMONIS and V. KOULOULIAS. Brachytherapy for prostate cancer: a systematic review. *Advances in urology*, 2009, **2009**, pp.1-11.
3. RIVARD, M.J., B.M. COURSEY, L.A. DEWERD, W.F. HANSON, M.S. HUQ, G.S. IBBOTT, M.G. MITCH, R. NATH and J.F. WILLIAMSON. Update of AAPM Task Group No. 43 Report: A revised AAPM protocol for brachytherapy dose calculations. *Medical Physics*, 2004, **31**, pp.633-674.
4. UK, C.R. *Prostate Cancer Incidence Statistics* [online]. 2014. [Accessed]. Available from: http://www.cancerresearchuk.org/cancer-info/cancerstats/types/prostate/incidence/uk-prostate-cancer-incidence-statistics.
5. UK, C.R.. *Prostate Cancer Survival Statistics* [online]. 2014. [Accessed]. Available from: http://www.cancerresearchuk.org/cancer-info/cancerstats/types/prostate/survival/prostate-cancer-survival-statistics.
6. PETER HOSKIN , G.K., MARCO VAN VULPEN , DIMOS BALTAS *GEC-ESTRO Handbook of Brachytherapy Second Edition - Prostate Cancer* [online]. 2014. [Accessed 9/12/2014]. Available from: http://www.estro.org/about/governance-organisation/committees-activities/gec-estro-handbook-of-brachytherapy.
7. VAN DEN BERGH, R.C., M.L. ESSINK-BOT, M.J. ROOBOL, T. WOLTERS, F.H. SCHRÖDER, C.H. BANGMA and E.W. STEYERBERG. Anxiety and distress during active surveillance for early prostate cancer. *Cancer*, 2009, **115**(17), pp.3868-3878.
8. WILT, T.J., R. MACDONALD, I. RUTKS, T.A. SHAMLIYAN, B.C. TAYLOR and R.L. KANE. Systematic review: comparative effectiveness and harms of treatments for clinically localized prostate cancer. *Annals of internal medicine*, 2008, **148**(6), pp.435-448.
9. GRIMM, P., I. BILLIET, D. BOSTWICK, A.P. DICKER, S. FRANK, J. IMMERZEEL, M. KEYES, P. KUPELIAN, W.R. LEE and S. MACHTENS. Comparative analysis of prostate-specific antigen free survival outcomes for patients with low, intermediate and high risk prostate cancer treatment by radical therapy. Results from the Prostate Cancer Results Study Group. *BJU international*, 2012, **109**(s1), pp.22-29.
10. HENRY, A.M., B. AL-QAISIEH, K. GOULD, P. BOWNES, J. SMITH, B. CAREY, D. BOTTOMLEY and D. ASH. Outcomes

following iodine-125 monotherapy for localized prostate cancer: the results of leeds 10-year single-center brachytherapy experience. *International Journal of Radiation Oncology* Biology* Physics*, 2010, **76**(1), pp.50-56.

11. DEARNALEY, D.P., M.R. SYDES, J.D. GRAHAM, E.G. AIRD, D. BOTTOMLEY, R.A. COWAN, R.A. HUDDART, C.C. JOSE, J.H.L. MATTHEWS and J. MILLAR. Escalated-dose versus standard-dose conformal radiotherapy in prostate cancer: first results from the MRC RT01 randomised controlled trial. *The lancet oncology*, 2007, **8**(6), pp.475-487.
12. ASH, D., A. FLYNN, J. BATTERMANN, T. DE REIJKE, P. LAVAGNINI and L. BLANK. ESTRO/EAU/EORTC recommendations on permanent seed implantation for localized prostate cancer. *Radiotherapy and oncology*, 2000, **57**(3), p.315.
13. NATH, R., W.S. BICE, W.M. BUTLER, Z. CHEN, A.S. MEIGOONI, V. NARAYANA, M.J. RIVARD and Y. YU. AAPM recommendations on dose prescription and reporting methods for permanent interstitial brachytherapy for prostate cancer: Report of Task Group 137. *Medical Physics*, 2009, **36**, pp.5310-5322.
14. SALEMBIER, C., P. LAVAGNINI, P. NICKERS, P. MANGILI, A. RIJNDERS, A. POLO, J. VENSELAAR and P. HOSKIN. Tumour and target volumes in permanent prostate brachytherapy: a supplement to the ESTRO/EAU/EORTC recommendations on prostate brachytherapy. *Radiotherapy and oncology*, 2007, **83**(1), pp.3-10.
15. HOSKIN, P.J., A. COLOMBO, A. HENRY, P. NIEHOFF, T. PAULSEN HELLEBUST, F.-A. SIEBERT and G. KOVACS. GEC/ESTRO recommendations on high dose rate afterloading brachytherapy for localised prostate cancer: An update. *Radiotherapy and oncology*, 2013, **107**(3), pp.325-332.
16. MORTON, G. and P. HOSKIN. Brachytherapy: Current Status and Future Strategies—Can High Dose Rate Replace Low Dose Rate and External Beam Radiotherapy? *Clinical Oncology*, 2013, **25**(8), pp.474-482.
17. BRENNER, D.J., A.A. MARTINEZ, G.K. EDMUNDSON, C. MITCHELL, H.D. THAMES and E.P. ARMOUR. Direct evidence that prostate tumors show high sensitivity to fractionation (low α/β ratio), similar to late-responding normal tissue. *International Journal of Radiation Oncology* Biology* Physics*, 2002, **52**(1), pp.6-13.
18. BAUMAN, G., M. HAIDER, U.A. VAN DER HEIDE and C. MÉNARD. Boosting imaging defined dominant prostatic tumors: A systematic review. *Radiotherapy and oncology*, 2013, **107**(3), pp.274-281.
19. MOURAVIEV, V., A. VILLERS, D.G. BOSTWICK, T.M. WHEELER, R. MONTIRONI and T.J. POLASCIK. Understanding the pathological features of focality, grade and tumour volume of early-stage prostate cancer as a foundation for parenchyma-sparing prostate cancer therapies: active surveillance and focal targeted therapy. *BJU international*, 2011, **108**(7), pp.1074-1085.

20. ARRAYEH, E., A.C. WESTPHALEN, J. KURHANEWICZ, M. ROACH, A.J. JUNG, P.R. CARROLL and F.V. COAKLEY. Does Local Recurrence of Prostate Cancer After Radiation Therapy Occur at the Site of Primary Tumor? Results of a Longitudinal MRI and MRSI Study. *International Journal of Radiation Oncology* Biology* Physics*, 2012, **82**(5), pp.e787–e793.
21. PUCAR, D., H. HRICAK, A. SHUKLA-DAVE, K. KUROIWA, M. DROBNJAK, J. EASTHAM, P.T. SCARDINO and M.J. ZELEFSKY. Clinically significant prostate cancer local recurrence after radiation therapy occurs at the site of primary tumor: magnetic resonance imaging and step-section pathology evidence. *International Journal of Radiation Oncology* Biology* Physics*, 2007, **69**(1), pp.62-69.
22. LIPS, I.M., U.A. VAN DER HEIDE, K. HAUSTERMANS, E.N. VAN LIN, F. POS, S.P. FRANKEN, A.N. KOTTE, C.H. VAN GILS and M. VAN VULPEN. Single blind randomized phase III trial to investigate the benefit of a focal lesion ablative microboost in prostate cancer (FLAME-trial): study protocol for a randomized controlled trial. *Trials*, 2011, **12**(1), p.255.
23. AHMED, H., A. FREEMAN, A. KIRKHAM, M. SAHU, R. SCOTT, C. ALLEN, J. VAN DER MEULEN and M. EMBERTON. Focal therapy for localized prostate cancer: a phase I/II trial. *The Journal of urology*, 2011, **185**(4), pp.1246-1255.
24. COSSET, J.-M., X. CATHELINEAU, G. WAKIL, N. PIERRAT, O. QUENZER, D. PRAPOTNICH, E. BARRET, F. ROZET, M. GALIANO and G. VALLANCIEN. Focal brachytherapy for selected low-risk prostate cancers: A pilot study. *Brachytherapy*, 2013, **12**(4), pp.331–337.
25. LANGLEY, S., H.U. AHMED, B. AL-QAISIEH, D. BOSTWICK, L. DICKINSON, F.G. VEIGA, P. GRIMM, S. MACHTENS, F. GUEDEA and M. EMBERTON. Report of a consensus meeting on focal low dose rate brachytherapy for prostate cancer. *BJU international*, 2012, **109**(s1), pp.7-16.
26. VAN DEN BOS, W., B.G. MULLER, H. AHMED, C.H. BANGMA, E. BARRET, S. CROUZET, S.E. EGGENER, I.S. GILL, S. JONIAU and G. KOVACS. Focal therapy in prostate cancer: international multidisciplinary consensus on trial design. *European urology*, 2014, **65**(6), pp.1078-1083.
27. KAMRAVA, M., M.P. CHUNG, O. KAYODE, J. WANG, L. MARKS, P. KUPELIAN, M. STEINBERG, S.-J. PARK and D.J. DEMANES. Focal high-dose-rate brachytherapy: A dosimetric comparison of hemigland vs. conventional whole-gland treatment. *Brachytherapy*, 2013, **12**(5), pp.434–441.
28. NGUYEN, P.L., M.-H. CHEN, Y. ZHANG, C.M. TEMPANY, R.A. CORMACK, C.J. BEARD, M.D. HURWITZ, W.W. SUH and A.V. D'AMICO. Updated results of magnetic resonance imaging guided partial prostate brachytherapy for favorable risk prostate cancer: implications for focal therapy. *The Journal of urology*, 2012, **118**(4), pp.1151–1156.

29. WILLIAMSON, J.F. Brachytherapy technology and physics practice since 1950: a half-century of progress. *Physics in medicine and biology*, 2006, **51**(13), p.R303.
30. NAG, S., W. BICE, K. DEWYNGAERT, B. PRESTIDGE, R. STOCK and Y. YU. The American Brachytherapy Society recommendations for permanent prostate brachytherapy postimplant dosimetric analysis. *International Journal of Radiation Oncology* Biology* Physics*, 2000, **46**(1), pp.221-230.
31. POTTERS, L., Y. CAO, E. CALUGARU, T. TORRE, P. FEARN and X.H. WANG. A comprehensive review of CT-based dosimetry parameters and biochemical control in patients treated with permanent prostate brachytherapy. *International Journal of Radiation Oncology* Biology* Physics*, 2001, **50**(3), pp.605-614.
32. STOCK, M.D., G. RICHARD, M.D. STONE, N. NELSON and M.S. TABERT. A dose-response study for I-125 prostate implants. *International Journal of Radiation Oncology* Biology* Physics*, 1998, **41**(1), pp.101-108.
33. RODRIGUES, G., X. YAO, D.A. LOBLAW, M. BRUNDAGE and J.L. CHIN. Low-dose rate brachytherapy for patients with low-or intermediate-risk prostate cancer: A systematic review. *Canadian Urological Association Journal*, 2013, **7**(11-12), p.463.
34. KOVACS, G., R. POTTER, T. LOCH, J. HAMMER, I.K. KOLKMAN-DEURLOO, J.J. DE LA ROSETTE and H. BERTERMANN. GEC/ESTRO-EAU recommendations on temporary brachytherapy using stepping sources for localised prostate cancer. *Radiotherapy and oncology*, 2005, **74**(2), pp.137-148.
35. MORTON, G., A. LOBLAW, P. CHEUNG, E. SZUMACHER, M. CHAHAL, C. DANJOUX, H.T. CHUNG, A. DEABREU, A. MAMEDOV and L. ZHANG. Is single fraction 15Gy the preferred high dose-rate brachytherapy boost dose for prostate cancer? *Radiotherapy and oncology*, 2011, **100**(3), pp.463-467.
36. ZAORSKY, N.G., L.A. DOYLE, K. YAMOAH, J.A. ANDREL, E.J. TRABULSI, M.D. HURWITZ, A.P. DICKER and R.B. DEN. High dose rate brachytherapy boost for prostate cancer: A systematic review. *Cancer treatment reviews*, 2014, **40**(3), pp.414-425.
37. HOSKIN, P.J., A.M. ROJAS, P.J. BOWNES, G.J. LOWE, P.J. OSTLER and L. BRYANT. Randomised trial of external beam radiotherapy alone or combined with high-dose-rate brachytherapy boost for localised prostate cancer. *Radiotherapy and oncology*, 2012, **103**(2), pp.217-222.
38. KIRISITS, C., M.J. RIVARD, D. BALTAS, F. BALLESTER, M. DE BRABANDERE, R. VAN DER LAARSE, Y. NIATSETSKI, P. PAPAGIANNIS, T.P. HELLEBUST and J. PEREZ-CALATAYUD. Review of clinical brachytherapy uncertainties: Analysis guidelines of GEC-ESTRO and the AAPM. *Radiotherapy and oncology*, 2014, **110**(1), pp.199-212.
39. RIVARD, M.J., J.L.M. VENSELAAR and L. BEAULIEU. The evolution of brachytherapy treatment planning. *Medical Physics*, 2009, **36**, p.2136.

40. BEAULIEU, L., Ã.C. TEDGREN, J.-F. CARRIER, S.D. DAVIS, F. MOURTADA, M.J. RIVARD, R.M. THOMSON, F. VERHAEGEN, T.A. WAREING and J.F. WILLIAMSON. Report of the Task Group 186 on model-based dose calculation methods in brachytherapy beyond the TG-43 formalism: Current status and recommendations for clinical implementation. *Medical Physics*, 2012, **39**, pp.6208-6236.
41. DIMOS BALTAS, L.S.N.Z. *The Physics of Modern Brachytherapy for Oncology*. Taylor & Francis, 2007.
42. ANAGNOSTOPOULOS, G., D. BALTAS, P. KARAISKOS, P. SANDILOS, P. PAPAGIANNIS and L. SAKELLIOU. Thermoluminescent dosimetry of the selectSeed I interstitial brachytherapy seed. *Medical Physics*, 2002, **29**, p.709.
43. MOBIT, P. and I. BADRAGAN. Dose perturbation effects in prostate seed implant brachytherapy with I-125. *Physics in medicine and biology*, 2004, **49**, pp.3171-3178.
44. CHIU-TSAO, S.T., D. MEDICH and J. MUNRO III. The use of new GAFCHROMIC EBT film for I seed dosimetry in Solid Water phantom. *Medical Physics*, 2008, **35**, p.3787.
45. HARTMANN, B., M. MARTIŠÍKOVÁ and O. JÄKEL. Technical Note: Homogeneity of Gafchromic EBT2 film. *Medical Physics*, 2010, **37**, p.1753.
46. PRESTIDGE, B.R., I. JURKOVIC, A.G. SADEGHI, L. SALINAS and W.S. BICE. Postoperative urethral dose assessment of I-125 prostate implants using in vivo MOSFET detectors. *Brachytherapy*, 2007, **6**(2), p.90.
47. CYGLER, J.E., A. SAOUDI, G. PERRY and C. MORASH. Feasibility study of using MOSFET detectors for in vivo dosimetry during permanent low-dose-rate prostate implants. *Radiotherapy and oncology*, 2006, **80**(3), pp.296-301.
48. LAMBERT, J., T. NAKANO, S. LAW, J. ELSEY, D.R. MCKENZIE and N. SUCHOWERSKA. In vivo dosimeters for HDR brachytherapy: a comparison of a diamond detector, MOSFET, TLD, and scintillation detector. *Medical Physics*, 2007, **34**, p.1759.
49. BLOEMEN-VAN GURP, E.J., B.K. HAANSTRA, L.H. MURRER, F.C. VAN GILS, A.L. DEKKER, B.J. MIJNHEER and P. LAMBIN. In Vivo Dosimetry with a Linear MOSFET Array to Evaluate the Urethra Dose during Permanent Implant Brachytherapy Using Iodine-125. *International journal of radiation oncology, biology, physics*, 2009, **73**(1), pp.314-321.
50. ZILIO, V.O., O.P. JONEJA, Y. POPOWSKI, A. ROSENFELD and R. CHAWLA. Absolute depth-dose-rate measurements for an Ir HDR brachytherapy source in water using MOSFET detectors. *Medical Physics*, 2006, **33**, p.1532.
51. THERRIAULT-PROULX, F., T.M. BRIERE, F. MOURTADA, S. AUBIN, S. BEDDAR and L. BEAULIEU. A phantom study of an in vivo dosimetry system using plastic scintillation detectors for real-time verification of 192Ir HDR brachytherapy. *Medical Physics*, 2011, **38**, pp.2542-2551.

52. PANTELIS, E., A.K. KARLIS, M. KOZICKI, P. PAPAGIANNIS, L. SAKELLIOU and J.M. ROSIAK. Polymer gel water equivalence and relative energy response with emphasis on low photon energy dosimetry in brachytherapy. *Physics in medicine and biology*, 2004, **49**, p.3495.
53. PANTELIS, E., G. LYMPEROPOULOU, P. PAPAGIANNIS, L. SAKELLIOU, E. STILIARIS, P. SANDILOS, I. SEIMENIS, M. KOZICKI and J.M. ROSIAK. Polymer gel dosimetry close to an 125I interstitial brachytherapy seed. *Physics in medicine and biology*, 2005, **50**, p.4371.
54. PAPAGIANNIS, P., E. PANTELIS, E. GEORGIOU, P. KARAISKOS, A. ANGELOPOULOS, L. SAKELLIOU, S. STILIARIS, D. BALTAS and I. SEIMENIS. Polymer gel dosimetry for the TG-43 dosimetric characterization of a new 125I interstitial brachytherapy seed. *Physics in medicine and biology*, 2006, **51**, p.2101.
55. MAZAHERI, Y., A. SHUKLA-DAVE, A. MUELLNER and H. HRICAK. MR imaging of the prostate in clinical practice. *Magnetic Resonance Materials in Physics, Biology and Medicine*, 2008, **21**(6), pp.379-392.
56. SEITZ, M., A. SHUKLA-DAVE, A. BJARTELL, K. TOUIJER, A. SCIARRA, P.J. BASTIAN, C. STIEF, H. HRICAK and A. GRASER. Functional magnetic resonance imaging in prostate cancer. *Eur Urol*, 2009, **55**(4), pp.801–814.
57. ARES, C., Y. POPOWSKI, S. PAMPALLONA, P. NOUET, G. DIPASQUALE, S. BIERI, O. ÖZSOY, M. ROUZAUD, H. KHAN and R. MIRALBELL. Hypofractionated Boost With High-Dose-Rate Brachytherapy and Open Magnetic Resonance Imaging–Guided Implants for Locally Aggressive Prostate Cancer: A Sequential Dose-Escalation Pilot Study. *International journal of radiation oncology, biology, physics*, 2009, **75**(3), pp.656-663.
58. GROENENDAAL, G., C.A.T. VAN DEN BERG, J.G. KORPORAAL, M.E.P. PHILIPPENS, P.R. LUIJTEN, M. VAN VULPEN and U.A. VAN DER HEIDE. Simultaneous MRI diffusion and perfusion imaging for tumor delineation in prostate cancer patients. *Radiotherapy and oncology*, 2010, **95**(2), pp.185-190.
59. OZER, S., D.L. LANGER, X. LIU, M.A. HAIDER, T.H. VAN DER KWAST, A.J. EVANS, Y. YANG, M.N. WERNICK and I.S. YETIK. Supervised and unsupervised methods for prostate cancer segmentation with multispectral MRI. *Medical Physics*, 2010, **37**, p.1873.
60. MCROBBIE, D.W., E.A. MOORE, M.J. GRAVES and M.R. PRINCE. *MRI From Picture to Proton.* 2nd ed. Cambridge University Press, 2007.
61. DESOUZA, N.M., S.A. REINSBERG, E.D. SCURR, J.M. BREWSTER and G.S. PAYNE. Magnetic resonance imaging in prostate cancer: the value of apparent diffusion coefficients for identifying malignant nodules. *British Journal of Radiology*, 2007, **80**(950), p.90.

62. HAIDER, M.A., T.H. VAN DER KWAST, J. TANGUAY, A.J. EVANS, A.T. HASHMI, G. LOCKWOOD and J. TRACHTENBERG. Combined T2-weighted and diffusion-weighted MRI for localization of prostate cancer. *American Journal of Roentgenology*, 2007, **189**(2), p.323.
63. MORGAN, V.A., S. KYRIAZI and S.E. ASHLEY. Evaluation of the potential of diffusion-weighted imaging in prostate cancer detection. *Acta Radiologica*, 2007, **48**(6), pp.695-703.
64. VAN AS, N. Correlation of diffusion-weighted MRI with whole mount radical prostatectomy specimens. *British Journal of Radiology*, 2008, **81**(966), p.456.
65. KAJIHARA, H., Y. HAYASHIDA, R. MURAKAMI, K. KATAHIRA, R. NISHIMURA, Y. HAMADA, K. KITANI, M. KITAOKA, Y. SUZUKI and M. KITAJIMA. Usefulness of diffusion-weighted imaging in the localization of prostate cancer. *International Journal of Radiation Oncology* Biology* Physics*, 2009, **74**(2), pp.399-403.
66. DESOUZA, N.M., S.F. RICHES, N.J. VANAS, V.A. MORGAN, S.A. ASHLEY, C. FISHER, G.S. PAYNE and C. PARKER. Diffusion-weighted magnetic resonance imaging: a potential non-invasive marker of tumour aggressiveness in localized prostate cancer. *Clinical radiology*, 2008, **63**(7), pp.774-782.
67. ITOU, Y., K. NAKANISHI, Y. NARUMI, Y. NISHIZAWA and H. TSUKUMA. Clinical utility of apparent diffusion coefficient (ADC) values in patients with prostate cancer: Can ADC values contribute to assess the aggressiveness of prostate cancer? *Journal of Magnetic Resonance Imaging*, 2011, **33**(1), pp.167-172.
68. TURKBEY, B., V.P. SHAH, Y. PANG, M. BERNARDO, S. XU, J. KRUECKER, J. LOCKLIN, A.A. BACCALA JR, A.R. RASTINEHAD and M.J. MERINO. Is apparent diffusion coefficient associated with clinical risk scores for prostate cancers that are visible on 3-T MR images? *Radiology*, 2011, **258**(2), pp.488-495.
69. WALKER-SAMUEL, S., M. ORTON, L.D. MCPHAIL and S.P. ROBINSON. Robust estimation of the apparent diffusion coefficient (ADC) in heterogeneous solid tumors. *Magnetic Resonance In Medicine*, 2009, **62**(2), pp.420-429.
70. KOH, D.M. and D.J. COLLINS. Diffusion-weighted MRI in the body: applications and challenges in oncology. *American Journal of Roentgenology*, 2007, **188**(6), p.1622.
71. RICHES, S.F., K. HAWTIN, E.M. CHARLES-EDWARDS and N.M. DE SOUZA. Diffusion-weighted imaging of the prostate and rectal wall: comparison of biexponential and monoexponential modelled diffusion and associated perfusion coefficients. *NMR in Biomedicine*, 2009, **22**(3), pp.318-325.
72. HRICAK, H., P.L. CHOYKE, S.C. EBERHARDT, S.A. LEIBEL and P.T. SCARDINO. Imaging Prostate Cancer: A Multidisciplinary Perspective1. *Radiology*, 2007, **243**(1), p.28.
73. ALONZI, R. and P. HOSKIN. Functional imaging in clinical oncology: magnetic resonance imaging-and computerised

tomography-based techniques. *Clinical Oncology*, 2006, **18**(7), pp.555-570.

74. ALONZI, R., A.R. PADHANI and C. ALLEN. Dynamic contrast enhanced MRI in prostate cancer. *European Journal of Radiology*, 2007, **63**(3), pp.335-350.
75. BUCKLEY, D.L. and G.J.M. PARKER. Measuring Contrast Agent Concentration in T1-Weighted Dynamic Contrast-Enhanced MRI. *In:* A. JACKSON, D. BUCKLEY and G. PARKER, eds. *Dynamic Contrast-Enhanced Magnetic Resonance Imaging in Oncolgoy*. Berlin Heidelberg New York: Springer, 2005.
76. TOFTS, P.S., G. BRIX, D.L. BUCKLEY, J.L. EVELHOCH, E. HENDERSON, M.V. KNOPP, H.B.W. LARSSON, T.Y. LEE, N.A. MAYR and G.J.M. PARKER. Estimating kinetic parameters from dynamic contrast-enhanced T1-weighted MRI of a diffusable tracer: standardized quantities and symbols. *Journal of Magnetic Resonance Imaging*, 1999, **10**(3), pp.223-232.
77. JACKSON, A.S.N., S.A. REINSBERG, S.A. SOHAIB, E.M. CHARLES-EDWARDS, S. JHAVAR, T.J. CHRISTMAS, A.C. THOMPSON, M.J. BAILEY, C.M. CORBISHLEY and C. FISHER. Dynamic contrast-enhanced MRI for prostate cancer localization. *British Journal of Radiology*, 2009, **82**(974), p.148.
78. LANGER, D.L., T.H. VAN DER KWAST, A.J. EVANS, A. PLOTKIN, J. TRACHTENBERG, B.C. WILSON and M.A. HAIDER. Prostate Tissue Composition and MR Measurements: Investigating the Relationships between ADC, T2, Ktrans, ve, and Corresponding Histologic Features1. *Radiology*, 2010, **255**(2), pp.485-494.
79. FRANIEL, T., C. STEPHAN, A. ERBERSDOBLER, E. DIETZ, A. MAXEINER, N. HELL, A. HUPPERTZ, K. MILLER, R. STRECKER and B. HAMM. Areas Suspicious for Prostate Cancer: MRâ€“guided Biopsy in Patients with at Least One Transrectal US-guided Biopsy with a Negative Findingâ€”Multiparametric MR Imaging for Detection and Biopsy Planning. *Radiology*, 2011, **259**(1), pp.162-172.
80. RAVIZZINI, G., B. TURKBEY, K. KURDZIEL and P.L. CHOYKE. New horizons in prostate cancer imaging. *European Journal of Radiology*, 2009, **70**(2), p.212.
81. PARKER, G.J.M. and D.L. BUCKLEY. Tracer Kinetic Modelling for T1-Weighted DCE-MRI. *In:* A. JACKSON, D. BUCKLEY and G. PARKER, eds. *Dynamic Contrast-Enhanced Magnetic Resonance Imaging in Oncolgoy*. Berlin Heidelberg New York: Springer, 2005.
82. DONALDSON, S.B., C.M.L. WEST, S.E. DAVIDSON, B.M. CARRINGTON, G. HUTCHISON, A.P. JONES, S.P. SOURBRON and D.L. BUCKLEY. A comparison of tracer kinetic models for T1-weighted dynamic contrast-enhanced MRI: Application in carcinoma of the cervix. *Magnetic Resonance In Medicine*, 2010, **63**(3), pp.691-700.
83. KOBUS, T., T. HAMBROCK, C.A. HULSBERGEN-VAN DE KAA, A.J. WRIGHT, J.O. BARENTSZ, A. HEERSCHAP and T.W.

SCHEENEN. In vivo assessment of prostate cancer aggressiveness using magnetic resonance spectroscopic imaging at 3 T with an endorectal coil. *European urology*, 2011, **60**(5), pp.1074-1080.

84. HRICAK, H., S. WHITE, D. VIGNERON, J. KURHANEWICZ, A. KOSCO, D. LEVIN, J. WEISS, P. NARAYAN and P.R. CARROLL. Carcinoma of the prostate gland: MR imaging with pelvic phased-array coils versus integrated endorectal--pelvic phased-array coils. *Radiology*, 1994, **193**(3), p.703.
85. HEIJMINK, S.W., J.J. FÜTTERER, T. HAMBROCK, S. TAKAHASHI, T.W.J. SCHEENEN, H.J. HUISMAN, C.A. HULSBERGEN–VAN DE KAA, B.C. KNIPSCHEER, L. KIEMENEY and J.A. WITJES. Prostate Cancer: Body-Array versus Endorectal Coil MR Imaging at 3 T—Comparison of Image Quality, Localization, and Staging Performance1. *Radiology*, 2007, **244**(1), p.184.
86. HOEKS, C.M.A., J.O. BARENTSZ, T. HAMBROCK, D. YAKAR, D.M. SOMFORD, S.W. HEIJMINK, T.W.J. SCHEENEN, P.C. VOS, H. HUISMAN and I.M. VAN OORT. Prostate cancer: multiparametric MR imaging for detection, localization, and staging. *Radiology*, 2011, **261**(1), pp.46-66.
87. VARGAS, H.A., C. WASSBERG, O. AKIN and H. HRICAK. MR imaging of treated prostate cancer. *Radiology*, 2012, **262**(1), pp.26-42.
88. PADHANI, A.R., A.D. MACVICAR, C.J. GAPINSKI, D.P. DEARNALEY, G.J.M. PARKER, J. SUCKLING, M.O. LEACH and J.E. HUSBAND. Effects of Androgen Deprivation on Prostatic Morphology and Vascular Permeability Evaluated with MR Imaging1. *Radiology*, 2001, **218**(2), p.365.
89. ALONZI, R., A.R. PADHANI, N.J. TAYLOR, J.J. STIRLING, M.I. SAUNDERS and P.J. HOSKIN. Physiological Changes within the Prostate Caused by Androgen Withdrawal. *Clinical Oncology*, 2007, **19**(3), p.6.
90. MUELLER-LISSE, U.G., M.G. SWANSON, D.B. VIGNERON, H. HRICAK, A. BESSETTE, R.G. MALES, P.J. WOOD, S. NOWOROLSKI, S.J. NELSON and I. BARKEN. Time-dependent effects of hormone-deprivation therapy on prostate metabolism as detected by combined magnetic resonance imaging and 3D magnetic resonance spectroscopic imaging. *Magnetic Resonance In Medicine*, 2001, **46**(1), pp.49-57.
91. MUELLER-LISSE, U.G., M.G. SWANSON, D.B. VIGNERON and J. KURHANEWICZ. Magnetic resonance spectroscopy in patients with locally confined prostate cancer: association of prostatic citrate and metabolic atrophy with time on hormone deprivation therapy, PSA level, and biopsy Gleason score. *European Radiology*, 2007, **17**(2), pp.371-378.
92. GROENENDAAL, G., M. VAN VULPEN, S.R. PEREBOOM, D. POELMA-TAP, J.G. KORPORAAL, E. MONNINKHOF and U.A. VAN DER HEIDE. The effect of hormonal treatment on conspicuity of prostate cancer: Implications for focal boosting radiotherapy. *Radiotherapy and oncology*, 2012, **103**(2), pp.233–238.

93. DIBIASE, S.J., K. HOSSEINZADEH, R.P. GULLAPALLI, S.C. JACOBS, M.J. NASLUND, G.N. SKLAR, R.B. ALEXANDER and C. YU. Magnetic resonance spectroscopic imaging-guided brachytherapy for localized prostate cancer. *International Journal of Radiation Oncology* Biology* Physics*, 2002, **52**(2), pp.429-438.
94. ZAIDER, M., M.J. ZELEFSKY, E.K. LEE, K.L. ZAKIAN, H.I. AMOLS, J. DYKE, G. COHEN, Y.C. HU, A.K. ENDI and C.S. CHUI. Treatment planning for prostate implants using magnetic-resonance spectroscopy imaging. *International journal of radiation oncology, biology, physics*, 2000, **47**(4), pp.1085-1096.
95. POULIOT, J., Y. KIM, E. LESSARD and I. HSU. Inverse planning for HDR prostate brachytherapy used to boost dominant intraprostatic lesions defined by magnetic resonance spectroscopy imaging* 1. *International Journal of Radiation Oncology* Biology* Physics*, 2004, **59**(4), pp.1196-1207.
96. KIM, Y., I. HSU, J. CHOW, E. LESSARD, J. KURHANEWICZ, S.M. NOWOROLSKI and J. POULIOT. Class solution in inverse planned HDR prostate brachytherapy for dose escalation of DIL defined by combined MRI/MRSI. *Radiotherapy and oncology*, 2008, **88**(1), pp.148-155.
97. VAN LIN, E., J.J. FÜTTERER, S.W. HEIJMINK, L.P. VAN DER VIGHT, A.L. HOFFMANN, P. VAN KOLLENBURG, H.J.J. HUISMAN, T.W.J. SCHEENEN, J.A. WITJES and J.W. LEER. IMRT boost dose planning on dominant intraprostatic lesions: gold marker-based three-dimensional fusion of CT with dynamic contrast-enhanced and 1H-spectroscopic MRI. *International Journal of Radiation Oncology* Biology* Physics*, 2006, **65**(1), pp.291-303.
98. KARAVITAKIS, M., H.U. AHMED, P.D. ABEL, S. HAZELL and M.H. WINKLER. Tumor focality in prostate cancer: implications for focal therapy. *Nature Reviews Clinical Oncology*, 2011, **8**(1), pp.48-55.
99. POLLACK, A., G.K. ZAGARS, L.G. SMITH, J.J. LEE, A.C. VON ESCHENBACH, J.A. ANTOLAK, G. STARKSCHALL and I. ROSEN. Preliminary results of a randomized radiotherapy dose-escalation study comparing 70 Gy with 78 Gy for prostate cancer. *Journal of Clinical Oncology*, 2000, **18**(23), pp.3904-3911.
100. ZELEFSKY, M.J., Y. YAMADA, Z. FUKS, Z. ZHANG, M. HUNT, O. CAHLON, J. PARK and A. SHIPPY. Long-term results of conformal radiotherapy for prostate cancer: impact of dose escalation on biochemical tumor control and distant metastases-free survival outcomes. *International Journal of Radiation Oncology* Biology* Physics*, 2008, **71**(4), pp.1028-1033.
101. PELOWITZ, D.B. MCNPX User's Manual Version 2.5.0. *Los Alamos National Laboratory Report*, 2005, **LA-CP-05–0369**.
102. MELHUS, C.S. and M.J. RIVARD. Approaches to calculating AAPM TG-43 brachytherapy dosimetry parameters for 137 Cs, 125 I, 192 Ir, 103 Pd, and 169 Yb sources. *Med Phys*, 2006, **33**(6), p.17291737.

103. GRANERO, D., J. VIJANDE, F. BALLESTER and M.J. RIVARD. Dosimetry revisited for the HDR Ir brachytherapy source model mHDR-v2. *Medical Physics*, 2011, **38**, pp.487-494.
104. FURSTOSS, C., B. RENIERS, M.J. BERTRAND, E. POON, J.F. CARRIER, B.M. KELLER, J.P. PIGNOL, L. BEAULIEU and F. VERHAEGEN. Monte Carlo study of LDR seed dosimetry with an application in a clinical brachytherapy breast implant. *Medical Physics*, 2009, **36**, pp.1848-1858.
105. DOLAN, J., Z. LI and J.F. WILLIAMSON. Monte Carlo and experimental dosimetry of an I brachytherapy seed. *Medical Physics*, 2006, **33**, p.4675.
106. KENNEDY, R.M., S.D. DAVIS, J.A. MICKA and L.A. DEWERD. Experimental and Monte Carlo determination of the TG-43 dosimetric parameters for the model 9011 THINSeed™ brachytherapy source. *Medical Physics*, 2010, **37**, p.1681.
107. RIVARD, M.J. Monte Carlo radiation dose simulations and dosimetric comparison of the model 6711 and 9011 I brachytherapy sources. *Medical Physics*, 2009, **36**, p.486.
108. ARYAL, P., J.A. MOLLOY and M.J. RIVARD. A modern Monte Carlo investigation of the TG-43 dosimetry parameters for an 125I seed already having AAPM consensus data. *Medical Physics*, 2014, **41**(2), p.021702.
109. Nuclear Data Sheets, Volume 113, issues 8-9, p1871-2111, August–September 2012, National Nuclear Data Center, Brookhaven National Laboratory.
110. PEREZ-CALATAYUD, J., F. BALLESTER, R.K. DAS, L.A. DEWERD, G.S. IBBOTT, A.S. MEIGOONI, Z. OUHIB, M.J. RIVARD, R.S. SLOBODA and J.F. WILLIAMSON. Dose calculation for photon-emitting brachytherapy sources with average energy higher than 50 keV: Report of the AAPM and ESTRO. *Medical Physics*, 2012, **39**, p.2904.
111. *Oncentra Prostate Reference Manual* [online]. Nucletron.
112. KIRISITS, C., F.A. SIEBERT, D. BALTAS, M. DE BRABANDERE, T.P. HELLEBUST, D. BERGER and J. VENSELAAR. Accuracy of volume and DVH parameters determined with different brachytherapy treatment planning systems. *Radiotherapy and oncology*, 2007, **84**(3), pp.290-297.
113. CHIBANI, O. and J.F. WILLIAMSON. MCPI: A sub-minute Monte Carlo dose calculation engine for prostate implants. *Medical Physics*, 2005, **32**, pp.3688-3698.
114. MEIGOONI, A.S., J.A. MELI and R. NATH. Interseed effects on dose for 125I brachytherapy implants. *Medical Physics*, 1992, **19**(2), pp.385-390.
115. BURNS, G.S. and D.E. RAESIDE. The accuracy of single-seed dose superposition for I-125 implants. *Medical Physics*, 1989, **16**, pp.627-631.
116. CARRIER, J.F., M. D'AMOURS, F. VERHAEGEN, B. RENIERS, A.G. MARTIN, É. VIGNEAULT and L. BEAULIEU. Postimplant dosimetry using a Monte Carlo dose calculation engine: A new

clinical standard. *International Journal of Radiation Oncology* Biology* Physics*, 2007, **68**(4), pp.1190-1198.

117. CHIBANI, O., J.F. WILLIAMSON and D. TODOR. Dosimetric effects of seed anisotropy and interseed attenuation for 103Pd and 125I prostate implants. *Medical Physics*, 2005, **32**(8), pp.2557-2566.
118. DEMARCO, J.J., J.B. SMATHERS, C.M. BURNISON, Q.K. NCUBE and T.D. SOLBERG. CT-based dosimetry calculations for 125I prostate implants. *International Journal of Radiation Oncology* Biology* Physics*, 1999, **45**(5), pp.1347-1353.
119. ZHANG, H., C. BAKER, R. MCKINSEY and A. MEIGOONI. Dose verification with Monte Carlo technique for prostate brachytherapy implants with 125I sources. *Medical Dosimetry*, 2005, **30**(2), pp.85-91.
120. LUXTON, G. Comparison of radiation dosimetry in water and in solid phantom materials for I-125 and Pd-103 brachytherapy sources: EGS4 Monte Carlo study. *Medical Physics*, 1994, **21**, p.631.
121. CHEN, Z. and R. NATH. Dose rate constant and energy spectrum of interstitial brachytherapy sources. *Medical Physics*, 2001, **28**, p.86.
122. DEWERD, L.A., G.S. IBBOTT, A.S. MEIGOONI, M.G. MITCH, M.J. RIVARD, K.E. STUMP, B.R. THOMADSEN and J.L.M. VENSELAAR. A dosimetric uncertainty analysis for photon-emitting brachytherapy sources: Report of AAPM Task Group No. 138 and GEC-ESTRO. *Medical Physics*, 2011, **38**, p.782.
123. LAVALLEE, M.C., L. GINGRAS and L. BEAULIEU. Energy and integrated dose dependence of MOSFET dosimeter sensitivity for irradiation energies between 30 kV and Co. *Medical Physics*, 2006, **33**, p.3683.
124. CARRIER, J.F., L. BEAULIEU, F. THERRIAULT-PROULX and R. ROY. Impact of interseed attenuation and tissue composition for permanent prostate implants. *Medical Physics*, 2006, **33**, pp.595-604.
125. LANDRY, G., B. RENIERS, J.P. PIGNOL, L. BEAULIEU and F. VERHAEGEN. The difference of scoring dose to water or tissues in Monte Carlo dose calculations for low energy brachytherapy photon sources. *Medical Physics*, 2011, **38**(3), pp.1526-1533.
126. MASON, J., B. AL-QAISIEH, P. BOWNES, A. HENRY and D. THWAITES. Monte Carlo investigation of I-125 interseed attenuation for standard and thinner seeds in prostate brachytherapy with phantom validation using a MOSFET. *Medical Physics*, 2013, **40**, pp.031717-031728.
127. MELHUS, C.S., J.K. MIKELL, S.J. FRANK, F. MOURTADA and M.J. RIVARD. Dosimetric influence of seed spacers and end-weld thickness for permanent prostate brachytherapy. *Brachytherapy*, 2013, (In Press).
128. AFSHARPOUR, H., M. D'AMOURS, B. COTÉ, J.F. CARRIER, F. VERHAEGEN and L. BEAULIEU. A Monte Carlo study on the effect of seed design on the interseed attenuation in permanent prostate implants. *Medical Physics*, 2008, **35**, p.3671.

129. LANDRY, G., B. RENIERS, L. MURRER, L. LUTGENS, E. BLOEMEN-VAN GURP, J.P. PIGNOL, B. KELLER, L. BEAULIEU and F. VERHAEGEN. Sensitivity of low energy brachytherapy Monte Carlo dose calculations to uncertainties in human tissue composition. *Medical Physics*, 2010, **37**, pp.5188-5198.
130. AL-QAISIEH, B. Pre-and post-implant dosimetry: an inter-comparison between UK prostate brachytherapy centres. *Radiotherapy and oncology*, 2003, **66**(2), pp.181-183.
131. BICE JR, W.S., B.R. PRESTIDGE and M.F. SAROSDY. Sector analysis of prostate implants. *Medical Physics*, 2001, **28**, pp.2561-2567.
132. GAUDET, M., E. VIGNEAULT, S. AUBIN, N. VARFALVY, F. HAREL, L. BEAULIEU and A.G. MARTIN. Dose Escalation to the Dominant Intraprostatic Lesion Defined by Sextant Biopsy in a Permanent Prostate I-125 Implant: A Prospective Comparative Toxicity Analysis. *International journal of radiation oncology, biology, physics*, 2010, **77**(1), pp.153-9.
133. HOUSRI, N., H. NING, J. ONDOS, P. CHOYKE, K. CAMPHAUSEN, D. CITRIN, B. ARORA, U. SHANKAVARAM and A. KAUSHAL. Parameters Favorable to Intraprostatic Radiation Dose Escalation in Men With Localized Prostate Cancer. *International Journal of Radiation Oncology* Biology* Physics*, 2011, **80**(2), pp.614-620.
134. OST, P., B. SPELEERS, G. DE MEERLEER, W. DE NEVE, V. FONTEYNE, G. VILLEIRS and W. DE GERSEM. Volumetric Arc Therapy and Intensity-Modulated Radiotherapy for Primary Prostate Radiotherapy With Simultaneous Integrated Boost to Intraprostatic Lesion With 6 and 18 MV: A Planning Comparison Study. *International Journal of Radiation Oncology* Biology* Physics*, 2011, **79**(3), pp.920-926.
135. ALONZI, R., A.R. PADHANI, N.J. TAYLOR, D.J. COLLINS, J.A. D'ARCY, J.J. STIRLING, M.I. SAUNDERS and P.J. HOSKIN. Antivascular effects of neoadjuvant androgen deprivation for prostate cancer: an in vivo human study using susceptibility and relaxivity dynamic MRI. *International Journal of Radiation Oncology* Biology* Physics*, 2011, **80**(3), pp.721-727.
136. BARRETT, T., A.B. GILL, M.Y. KATAOKA, A.N. PRIEST, I. JOUBERT, M.A. MCLEAN, M.J. GRAVES, S. STEARN, D.J. LOMAS and J.R. GRIFFITHS. DCE and DW MRI in monitoring response to androgen deprivation therapy in patients with prostate cancer: A feasibility study. *Magnetic Resonance In Medicine*, 2011, **67**(3), pp.778-785.
137. *Common Terminology Criteria for Adverse Events (CTCAE).* Version 4.0. National Institutes of Health: National Cancer Institute, 2009.
138. DICKINSON, L., H.U. AHMED, C. ALLEN, J.O. BARENTSZ, B. CAREY, J.J. FUTTERER, S.W. HEIJMINK, P.J. HOSKIN, A. KIRKHAM and A.R. PADHANI. Magnetic resonance imaging for the detection, localisation, and characterisation of prostate cancer:

recommendations from a European consensus meeting. *European urology*, 2011, **59**(4), pp.477-494.

139. BARENTSZ, J.O., J. RICHENBERG, R. CLEMENTS, P. CHOYKE, S. VERMA, G. VILLEIRS, O. ROUVIERE, V. LOGAGER and J.J. FÃ¼TTERER. ESUR prostate MR guidelines 2012. *European Radiology*, 2012, pp.1-12.
140. KERSHAW, L.E., C.E. HUTCHINSON and D.L. BUCKLEY. Benign prostatic hyperplasia: Evaluation of T1, T2, and microvascular characteristics with T1â€ weighted dynamic contrastâ€ enhanced MRI. *Journal of Magnetic Resonance Imaging*, 2009, **29**(3), pp.641-648.
141. SCHERR, M.K., M. SEITZ, U.G. MÃ¼LLER-LISSE, M. INGRISCH, M.F. REISER and U.L. MÃ¼LLER-LISSE. MR-perfusion (MRP) and diffusion-weighted imaging (DWI) in prostate cancer: Quantitative and model-based gadobenate dimeglumine MRP parameters in detection of prostate cancer. *European Journal of Radiology*, 2010, **76**(3), pp.359-366.
142. SOURBRON, S., M. INGRISCH, A. SIEFERT, M. REISER and K. HERRMANN. Quantification of cerebral blood flow, cerebral blood volume, and blood-brain-barrier leakage with DCE-MRI. *Magnetic Resonance In Medicine*, 2009, **62**(1), pp.205-217.
143. MCKENZIE, A., M. COFFEY, T. GREENER, C. HALL, M. VAN HERK, B. MIJNHEER and A. HARRISON. *Technical overview of geometric uncertainties in radiotherapy* [online]. The British Institute of Radiology, London 2003.
144. GROENENDAAL, G., A. BORREN, M.R. MOMAN, E. MONNINKHOF, P.J. VAN DIEST, M.E.P. PHILIPPENS, M. VAN VULPEN and U.A. VAN DER HEIDE. Pathologic Validation of a Model Based on Diffusion-Weighted Imaging and Dynamic Contrast-Enhanced Magnetic Resonance Imaging for Tumor Delineation in the Prostate Peripheral Zone. *International Journal of Radiation Oncology* Biology* Physics*, 2011.
145. MORTON, G.C., D.A. LOBLAW, H. CHUNG, G. TSANG, R. SANKREACHA, A. DEABREU, L. ZHANG, A. MAMEDOV, P. CHEUNG and D. BATCHELAR. Health-related quality of life after single-fraction high-dose-rate brachytherapy and hypofractionated external beam radiotherapy for prostate cancer. *International Journal of Radiation Oncology* Biology* Physics*, **80**(5), pp.1299-1305.
146. BALTAS, D., C. KOLOTAS, K. GERAMANI, R.F. MOULD, G. IOANNIDIS, M. KEKCHIDI and N. ZAMBOGLOU. A conformal index (COIN) to evaluate implant quality and dose specification in brachytherapy. *International Journal of Radiation Oncology* Biology* Physics*, 1998, **40**(2), pp.515-524.
147. TODOR, D.A., I.J. BARANI, P.-S. LIN and M.S. ANSCHER. Moving toward focal therapy in prostate cancer: dual-isotope permanent seed implants as a possible solution. *International Journal of Radiation Oncology* Biology* Physics*, 2011, **81**(1), pp.297-304.

148. KAZI, A., G. GODWIN, J. SIMPSON and G. SASSO. MRS-guided HDR brachytherapy boost to the dominant intraprostatic lesion in high risk localised prostate cancer. *BMC cancer*, 2010, **10**(1), p.472.
149. MASON, J., B. AL-QAISIEH, P. BOWNES, D. WILSON, D.L. BUCKLEY, D. THWAITES, B. CAREY and A. HENRY. Multi-parametric MRI-guided focal tumor boost using HDR prostate brachytherapy: A feasibility study. *Brachytherapy*, 2013.
150. SCHICK, U., Y. POPOWSKI, P. NOUET, S. BIERI, M. ROUZAUD, H. KHAN, D.C. WEBER and R. MIRALBELL. High-dose-rate brachytherapy boost to the dominant intra-prostatic tumor region: Hemi-irradiation of prostate cancer. *The Prostate*, 2011, **71**(12), pp.1309-1316.
151. HOSKIN, P., A. ROJAS, P. OSTLER, R. HUGHES, R. ALONZI, G. LOWE and L. BRYANT. High-dose-rate brachytherapy alone given as two or one fraction to patients for locally advanced prostate cancer: Acute toxicity. *Radiotherapy and oncology*, 2013.
152. PRADA, P.J., I. JIMENEZ, H. GONZÁLEZ-SUÁREZ, J. FERNÁNDEZ, C. CUERVO-ARANGO and L. MENDEZ. High-dose-rate interstitial brachytherapy as monotherapy in one fraction and transperineal hyaluronic acid injection into the perirectal fat for the treatment of favorable stage prostate cancer: treatment description and preliminary results. *Brachytherapy*, 2012, **11**(2), pp.105-110.
153. MAVROIDIS, P., N. MILICKOVIC, W.F. CRUZ, N. TSELIS, A. KARABIS, S. STATHAKIS, N. PAPANIKOLAOU, N. ZAMBOGLOU and D. BALTAS. Comparison of Different Fractionation Schedules Toward a Single Fraction in High-Dose-Rate Brachytherapy as Monotherapy for Low-Risk Prostate Cancer Using 3-Dimensional Radiobiological Models. *International Journal of Radiation Oncology* Biology* Physics*, 2014, **88**(1), pp.216-223.
154. BUES, M., E.J. HOLUPKA, P. MESKELL and I.D. KAPLAN. Effect of random seed placement error in permanent transperineal prostate seed implant. *Radiotherapy and oncology*, 2006, **79**(1), pp.70-74.
155. WHITAKER, M., G. HRUBY, A. LOVETT and N. PATANJALI. Prostate HDR brachytherapy catheter displacement between planning and treatment delivery. *Radiotherapy and oncology*, 2011, **101**(3), pp.490-494.
156. MILICKOVIC, N., P. MAVROIDIS, N. TSELIS, I. NIKOLOVA, Z. KATSILIERI, V. KEFALA, N. ZAMBOGLOU and D. BALTAS. 4D analysis of influence of patient movement and anatomy alteration on the quality of 3D U/S-based prostate HDR brachytherapy treatment delivery. *Medical Physics*, 2011, **38**, p.4982.
157. MASHOUF, S., E. LECHTMAN, L. BEAULIEU, F. VERHAEGEN, B.M. KELLER, A. RAVI and J.-P. PIGNOL. A simplified analytical dose calculation algorithm accounting for tissue heterogeneity for low-energy brachytherapy sources. *Physics in medicine and biology*, 2013, **58**(18), p.6299.
158. LANDRY, G., B. RENIERS, P.V. GRANTON, B. VAN ROOIJEN, L. BEAULIEU, J.E. WILDBERGER and F. VERHAEGEN.

Extracting atomic numbers and electron densities from a dual source dual energy CT scanner: experiments and a simulation model. *Radiotherapy and oncology*, 2011, **100**(3), pp.375-379.

159. ENGER, S.A., A. AHNESJÖ, F. VERHAEGEN and L. BEAULIEU. Dose to tissue medium or water cavities as surrogate for the dose to cell nuclei at brachytherapy photon energies. *Physics in medicine and biology*, 2012, **57**(14), p.4489.
160. TEDGREN, Å.C. and G.A. CARLSSON. Specification of absorbed dose to water using model-based dose calculation algorithms for treatment planning in brachytherapy. *Physics in medicine and biology*, 2013, **58**(8), p.2561.
161. THOMSON, R., Å.C. TEDGREN and J. WILLIAMSON. On the biological basis for competing macroscopic dose descriptors for kilovoltage dosimetry: cellular dosimetry for brachytherapy and diagnostic radiology. *Physics in medicine and biology*, 2013, **58**(4), p.1123.
162. SHAH, V., B. TURKBEY, H. MANI, Y. PANG, T. POHIDA, M.J. MERINO, P.A. PINTO, P.L. CHOYKE and M. BERNARDO. Decision support system for localizing prostate cancer based on multiparametric magnetic resonance imaging. *Medical Physics*, 2012, **39**(7), pp.4093-4103.
163. VOS, P., J. BARENTSZ, N. KARSSEMEIJER and H. HUISMAN. Automatic computer-aided detection of prostate cancer based on multiparametric magnetic resonance image analysis. *Physics in medicine and biology*, 2012, **57**(6), p.1527.
164. LIU, X., L. ZHOU, W. PENG, C. WANG and H. WANG. Differentiation of central gland prostate cancer from benign prostatic hyperplasia using monoexponential and biexponential diffusion-weighted imaging. *Magnetic resonance imaging*, 2013, **31**(8), pp.1318-1324.
165. ABOUMARZOUK, O.M., S. OGSTON, Z. HUANG, A. EVANS, A. MELZER, J.U. STOLZENBERG and G. NABI. Diagnostic accuracy of transrectal elastosonography (TRES) imaging for the diagnosis of prostate cancer: a systematic review and meta-analysis. *BJU international*, 2012, **110**(10), pp.1414-1423.
166. BROCK, M., T. EGGERT, R.J. PALISAAR, F. ROGHMANN, K. BRAUN, B. LÖPPENBERG, F. SOMMERER, J. NOLDUS and C. VON BODMAN. Multiparametric ultrasound of the prostate: adding contrast enhanced ultrasound to real-time elastography to detect histopathologically confirmed cancer. *The Journal of urology*, 2013, **189**(1), pp.93-98.
167. REYNIER, C., J. TROCCAZ, P. FOURNERET, A. DUSSERRE, C. GAY-JEUNE, J.L. DESCOTES, M. BOLLA and J.Y. GIRAUD. MRI/TRUS data fusion for prostate brachytherapy. Preliminary results. *Medical Physics*, 2004, **31**, p.1568.
168. MURRAY, L.J., J. LILLEY, C.M. THOMPSON, V. COSGROVE, J. MASON, J. SYKES, K. FRANKS, D. SEBAG-MONTEFIORE and A.M. HENRY. Prostate Stereotactic Ablative Radiation Therapy Using Volumetric Modulated Arc Therapy to Dominant

Intraprostatic Lesions. *International Journal of Radiation Oncology* Biology* Physics*, 2014, **89**(2), pp.406-415.